Universiteit Utrecht

CHEMISTRY AND FABRIC OF OLIVINE MICROSTRUCTURES IN COLD, ULTRA-DEPLETED SPINEL MANTLE WEDGE PERIDOTITE, SEVE NAPPE COMPLEX (CENTRAL SWEDISH CALEDONIDES)

MSc student : Frediano Clos Clos.Frediano@gmail.com

Supervisor: Dr. Herman L.M. van Roermund

ABSTRACT

This thesis investigates the formation conditions of olivine microstructures in the Kittelfjäll spinel peridotite (KSP), a fragment of lithospheric mantle which occurs as an isolated body within high grade metamorphic crustal rocks in the Seve Nappe Complex (SNC) of Northern Jämtland, central Sweden. The KSP is an orogenic peridotite containing a well developed penetrative compositional layering, defined by highly depleted dunites (high olivine Mg# (Mg/Mg+Fe = 0,92–0,93) and spinel Cr# (Cr/Cr+Al = 0,89-0,96)), and harzburgites (with lower Mg# (0,91–0,92) and higher whole-rock Ca and Al contents). Dunites are characterized by three contrasting olivine microstructures formed in response to different tectono-metamorphic conditions: 1) Coarse-grained, highly strained olivine porphyroclasts (M1) up to 20 cm are surrounded by 2) dynamically recrystallized olivine grains (M2) defining a characteristic olivine "foam" microstructure (200-2000 um). In strongly localized shear zones 3) an olivine "mortar" structure (10-50 um). Olivine fabric analysis (microstructure + Crystallographic Preferred Orientations (CPO)), EMP and XRF analyses reveal a retrograde evolution for the KSP. Olivine porphyroclasts (M1) grew at high temperature during cooling following Archean melt extraction (<50%) and possible Proterozoic refertilization events. The onset of the Caledonian deformation is interpreted to be related to the crustal emplacement of the KSP during eduction of the SNC. This phase is characterized by the development of the olivine M2 foam microstructure, formed at 750-830°C – 2±1 Gpa by dislocation creep processes producing dominant E-type CPO's by the operation of the [100](001) slip systems. The formation of an olivine M3 "mortar" structure in localized shear zones at 550-600°C-0,45-0,6 Gpa represents further stage during eduction.

Mineralogical, geochemical and structural evidence clearly demonstrates that the KSP peridotite represents old, possibly Archean sub-continental lithosphere mantle (partial melting >50%) that was crustally emplaced into the Caledonian tectonic edifice during the Jämtlandian orogeny (~450 Ma). The "relatively LT" olivine M2 "foam" microstructure can be proposed as a tool to easily discriminate mantle wedge peridotites (i.e. sub-continental affinity) from ophiolite (i.e. sub-oceanic affinity) in the Scandinavian Caledonides.

Table of Contents

Abbreviations

Atg	Antigorite
BLG	Bulging
Chr	Chromite
CPO	Crystallographic Preferred Orientations
Cpx	clinopyroxene
Cr#	(Cr)/(Cr+Al)
EMP	Electron microprobe
EMPA	Electron microprobe analysis
Fe^{3+}#	$(Fe^{3+})/(Fe^{3+}+Al+Cr)$
FGP	Friningen garnet peridotite
GBM	Grain Boundary Migration
GSI	Grain Size Insensitive
GSS	Grain Size Sensitive
HP	High pressure
IP	Intermediate pressure
KNC	Köli Nappe Complex
KSP	Kittelfjäll spinel peridotite
LP	Low Pressure
Mg#	(Mg)/(Mg+Fe)
OCT	Ocean-Continent Transition
Ol	Olivine
Opx	Orthopyroxene
PT	Pressure-Temperature
SC	Scandinavian Caledonides
SCLM	Sub-Continental Lithospheric Mantle
SGR	Subgrain Rotation
SNC	Seve Nappe Complex
SOLM	Sub-Oceanic Lithospheric Mantle
TEM	Transmission Electron Microprobe
Tc	Talc
Tr	Tremolite
UHP	Ultra High Pressure
XRF	X-Ray Fluorescence

1 INTRODUCTION

One of the major issues encountered when attempting to decipher the evolution of orogens is the reconstruction of complex events from an incomplete geological record. In fact, orogenic belts can be considered as the final product of geological cycles, alternating ocean spreading and closure. Newly-formed oceanic crust and volcanic arcs alongside with sedimentary sequences are rapidly developed and successively subducted into the mantle, before the complete ocean closure and final continent-continent collision. Only part of the original geological record is finally educted (exhumed) back to the surface. Thus far, one of the most effective solutions adopted to unravel the tectono-metamorphic evolution of mountain belts from the incomplete geological records is the detailed study of tectono-stratigraphic areas defining fossil plate boundaries. Such former suture zones are outlined by the scattered presence of (orogenic) peridotite bodies (Coleman, 1971). The strategic importance of ultramafic bodies lies in their ability to preserve mineral traces of early geological evolution, otherwise overprinted by later events in the surrounding continental rocks. Therefore, a deep understanding of ultramafic bodies and the mechanisms responsible for their emplacement in such suture zones is of paramount importance for paleogeographic and geodynamic reconstructions in all orogenic belts.

The Scandinavian Caledonides (SC) provides one of the most appropriate locations for the case study of ultramafic massifs. This orogenic belt represents a complex early Paleozoic collision belt exposed along the Scandinavian peninsula for more than 2000 km. Several stages of Precambrian terrane formation and reworking lead to the development of the supercontinent Rhodinia around 900 Ma, which subsequently rifted apart into 4 major continents (Baltica, Laurentia, Siberia and Gondwana). The formation of the SC is related to the closure of the ocean dividing Laurasia and Baltica, the Iapetus ocean (*Cocks & Torsvik, 2006)*. Convergence between Baltica and Laurentia resulted in a series of collisional events, namely the Finnmarkian orogeny (520-500 Ma), the Jämtlandian orogeny (~454 Ma) and the final continent-continent collision by underthrusting of Baltica beneath Laurentia, which occurred during the Scandian orogeny (430-400 Ma) (Roberts 2003). A series of nappes were thrusted eastwards over the Baltoscandian basement and its autochtonous Vendian to early Paleozoic sedimentary cover (Gee, 2008). The tectonostratigraphy of the nappes, now overlying the authoctonous units, is divided from base to top into Lower, Middle, Upper and Uppermost allochthons (Roberts & Gee,1985). The Lower allochthon is comprised of westward-stacked autochtonous/parautochtonous units (Roberts and Gee, 1985). The Middle allochthon is composed of metasediments representing the ocean-continent transition zone (OCT) apart from the Baltic Shield (Seve Nappe Complex, SNC), and by a crystalline basement and late Proterozoic feldspathic sandstones of Baltica affinity (Sarv Nappe) (Gee, 2008). The Upper allochthon is characterized by rocks of oceanic affinity representing relics of the former Iapetus ocean associated with marginal basin deposits and island arcs proximal to the western edge of Baltica (Roberts, 2003). The Uppermost allochthon preserves thick pre-Paleozoic carbonate sequences on crystalline basement structures and is considered to represent part of Laurentia's foreland (Yoshinobu et al, 2002).

Within the SC orogenic mantle fragments are found in the metamorphic rocks of the Western Gneiss Region (WGR; a tectonic window exposing reworked Scandian Baltic basement), Upper (Köli Nappe Complex, KNC) and Middle allochthons (SNC). The area of interest for this MSc thesis is located in the SNC, the orogenic peridotites of which are so far interpreted as either: 1) lower sections of dismembered ophiolite complexes (Du Rietz, 1935; Zachrisson, 1969; Zwart, 1974; Stigh, 1979; Qvale & Stigh, 1985; Bucher-Nurminen, 1988, 1991; Andreasson, 1994) 2) or as peridotite massifs related to hyperextension along the Baltic margin (Anderson et al., 2012). Most of these mantle fragments are dunitic/harzburgitic in their bulk rock chemistry, making it difficult to reconstruct their structural-metamorphic evolution, hence the sub-continental/sub-oceanic mantle affinity. However, recent work on orogenic garnet peridotites from the SNC has demonstrated an alternative tectonic scenario in which intermediate to high pressure sub-continental mantle rocks become involved in a

prograde subduction zone in which they become subducted down to coesite-stable, Ultra High Pressure (UHP) metamorphic conditions (van Roermund, 1989; Janak et al, 2013). Nevertheless the great majority of ultramafic bodies in the SNC lack a garnet bearing mineral assemblage. An extremely depleted bulk rock composition in composition with the minor mineralogical variety complicates the pressure-temperature (PT) estimates, making it difficult if not impossible, to define their origin (i.e. sub-continental vs sub-oceanic) and for structural-metamorphic evolution.

The idea of studying and unravelling the tectono-metamorphic evolution of dunite bodies is intriguing but studies of dunite massifs have so far been discarded in favour of more profitable areas, richer in geological information. However, will it be possible in the absence of stable mineral assemblages to determine PT conditions associated with re-crystallised microstructures in olivine? Would it be possible to mutually compare the olivine microstructures of well-known ultramafic lenses with highly depleted ultramafic massifs? The aim of the present thesis is to define a microstructural olivine method able to easily discriminate ultramafic fragments based on their sub-continental or sub-oceanic provenance.

The metamorphic conditions primarily associated with olivine fabrics in one of the largest dunitic/harzburgitic bodies in the SNC, the Kittelfjäll spinel-bearing peridotite (KSP) in the central Swedish Caledonides are re-investigated. Microstructural, geochemical and petrological evidences clearly demonstrate that the KSP represents an old, possibly Archean, sub-continental lithospheric mantle (SCLM) fragment, that was transported from deep mantle levels into the continental crust during eduction (exhumation) of the SNC. Similar orogenic peridotites have thus far only been found within the Western Gneiss Region of SW Norway (Brueckner et al., 2010). Three contrasting olivine microstructures are formed in response to different metamorphic and deformation conditions. Coarse-grained (up to 20 cm), highly strained olivine crystals (M1) are surrounded by dynamically recrystallized olivine grains (M2) defining a characteristic olivine “foam” microstructure (200-2000 um). In strongly localized shear zones a third fabric is developed, named olivine “mortar” structure (10-50 um). Detailed investigations concerning deformation mechanisms which have generated the aforementioned olivine microstructures are presented herein and ultimately are interpreted to be related to retrogression from sub-continental mantle conditions to shallower crustal levels due to eduction. In particular, the penetrative M2 olivine microstructure reveals strong analogies with olivine microstructures in the orogenic Friningen garnet peridotite (MSc thesis Gilio, 2013) and can be associated to early-Caledonian subduction and/or eduction processes. The latter ductile-olivine microstructures thus represent a powerful tool which enables easy discrimination between orogenic peridotites with sub-continental affinity and other types of orogenic peridotites (i.e. ophiolites) in which similar olivine microstructures are lacking.

2 GEOLOGICAL SETTING

2.1 Paleogeography of Baltica and Caledonian Orogeny

The Baltic shield is the result of a complex geological history, characterized by several stages of terrane formation and reworking. Crustal accretion, leading to the formation of the ancestral Baltic shield (termed Protobaltica), occurred during Saamian orogeny (>3,1Ga), Lopian orogeny (2,9-2,6 Ga; (Spengler et al., 2006)) Svecofennian orogeny (1,75 – 2,0 Ga; Bogdanova, Gorbatschev, & Stephenson, 2001) and the subsequent Gothian orogeny (1,5 – 1,75; Gaál and Gorbatscheb, 1987). In the late Proterozoic a large area of Protobaltica was reworked by the Sveconorwegian-Greenvillian Orogeny (1,05-0.9 Ga) in order to form the supercontinent Rhodinia.

The onset of the break up/rifting in the supercontinent Rhodinia is dated around 750 – 800 Ma (Torsvik & Cocks, 2009) . As a result, 4 new continents were formed: Laurentia, Baltica, Siberia and Gondwana. In a first phase Baltica and Laurentia remained attached, and only at 650 Ma they started to rift away. The formation of the Iapetus Ocean is signed by mafic dykes intrusions at c. 600 Ma *(Cocks & Torsvik, 2007; Majka et al., 2012) .* The shifting, from an extensional regime to a compressional state that closed the Iapetus ocean and formed Laurussia, is firstly marked by the Finnmarkian event in Late Cambrian (520-500 Ma; (Roberts, 2003). In this phase the Baltoscandian margin collided with an inferred magmatic arc (Dallmeyer and Gee, 1986) or a microcontinent with Baltic affinity. Progress of the oceanic closure caused subduction of Baltoscandian margin beneath Laurentia (Brueckner & Van Roermund, 2004; Roberts, 2003), during the Scandian phase (430-400 Ma). Early Scandian (430-410 Ma) metamorphic phase is characterized by low amphibolite to UHP eclogite facies paragenesis, and is followed by an overprint from granulite to amphibolite facies during the late Scandian (396-390 Ma; Terry and Robinson, 2003; Tucker et al, 2004). The buoyancy driven eduction of the subducted terranes in the Scandinavian Caledonides occurred relatively fast, in a time period of maximum 10 Ma (Spengler et al., 2006).

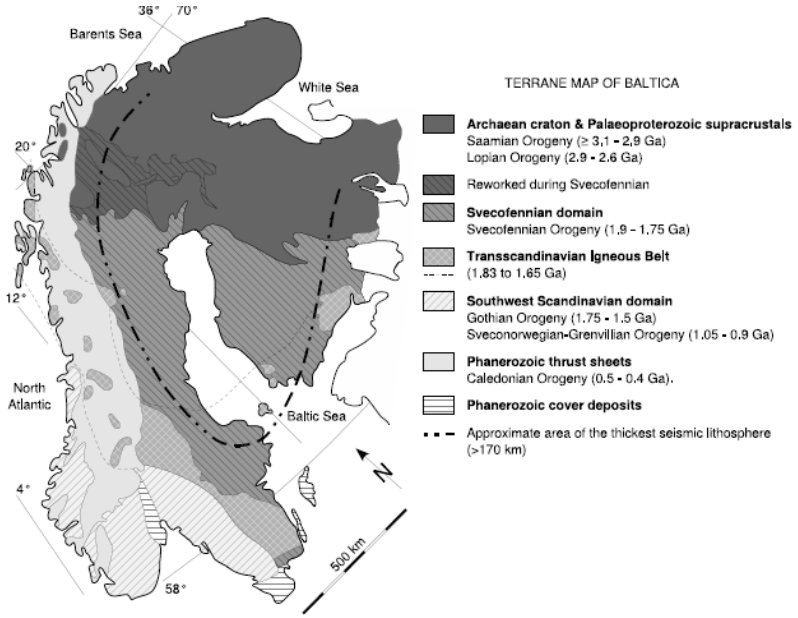

Figure 1:Simplified geological map displaying the major tectono-metamorphic units of the Baltic Shield. Dashed dotted line is the boundary in which the lithosphere is inferred to be thickest (modified after Spengler, 2006)

2.2 Allochthons and Autochthons

SC are formed by a series of allochthons divided by major tectonic contacts: from top to bottom Uppermost, Upper, Middle and Lower allochthon (Roberts & Gee, 1985). The Uppermost allochthon preserves early structures and is considered as part of the Laurentia's foreland (Roberts et al., 2001; Yoshinobu et al, 2002). The unit is characterized by high grade metamorphic metasediment, migmatitic paragneiss, marble and ophiolite of Paleozoic ages intruded by peralouminous and calc-alkaline rocks and it is generally thought to be part of the Laurentia tectonic plate (Stephens & Gee, 1985; Roberts et al, 2001). The Upper allochthon was classically divided in Sweden in Köli Nappe Complex (KNC) and Seve Nappe Complex (SNC), even though affinities with rocks of the Middle allochthon in Norway, recently placed the SNC in the Middle allochthon (Gee, 2008). The KNC present a sequence of late Cambrian to early Ordovician ophiolites and volcanic arc rocks covered by Laurentia affinity conglomerate and turbidites ((Roberts, 2003); Gee et al, 2010). The KNC has been

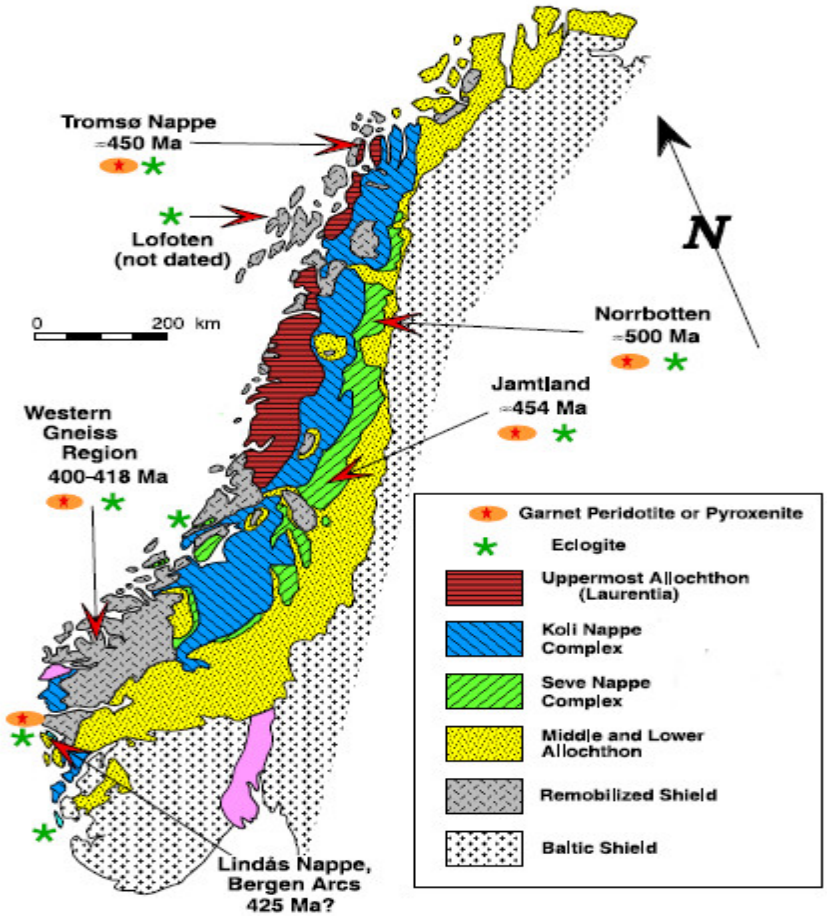

Figure 2: Geological map of the Scandinavian Caledonides illustrating N-S running allochthons in relationship with the occurence of Garnet peridotite and eclogites.

metamorphosed only during the Scandian orogeny and the maximum metamorphic grade is greenschist facies. Middle allochthon lithology is dominated by crystalline basement and late Proterozoic feldspatic sandstones, which origin is probably the continental margin of Baltica. In the lower part of the Middle allochthon dominates rocks metamorphosed under greenschist facies whereas in the upper part (i.e. SNC) amphibolite-granulite facies with preservation of local eclogites and relics of UHP.

The Lower allochthon is composed of westwards piled up autochtonous/ parautochtonous

sediments with a metamorphic gradient from low/medium greenschist facies to amphibolite (Andreasson*,1980;* Roberts and Gee, 1985). The allochthons lain over autochthonous Precambrian crystalline basement of the Baltic Shield and overlying parautochthonous units mainly composed of blackshales of Middle to Late Cambrian age.

2.3 Seve Nappe Complex

The SNC was at first considered to be part of the the Upper Allochthon because of the metamorphic grade (Roberts & Gee, 1985). More recently the SNC is classified as part of the Middle Allochthon because the rocks of the Seve Nappe Complex have more affinity with the metasedimentary units of those in the Middle Allochthon (Gee et al. 2008).

The (SNC) is a 800 km long assemblage of imbricated thrust sheets with different lithologies and metamorphic grades. The complex is overlain by the Köli Nappe Complex (KNC) and overlain Middle and Lower Nappes in the east (Zwart, 1974). The Lower part of the KNC consists of Early Ordovician volcano-sedimentary sequences overlain by metagreywacke, conglomerate and graphitic phyllites metamorphosed under lower greenschist conditions.

The SNC in North Jämtland/South Västerbotten is considered the upper part of the Middle allochthon (Gee, 2008) and is subdivided in three N-S running belts separated by major contacts (Zwart 1974) : Western, Central and Eastern belt (Fig.3). Tectonic nature of the contacts amongst units are emphasized by a clear E-W metamorphic gradient: metamorphic grade (Temperature) increase from lower amphibolites facies (Western Belt) to upper amphibolite-granulite facies (Central Belt),and then decrease again to lower amphibolite-upper greenschist facies (Eastern Belt) (Trouw, 1973).

The Western belt is formed by the Svartsjobacken Schists, mainly composed of garnet-micaschist with intercalated lenses of amphibolite. A low-medium amphibolite facies metamorphism characterizes the northern part of the belt (Trouw, 1973); Zwart 1974), whereas the southern part can not accurately be determined because of scarce exposure. Recent investigation on the area revealed monazites age of 488-491 Ma (MSc thesis Hogerwerf, 2010). The Eastern belt consists of garnet-mica schists, marbles, kyanite-staurolite schists, quartzo-feldspatic gneisses, amphibolites, quartzites and garnet-biotite rocks (Zwart, 1974; Roermund & Bakker, 1984) metamorphosed under lower amphibolite to upper greenschist facies.

The Central belt consists of rocks metamorphosed under upper amphibolite to granulite facies, overprinted by lower amphibolite and greenschist facies conditions (Zwart, 1974; Williams and Zwart, 1977). Three units compose the belt: Marsfjället gneiss, Avardo gneiss and Lillfjället gneiss (Fig.3). In the northernmost part, kyanite-Kfeldspar gneiss of the Marsfjället gneiss records intermediate range of pressure at ~12-17 kbar and ~550-800 °C (MSc thesis Hogerwerf, 2010). The Avardo gneiss exposes quartzo-feldspatic gneiss and amphibolites, in which monazites crystals indicate recrystallization ages of 520-500 Ma at 700-800 °C and > 18,5 kbar (MSc thesis Hogerwerf, 2010 and Gademan, 2010). The Lillfjället gneiss is exposed mainly in the southernmost areas as klippen on top of the Avardo gneisses (Fig.3). Mineral paragenesis indicate re-equilibration conditions of 9 –10 kbar at 750 – 800 °C (Gademan, 2010)

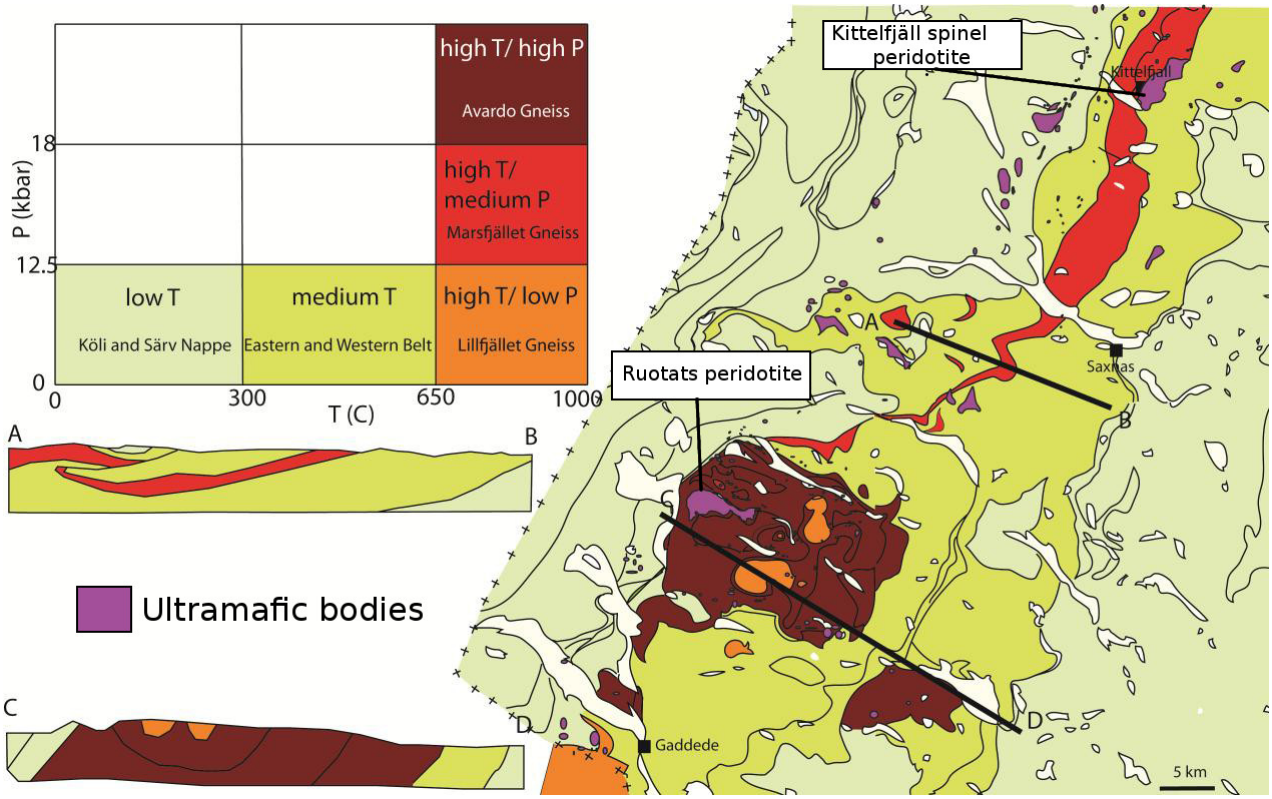

Figure 3: Metamorphic map showing the PT conditions at the metamorphic peak for each unit. Central Belt of the SNC is characterized by a N-S pressure gradient. Kittelfjäll spinel peridotite is considered part of the Marsfjället gneiss and the Ruotats peridotite lens part of the Avardo HP gneiss. (Modified after Verbaas, 2011)

The geological object of this MSc thesis is the Kittelfjäll spinel peridotite, a N-S elongated ultramafic mantle fragment in a crustal envelope, formed by Kittelfjäll amphibolite (Biermann, 1979)- Marsfjället gneiss (Trouw, 1973) and the garnet micaschist of the Eastern Belt (Fig.4). The amphibolite (Kittelfjäll amphibolite) and gneisses (Marsfjället gneisses) composing the Central Belt are characterized by similar peak metamorphic conditions as the Kittelfjäll peridotite: upper amphibolite to granulite facies (M2) metamorphic conditions.

- **Kittelfjäll amphibolite**

Kitttelfjäll amphibolite (Biermann, 1979), lying on top of the Kittelfjäll spinel peridotite (Appendix 1; Fig.4), is mainly formed by clinopyroxene bearing amphibolite and hornblendites (Biermann, 1979). The rocks are strongly re-equilibrated with stable assemblage of clinopyroxene, green hornblende, Ca-rich plagioclase and quartz. Preserved relics in gneisses and schists indicate the presence of a stable mineral assemblage of kyanite-Kfeldspar (Biermann, 1979). Positive feedback comes from the correlation with the KSP. In fact, in both units it is possible to observe a penetrative ductile deformation that was formed under upper amphibolite facies (M2) conditions and overprinted by metamorphism under low to medium amphibolite facies (M3) assemblages.

- **Marsfjället gneisses**

The Central Belt (Middle Belt) is mainly formed by pelitic and quartzo-feldspatic gneisses with minor metabasic rocks. Coarse grained, leucocratic gneisses overlie the Kittelfjäll amphibolite in the northernmost areas and are characterized by kyanite-Kfeldspar mineral assemblages (Trouw, 1973). Metabasic rocks are defined by the coeval stability of hornblende + plagioclase + garnet + clinopyroxene. The metamorphic peak assemblage (M2) is inferred to have formed at upper-amphibolite to granulite conditions. Migmatites are present only within few horizons (Trouw, 1973). Structure show positive correlation with both Kittelfjäll

amphibolite and peridotite even if early assemblages are better preserved because the metamorphic overprint was weaker, due to greater distance from the major contact (Fig.3-4). Metamorphic temperature, defined by mineral assemblages in the Central Belt of the SNC, remains approximately constant (650-800°C) but exhibit a N-S pressure gradient parallel to the axis of the belt (Fig.3). This change in metamorphic facies, from north to south, is exclusively restricted to the Central Belt of the SNC and a widely accepted model, explaining such gradient, has not been formulated yet.

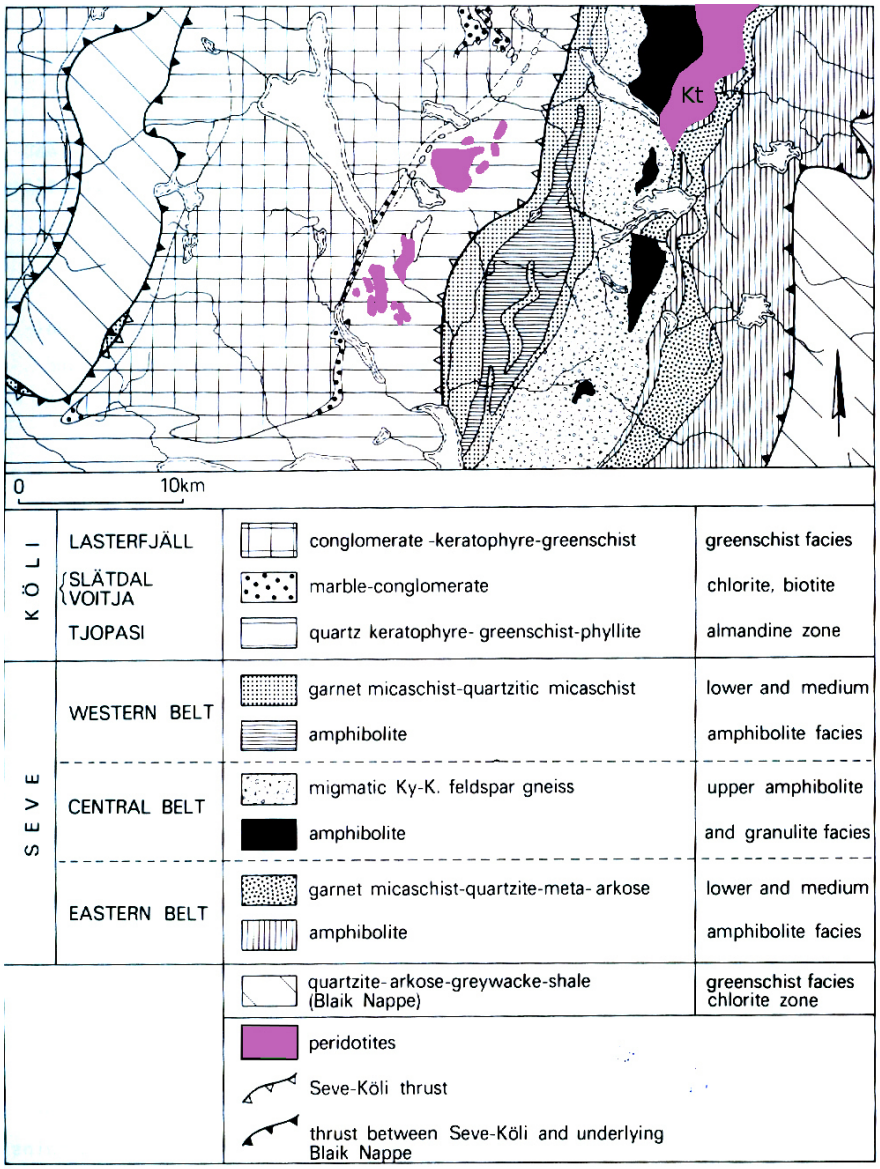

Figure 4: Geological map of the Marsfjället and adjacent areas. Kittelfjäll spinel peridotite (Kt) is located in the Central Belt, at the lower boundary with the Eastern Belt (Modified after Biermann, 1979)

2.4 Eclogites of the SNC

Within the SNC, there are two main eclogite-bearing terranes, 1) in northern Jämtland (Zwart, 1974) and 2) Norrbotten (Andreasson, 1994) located more in the north (Fig.2). Geodynamic interpretations relate SNC eclogite generation to Ordovician subduction of the Baltoscandian outer margin (Brueckner and van Roermund, 2004). Several attempts to date the metamorphism in eclogite bearing-regions and ultramafic bodies in the SNC, all came to ages in the range 500-445 Ma (Mørk et al., 1988; Brueckner et al., 2004; Gademan et al., 2011; Root & Corfu, 2011). This means that the metamorphism in the SNC occurred several millions year before the main Scandian phase, recorded by eclogites yielding ages from 420 to 400 Ma in the WGR (Carswell et al, 2003a; Krogh et al, 2011).

Eclogites in the Norrbotten terranes record Sm-Nd ages of 505 Ma *(Mørk* et al, 1988) and metamorphic zircon ages of 482 *(*Root and Corfu, 2011*).* In North Jämtland there are two high pressure lenses with different metamorphic P-T conditions. The Ertsekey lens (Central Belt) peak is at 780°C, 18-24 kbar and the Tjeliken lens (Eastern Belt) at 550-620°C, 14-16 kbar (van Roermund, 1989). Eclogites in these two HP regions are always associated with ultramafic bodies, more specifically with the presence of garnet peridotites (only in the Western Belts are absent). In the Central belt, Sm-Nd age of eclogite associated with migmatic gneiss is 455 +/-10 (Brueckner and van Roermund, 2007), and a layer of pyroxenite incorporated in the Friningen garnet peridotite, has been dated around 445 Ma (Brueckner et al., 2004) with metamorphic conditions 30 kbar and 800°C within the stable field of coesite (Janak at al, 2013).

The HP unit of the Eastern Belt is characterized by an eclogite Sm-Nd age of 460+/- 4 M and 464 Ma in garnet peridotite (Brueckner et al, 2004) and a U-Pb age of 446 Ma from zircons (Root & Corfu, 2011) and 453 Ma in pyroxenites cross-cutting garnet peridotites.

Differences in age using the Sm-Nd isochron rather than U-Pb zircon method are due to which rock the method is applied. In fact the Sm-Nd method is particularly suitable for garnet-bearing basic rocks and ultramafic bodies that generally lack in zircon. In addition Sm-Nd ages represent cooling age and it may dates the metamorphic peak only when the rock cooled rapidly down after HP formation (Brueckner and Van Roermund, 2004). In this regard, several works demonstrate rapid exhumation/eduction (Terry et al, 2000a; Carswell et al, 2003b), therefore the ages are interpreted here as reasonable time-estimates of the metamorphic peak (Brueckner and van Roermund, 2004).

A strong support to the theory of a rapid uplift comes from a recent work on Central Belt rocks in southern Jämtland (Areskutan) where granulite facies migmatites provide evidences of decompressional melting at 442-436 Ma (Majka et al, 2012).

2.5 Geodynamic model

The Caledonian orogeny can not be simply explained by the continent-continent collision between Baltica and Laurentia. The most accepted model is based on the idea of Brueckner & van Roermund (2004), who incorporated multiple terrane accretion in relation with (U)HP metamorphic phases and presence of orogenic peridotites. After the break up of the supercontinent Gondwana, Baltica rotated anticlockwise (Roberts, 2003) facing firstly Aegir sea and Siberia (Fig.5A-B) and after Iapetus ocean and Laurentia (Fig.5C-D). Terrane accretion occurred along the westernmost edge of the Baltic shield in the following phases:

1. **Finnmarkian phase (~500 Ma)**

The Finnmarkian is an orogenic event that occurred at 520-500 Ma and involves a collision between a microcontinent (Baltica affinity) and Virisen island arc (Fig.5B) with emplacement of mantle peridotites of oceanic affinity from the Virisen mantle wedge (Spengler, 2006). This event involved eclogite facies metamorphism with Sm-Nd age of 505 Ma *(Mørk et al*, 1988) and metamorphic zircon age of 482 *(*Root & Corfu, 2011). The resulting composite terrane is termed as Virisen-Norrbotten-Composite-Terrane (VNCT).

2. **Jämtlandian phase (~450 Ma)**

Thinned edge of Baltica (SNC in North Jämtland) is subducted below the VNCT composite terrane (Fig.5C). Subduction is recorded by subcontinental peridotite emplacement and eclogite facies (HP and UHP) metamorphism with Sm-Nd ageS of 460+/- 4 M and 464 Ma in garnet peridotites (Brueckner et al, 2004) and a U-Pb age of 446 Ma from zircons (Root & Corfu, 2011).

3. **Scandian phase (430-395 Ma)**

The final collision Baltica and Laurentia occurred during last stage of the Caledonian orogeny, called the Scandian phase at 430-395 Ma (Fig.5D). Baltic plate was subducted to exceptional depths, greater than 150 Km as witnessed by widespread presence of orogenic peridotites in the Western Gneiss Region (WGR) (Spengler, 2006).

Late to post Scandian deformation is characterized by widespread extension related to orogenic collapse, which transported and reworked the nappes eastwards. As a result, a series of allochthons, separated by low angle faults, were piled up on the stable Baltic Shield forming the current Scandinavian rock configuration.

The model is based on the concept called "dunk tectonics", in which an orogenic event is characterized by several intermediate micro-collisional events involving collisions between oceanic and/or continental plate, prior to the final continent -continent collision. Each time a plate is subducted deep into the mantle. The model involves a slab break off of the oceanic plate (Wortel & Spakman, 2000), followed by a buoyancy driven eduction. For more detailed information about the model see Chapter 2.5. The most important implication of the model is the fast subduction-eduction cycle that can explain ultra high pressure (UHP) conditions and orogenic peridotites.

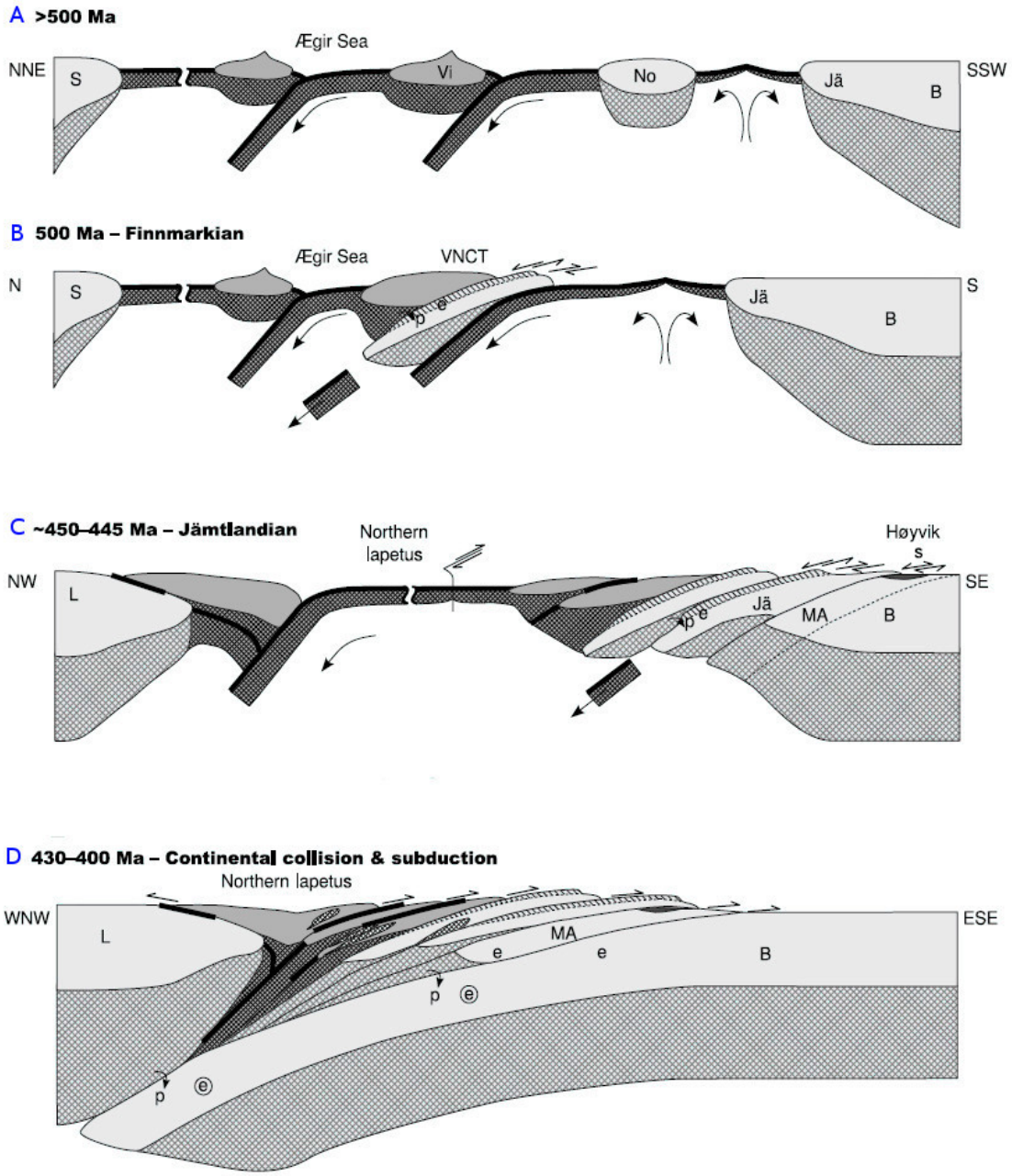

Figure 5: Simplified cartoon showing a proposed model for the evolution of the Northern Caledonides. A)Initial situation prior onset of convergence is defined by Baltica facing Siberia and the Aegir Sea. Oceanic configuration included an island arc (Virisen) and an extensional outboard terrane (Baltica affinity) termed Norrbotten. B)Compressive phase is generally associated to Finnmarkian Phase (~500 Ma), when Norrbotten micro-continent subducted underneath Virisen arc. The following eduction formed a new terrane, called Virisen-Norrbotten-Composite-Terrane (VNCT). C) Continental margin of Baltica (current Jämtland) was subducted below VNCT. This phase is dated around 465 Ma and is related to orogenic peridotite emplacement and eclogite facies metamorphism (UHP at 3 Gpa-800°C; Janak, 2012). Subduction was coupled with an anticlockwise rotation of Baltica towards Laurentia. D)Baltica and Laurentia finally collide in a continent-continent collision during last stage of Caledonian orogeny, namely Scandian phase at 430-395 Ma. Baltic plate was buried at exceptional depth, greater than 150 Km as witnessed by widespread presence of orogenic peridotites in the Western Gneiss Region (WGR). (modified after Spengler, 2006)

Abbreviations: Laurentia (L), Baltica (B), Siberia (S), Virisen arc (Vi), Norrbotten micro-continent (No), Jamtland continental margin (Ja), Middle allochthon (Ma), sediment (s), peridotite (p), HP eclogite (e), UHP eclogites (circled e) (modified after Spengler, 2006).

3 PERIDOTITE TYPES AND PROVENANCE

3.1 Lithospheric mantle

The genetic setting in which ultramafic rocks (i.e. peridotites) generate deeply influence their bulk rock chemical composition and its geodynamic interpretation. A first subdivision of rocks with ultramafic compositions is related to the crustal vs mantle genesis (Table 1). Crustal peridotites are generally interpreted as a subsurface complex of layered basic/ultrabasic cumulates, dikes and sills and are clearly differentiated from the geochemical standpoint with respect to the mantle type. Indeed mantle peridotites are rocks rich in Mg (35-46%)-Cr-Ni and low in Fe (5-10%), clearly in opposition with the rich Fe (12-25%)- TiO_2- Zr and poor Mg (15-26%)-Cr crustal rocks type (Reverdatto et al, 2008). Peridotites formed in the crust represent an extremely small percentage of the total exposed ultramafites on earth.

Most of the peridotites found in mountain belts or on the ocean floors genetically belong to the lithospheric mantle. Most of the data concerning to chemical composition of the Earth's upper mantle comes from study of mantle xenoliths or from tectonically emplaced orogenic, ophiolitic or oceanic peridotites (Chapter 3.2). Studies revealed a well defined geochemical trend linked to the degree of depletion the fertile peridotite underwent. In fact during progressive partial melting, some elements are preferentially partitioned in the solid phase (Cr-Mg) and others into the melt (K-Na-Ca-Al-Fe-Si). Thus, during partial melting mineral destabilized on a precise sequence, first clinopyroxene and then orthopyroxene. Hence a fertile peridotite evolve from lherzolite to harzburgite and in case of extremely high degree of depletion, to dunite (Fig.6).

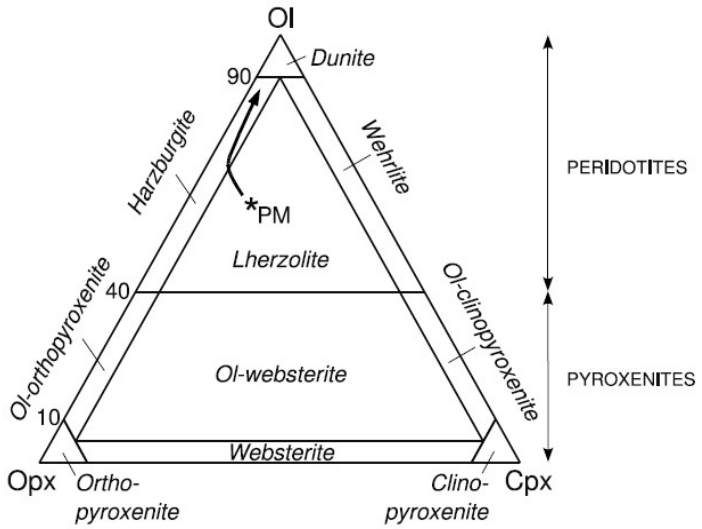

Figure 6: Classification for ultramafic rocks on the basis of mineral mode (Ol-Opx-Cpx). Black arrow indicate residual trend of peridotite during partial melting. Generally, from an average fertile mantle composition (PM), the rock is depleted firstly on the clinopyroxene and then by the orthopyroxene component. Peridotite evolution from lherzolite to harzburgite and finally to dunite is characteristic for most of the known geodynamic settings (after Spengler, 2006).

The above mentioned depletion process always occurs in the mantle and can thus be categorized in Sub-Oceanic Lithospheric Mantle (SOLM) and/or Sub-Continental Lithospheric

Mantle (SCLM) (after Spengler, 2006).

SOLM is related to rising hot asthenosphere underneath middle ocean ridges. Partial melting is related to decompression during upwelling and the resulting restite (i.e. depleted peridotite) will form, during subsequent cooling, the lithosphere underlying oceanic crust. Maximum age of ~200 Ma prior than the main orogeny is the inferred partial melting age for the SOLM, this important age constraint is related to ocean expansion and contraction. In fact, the extensive phase, during which SOLM forms, never exceed 180-200 Ma (Condie, 1997). Clearly, in case of ophiolite obduction the partial melting age is older than the collision event but it is always related to the onset of rifting that lead to the ocean formation. As an instance, in the Scandinavian Caledonides the onset of the rifting in the super-continent Rhodinia, dated around 750 – 800 Ma (Torsvik & Cocks, 2009),gives severe maximum age constraint for ultramafites forming the SOLM of Iapetus.

SCLM are generally subdivided in two categories based on the partial melting age. Old Archean SCLM formed between 2.5-3.8 Ga and represents the highly depleted lithosphere below the oldest cratons. The genesis is linked to high temperature (~1800°C) and pressure (3-7 Gpa) during partial melting, with extraction of komatiitic melts (Walter, 1999). The degree of partial melting inferred from restites is extremely high, generally > 40% (Herzberg, 1999). In fact, during Archean, heat flow in the mantle was about three times higher than in modern times, allowing extraction of komatiite and picritic melts from fertile mantle peridotites (Walter, 1998). During Proterozoic and Phanerozoic time, earth heat flow gradually decreased, causing a different depletion trend (Fig.46). As a result, young (post-Archean) SCLM is less depleted than the older Archean mantle, with melt extraction volume steadily decreasing from < 30% in the Proterozoic and 10-20% in more recent ages (Walter, 1998).

3.2 Classification of mantle peridotite

3.2.1 Initial nomenclature

Ultramafic bodies found high grade metamorphic rocks within the Scandinavian Caledonides are in literature generally defined as orogenic, Alpine type or Mg-Cr type peridotite (Menzies and Dupuy, 1991). An initial classification distinguished between "ophiolite" and "root zone", with oceanic and/or continental affinities respectively (den Tex, 1969). Root zone type was later replaced by the Alpine type peridotite, which was sub-divided after the discovery of the occurrence of garnet-bearing peridotite in UHP terranes of the WGR (Van Roermund, 2009). Thus, the necessity to create new models and a more accurate nomenclature, explaining the emplacement of orogenic garnet peridotite in crustal rocks that have experienced subduction, at depth greater than 150 km, leads to a more specific subdivision for orogenic peridotites with subcontinental affinities.

Current terminology is defined by the structural position in the mantle before the crustal emplacement. On the basis of sub-continental or sub-oceanic affinity, peridotites are subdivided into **orogenic peridotites massifs** (i.e. Root zone/Alpine type peridotite) and **ophiolitic mantle rocks** (Bodinier and Godard, 2005).

3.2.2 Orogenic peridotite massifs

The size of orogenic peridotite massifs is extremely variable , varying from a few meters to several Km's (up to 300 km2) like the Ronda massif in southern Spain or the Almklovdalen massif in the WGR. However most of the peridotite bodies outcropping along major suture zones have intermediate sizes. With a few exceptions the bulk rock composition of orogenic peridotite massif is characterized by the predominance of lherzolites equilibrated in the garnet, spinel or plagioclase field but more refractory compositions, as harzburgite and dunites have been observed, especially in the Caledonides. Most of the bodies are transected by a wide variety of dikes and veins composed by pyroxenytes, garnet, amphibole or gabbros. The degree of serpentinization is highly variable but in most of the bodies is mostly concentrated at the rim or along main faults and veins.

Based on mineral assemblages and tectonometamorphic evolution, orogenic peridotites amssifs can be divided in 3 main groups (Bodinier et al, 2005):

1. **HP/UHP massifs**: equilibrated or re-equilibrated at high or ultra-high pressure, in the stability field of garnet. They are generally termed as **Mantle Wedge type** (Van Roermund, 2009) or **Relict** (Brueckner and Medaris, 2000) peridotite and they represent old cratonic sub-continental lithosphere partially to completely overprinted by subduction fabric:

    - Prograde type

      Crustal intrusion at shallow to intermediated depth, in the stability field of plagioclase or spinel (< 50 km). After an initial prograde fabric and mineral assemblage is acquired during subduction related prograde metamorphism (Friningen garnet peridotite, SNC)

    - HP-HT type

      Crustal intrusion from the mantle wedge within the garnet stability field at depth greater than 50 km.

    - Retrograde type

      Mantle wedge peridotite in which the protolith assemblage define an early HP or/and HT assemblage upon which retrograde metamorphic minerals are superimposed (Almklovdalen garnet peridotite, WGR)

2. **Intermediate Pressure (IP) massifs**: when the rocks is mainly equilibrated in the stability field of spinel or plagioclase but it is possible to recognize some high pressure relics. (examples: Beni-Bousera, Morocco and Ronda, Spain). They often preserve melt related structures.
3. **Low Pressure (LP) massifs**: mantle rocks exhumed at very shallow levels or forming sea-floor in early extensional stages. Strongly re-crystallized in the stability field of plagioclase (Examples: Lanzo massif, Northern Italy)
4. **Subduction type**

   Peridotite characterized by early stage of low temperature serpentinization (group LP orogenic massifs or crustal peridotites) in the crust, followed by the superimposition of prograde metamorphism at HP, developed during the subduction cycle.

<table>
<tr><td colspan="2">Crustal origin</td><td colspan="2">CRUSTAL PERIDOTITES</td></tr>
<tr><td rowspan="3">Mantle origin</td><td rowspan="2">Sub-continental Affinity</td><td rowspan="2">OROGENIC PERIDOTITE MASSIFS
(Root zone/Alpine type)</td><td>HP/UHP OROGENIC PERIDOTITES</td></tr>
<tr><td>IP OROGENIC PERIDOTITES
LP OROGENIC PERIDOTITES</td></tr>
<tr><td>Sub-oceanic Affinity</td><td colspan="2">OPHIOLITIC MANTLE ROCKS</td></tr>
</table>

Table 1 Peridotite classification based on provenance (Crustal vs Mantle) with distinction between sub-continental (SCLM) and sub-oceanic mantle provenance.

3.2.3 Ophiolitic peridotites

Ophiolites represent fragments of oceanic lithosphere obducted onto continental or oceanic crust. A global agreement amongst geologist concerning the definition of the term "Ophiolite" was reached during the Penrose Conference (Anonymous, 1972). A complete ophiolitic sequence is, from the bottom to the top, composed by ultramafic complex (depleted + fertile mantle), gabbroic complex (cumulate + non cumulate + sheeted dykes) and basalt pillow lavas covered by oceanic sediments (Fig.7). Complete sequences are typical in relatively fast spreading oceanic ridges. However, in magma-poor ridges the sequence above described is often incomplete and is typical the occurrence of sedimentary covers lying on top of strongly serpentinized peridotites (Muntener and Manatschal, 2004). Noteworthy to mention is the absence of garnet bearing assemblage for the SOLM peridotites. In fact they are generally completely re-equilibrated in the spinel or plagioclase stability field.

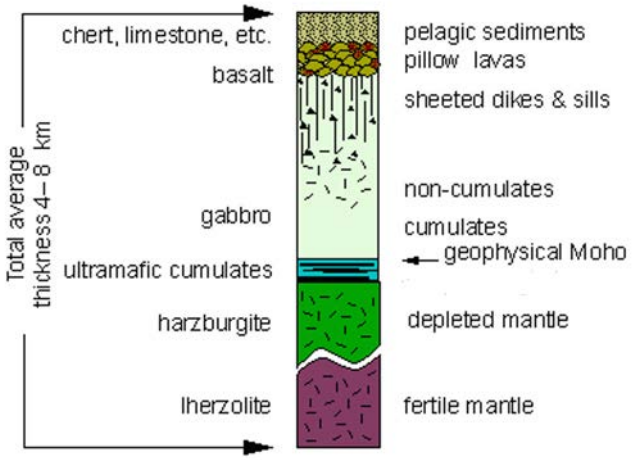

Figure 7: Idealized cross section of an ophiolite sequence comprising ultramafic rocks, gabbroic complex, basalts and sedimentary covers (Modified after Coleman, 1977).

3.3 Mechanism of crustal emplacement

3.3.1 Subduction/eduction

The discovery of high pressure minerals, as diamond and coesite, within eclogite bearing terranes is a further proof that continental crust is subducted deeply in the mantle, at depth greater than 100 Km (Brueckner, 1998). In addition, preservation of HP/UHP lenses is interpreted to be due to a relatively fast eduction, which did not kinetically allowed a complete re-equilibration at lower PT conditions. One of the mainstream models able to explain UHP and fast eduction is named "dunk" tectonics (Brueckner & Van Roermund, 2004) This model is based on the idea that during subduction the "unsubductable", buoyant continental lithosphere is pulled after the down-going oceanic lithosphere (Fig.8A). The greater density of the oceanic crust may result in the rupture, or "slab break off (Wortel and Spakman, 2000) of the down-going plate (Fig.8B). As a result, the subduction is effectively stopped and the crustal rocks can return to the surface through delamination from the underlying mantle (Brueckner & Van Roermund, 2004). Final eduction juxtapose HP/UHP units within LP units along main shear zones, likely to be the same planes active during subduction (Fig.8C).

The dunk tectonics model can easily explain the coeval presence of ultramafites and HP/UHP eclogitic lenses because the subducted slab is in a favourable geometrical position for crustal emplacement of peridotites. In fact dense mantle rocks are on top of less dense crustal rocks, along a boundary affected by active shear as the crust subducts and subsequently educted back move back to the surface. In this geodynamic setting, ultramafic bodies can be transferred to the continental crust either by brittle transfer during shearing or by ductile sinking caused by density inversion, named "reverse diapirism" (Brueckner, 1998). The chemistry of emplaced peridotites always shows features due to partial melting, varying from slightly depleted lherzolite to strongly depleted harzburgites and/or dunites (Brueckner & Van Roermund, 2004). The initial mantle texture starts to deform since the emplacement and shows an extensive prograde (if emplaced during subduction) or retrograde (if emplaced during eduction) overprint.

During subduction spinel or garnet peridotites can be introduced into the sibducted continental crust only from the hangingwall side of the subducted system (i.e. Mantle Wedge; Fig.8B). Instead during eduction part of the deformation is localized also in the footwall, hence the possibility of spinel peridotites emplacement either from the footwall and hanginwall (Fig.8B). Interesting to note that exhumation occurs along previous descending paths and provokes the juxtaposition of HP/UHP rocks within lower pressure rock (Fig.8C).

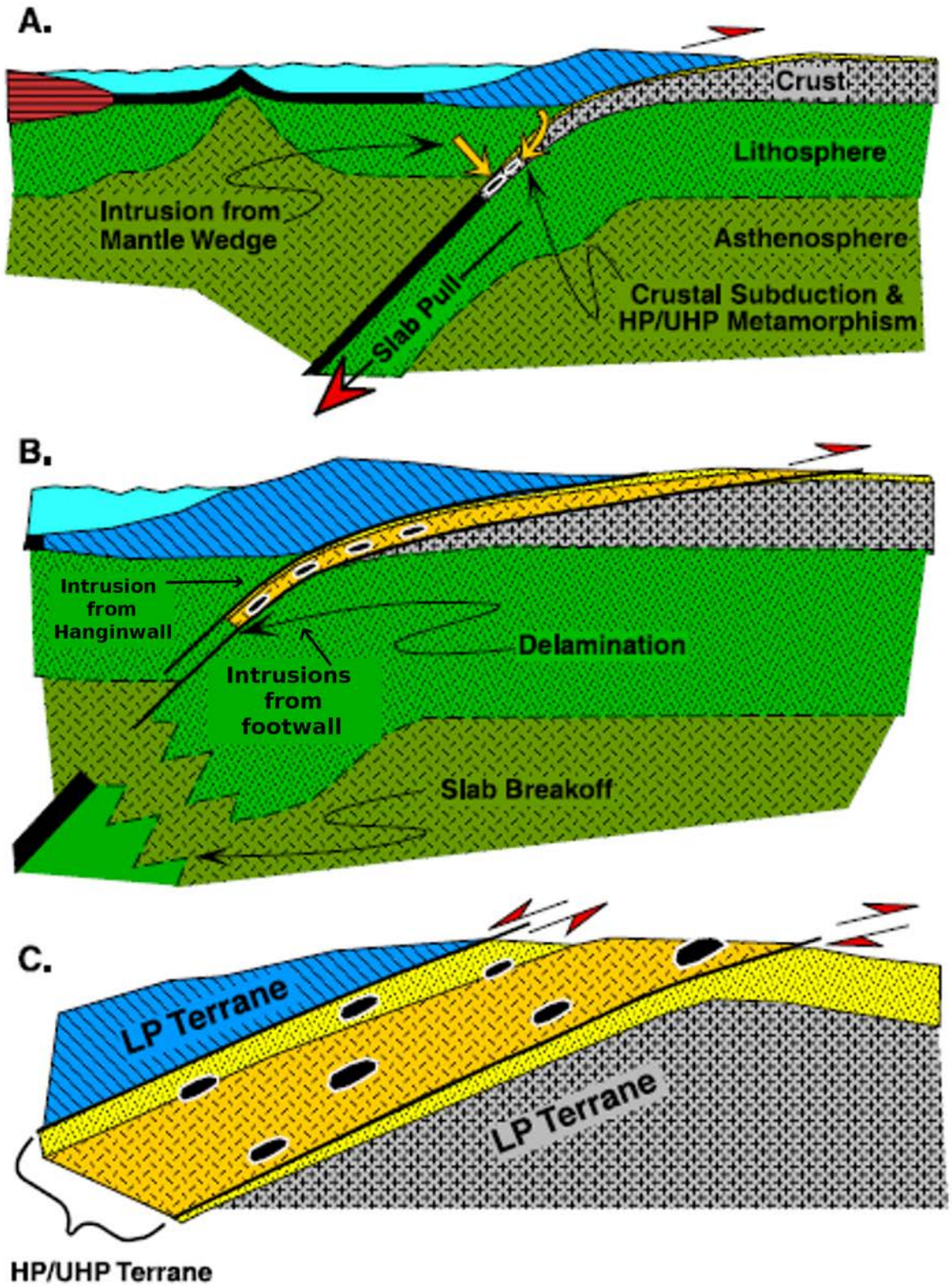

Figure 8: Simplified cartoon illustrating "dunk tectonics" model with characteristic subduction/eduction cycle for an arc-continent collision. A) Subduction of continental crust into the mantle, metamorphosed under HP/UHP conditions and invaded by peridotite fragments from the mantle wedge (hanginwall); B)Consequent slab break off of the oceanic plate cause buoyant, rapid exhumation of remaining slab (continental rock association). During retrograde path, mantle fragments might emplace either from hanginwall and footwall; C) Eduction/Exhumation occur along previous descending path and provoke the juxtaposition of HP/UHP rocks within lower pressure rock. Peridotite bodies are shown as black lenses. Hangingwall =Mantle Wedge (Modified after Brueckner & Van Roermund, 2004)

3.3.2 Obduction

Plate tectonic theory involves the idea that oceanic crust and its lithosphere are mainly subducted in oceanic trenches (Dewey, 1976). Thus, great interest is generated around the mechanism responsible for tectonic emplacement of ophiolites in orogenic belts, first referred as "obduction" by Coleman (1971). Obducted ophiolite complexes vary greatly in size, occurring in a wide variety of tectonic positions within orogenic belts, but they always overlie less dense continental rocks. Therefore one of the most complex and intriguing problem in plate tectonics, is to explain how ophiolites with densities of 3.0-3.3 g/cm3 are elevated from their natural position beneath the ocean floor and how they rode over continental crust, with densities in the order of 2.7-2.8 g/cm3.

For this research, the mechanism of ophiolite emplacement will be briefly analysed in a well studied arc-continent collision in the South-West Pacific (Fig.9)(Whattam, 2009). Similarity can be drawn between the current geographic setting of the eastern Australian margin and the thinned margin of the Baltic shield in the Cambrian-Ordovician (Chapter 2.5). The collision of an intra-oceanic arc with a continental margin or a rifted continental fragment results in the "obduction" of nappes composed of complete ophiolite sequences or solitary ophiolite fragments. Such ophiolites are defined as supra-subduction zone (SSZ) and are usually emplaced within ~10 Ma since their formation via arc-continent collision (Whattam, 2009). During the subduction process, the buoyant, 'unsubductable' continental lithosphere initially follows the oceanic lithosphere into the subduction zone (Fig.9a). After slab break off a subduction polarity flip occurs, catalysing ophiolite obduction during the final crustal shortening (Fig.9b). Such collision can be interpreted as a micro-orogeny, with an initial subduction, followed by ophiolite obduction and the final eduction (Fig.9c). In contrast to continent-continent collision, arc-continent collisions are inherently short-lived (~20 Ma) and can not reach great depth because of subduction impedance of buoyant continental lithosphere coupled with subduction polarity flip that follows (Whattam, 2009).

The possibility to preserve complete ophiolitic sequences or just ultramafic isolated bodies is determined by the interplaying of many factors, as plate tectonic configuration, rate of convergence, erosion etc... When a thick sequence is preserved (i.e Oman), it is possible to recognize a metamorphic sole at the interface between ophiolite and continental rocks. Such layer is generally metamorphosed under granulite facies for the first 20-30 meters and in amphibolite facies for the next 200-300.

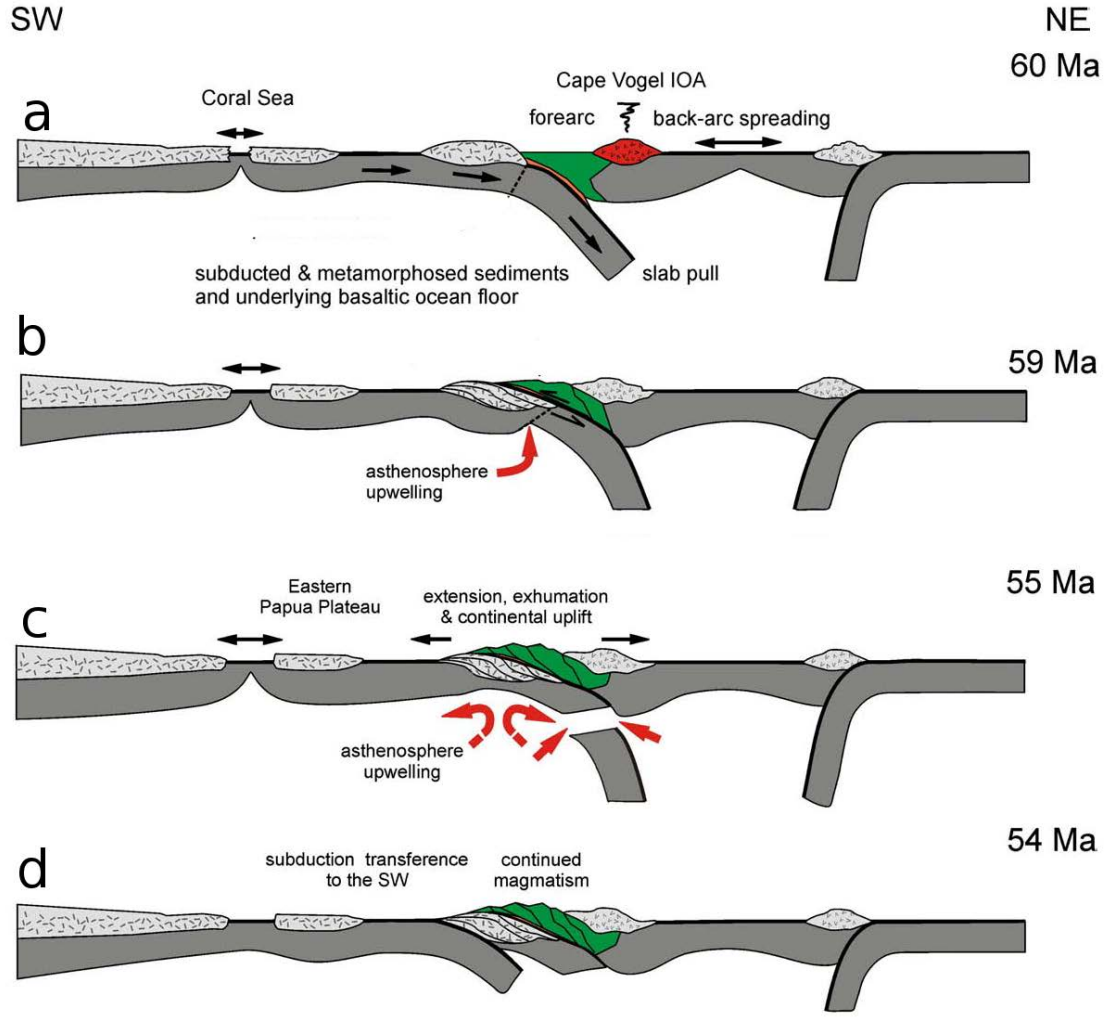

Figure 9: Tectonic reconstruction of obduction of SOLM in the region to the NE of the Papuan Peninsula. The model must be regarded only as representative of obduction of ultramafic rocks in continental terranes and must not be correlated with the tectonic setting in which was extrapolated. A) During subduction process, the buoyant, 'unsubductable' continental lithosphere initially follow the oceanic lithosphere into the subduction zone; B) After slab break off a subduction polarity flip occur, catalysing ophiolites obduction during the final crustal shortening C) Immediate consequence of slab break off is the establishment of an extensional state of stress which cause fast (~ 10 Ma) exhumation of the new formed complex; D) After exhumation, the subduction is transferred to next suitable area. Abbreviations: IOA=intra-oceanic arc; PP BAB=Papuan Peninsula back arc basin; RAF=rifted Australian fragment. (Modified after (Whattam, 2009)

4 METHODS

Field sampling

Seven samples from different layers of the compositionally layered KSP were selected for analysis on bulk rock composition (XRF analysis) and mineral chemistry (EMP). The locations , lithology and number of samples of samples that were gathered directly from the outcrop are depicted in Appendix 1.

Optical microscopy

Thin sections of each hand sample were made for investigations using optical and electron optical techniques. Samples were cut where microstructures in the hand-samples showed the least retrogression.

Thin-sections for olivine fabric analysis were cut parallel to the lineation and perpendicular to the foliation. CPO of olivine was measured for monomineralic dunites using a Universal Stage (U-stage) applied to an optical microscope. The U-stage, with its five axes of rotation, allows precise measurements (+/- 5° mechanical error) of crystallographic directions alfa (α), beta (β) and gamma(γ) in olivine.

Electron microprobe analysis (EMP)

Electron Microprobe (EMP) analyses were performed using a JEOL JXA-1800 Superprobe equipped with an energy dispersive detection system and five wavelength dispersive spectrometers (WDS) at Utrecht University. Carbon coated thin sections were initially analysed with Energy Dispersive Spectrometry (EDS) for quick identification of minerals and Wavelength Dispersal Spectrometry (WDS) for high resolution mineral chemical analyses.

X-Ray Fluorescence (XRF)

XRF analyses have been performed on representative samples. Small fragments were initially crushed with an hammer mortar and pestle and, at a later stage, in a automatic crusher. Resulting powder (< 73 um) was used on a sequential ARL 9400 WD-XRF in order to obtain representative bulk rock compositions for both dunite and harzburgite layers.

Theriak Domino

Theriak Domino is a programs that thermodynamically calculates phase diagrams for specific bulk rock composition used an input data. The software uses Gibbs Free Energy minimization (De Capitani and Petrakakis, 2010*)* to compute pseudosections under the assumption of chemical equilibrium throughout a certain bulk rock volume.

Thin section decoration

Dislocations are too small to be observable in a thin section but the staining method of Kohlstedt(1976) provide an alternative possibility. In fact in olivine crystals it is possible to decorate dislocations with iron oxides. Dunite sample has been warmed up at the temperature of 1000°C for a short period of time, in which oxygen diffuses rapidly along dislocations, oxidizing some of the iron present within olivine lattice. At this point, dislocation sub-structures are revealed in oxidized lines in the optical microscope.

5 KITTELFJÄLL SPINEL PERIDOTITE

5.1 Early study and basic definitions

5.1.1 Location and previous study

The Kittelfjäll spinel bearing peridotite (KSP is located geographically in the central part of the Västerbotten province (Sweden), more precisely in the Northern part of the Marsfjäll area (GPS 33W 05232991 7234141). The KSP is one of the largest in the nappe complex with its 24 km^2 of inferred outcrop (Calon, 1979). Unfortunately, due to bad exposure, only a small fraction around the village of Kittelfjäll is available for a geological survey (Appendix 1). Best outcrops are located in the hill of Lebnjesnuone, in the gullies above the city centre of Kittelfjäll and in the valley of Vojman. In the following chapter a brief summary is presented of the lithological variability, structures and metamorphism affecting KSP. For more detailed information, the reader is referred to the work of Calon (1979).

5.1.2 Lithologies

The body is mainly composed of dunite and harzburgite (reciprocal ratio 2:3), with minor but widespread occurrence of chromitites and orthopyroxenites. The bulk rock composition is monotonously uniform throughout the body (Calon, 1979) for either dunite and harzburgite. Serpentinites are present only at the rim of the body. Rare carbonate-bearing ultramafic rocks formed by CO_2 metasomatism are present at the edges of the KSP.

Dunite

In the central part of the body the dunites are well preserved and almost entirely composed of olivine with minor (5-10%) orthopyroxene, tremolite and chromite. At the margin of the body, dunites are enriched in tremolite, chlorite and talc/antigorite.

Harzburgite

In the inner areas of the peridotite, harzburgite layers are characterized mainly by olivine and orthopyroxene (10-30% Enstatite) with minor tremolite, chlorite and sparse chromite. Towards the rim tremolite and chorite contents increase and orthopyroxene is consistently replaced by talc and/or serpentine (bastite).

Serpentinite

Massive and highly foliated. Present at the rim of the body or along major fractures.

Chromitite

Chromitite occurs preferentially in dunite layers with a wide variety of shapes. They generally occur as boudinated aggregates less than 30 cm thick and one meter long.

Orthopyroxenite

They occur exclusively within harzburgites as thin vein (up to 10 cm) containing subordinate olivine, reddish-brown chrome spinel and tremolite (Calon, 1979). In the outer part of the body the metamorphic overprint produces an assemblage of talc and serpentine.

5.1.3 Structures

S_0 Compositional layering

KSP exhibits a well developed compositional layering consisting of alternating dunite and harzburgite layers. Transition from one layer to another, is mainly due to a variation in the volume ratio of olivine/orthopyroxene. Thickness of individual layers is highly variable, from few millimetres to several metres, and is constant along the strike in most of the outcrops. A regular pattern of repetition of the layered sequence is not present. The compositional layering layering is parallel to the earliest tectonic fabric (Pre-D1) and to chromitite layers.

Pre-D1

In dunite a strong planar fabric is highlighted by the preferential shape orientation of coarse olivine porphyroclasts, with grain sizes ranging from few millimetres up to 20 cm. The grains are strongly elongated with reciprocal proportions of 50:1 (length/thickness) and define a foliation (Pre-S1) at high angles to the compositional layering S_0. Olivine porphyroclasts often contain an internal foliation (S_i) outlined by a preferential orientation of chromite grains, which runs most of the time parallel to the compositional layering but in rare case a deviation up to 30° is observed (Calon, 1979).

D1

Rare isoclinal, intrafolial and rootless folds (F1) have been found, mostly in chromitite and pyroxenite layers (Calon, 1979). The shape of folds is defined by thickened hinges and strongly stretched limbs, often presenting pinch ad swell structures. F1folds are associated with a distinct axial plane foliation (S1) in which orthopyroxene and olivine porphyroclasts are weakly oriented (L1). In folded chromitites, the fabric in the hinge area is characterized by anhedral, tabular shaped single grains of chromite. D1 structures are associated to a fine grained matrix composed by strain free olivine. This microstructure is termed the "olivine foam microstructure" and its morphological characteristics and origin are discussed in detail in chapter 5.3. Such fabric develops throughout the body and result massive and non-foliated, but in rare cases a preferential grain orientation (L1) is developed. Towards the rim, a strong overprint makes it difficult to recognize D1 related structures and fabric due to subsequent overprint.

D2

D2 structures are grouped in two different sets of structures that vary in style and distribution:

- Folds (F2) with axial plane foliation (S2)

  D2 folds are developed in the whole body and they affect previous D1 structures. Mesoscopic folds (F2) range from parallel to similar with open to tight limbs but never isoclinal. The development of axial plane foliations (S2) and lineations (L1) is markedly influenced by the distance from the rim of the KSP body and by the lithology. In fact in the interior part of the body, dunites are affected by a S2 foliation developed as regularly spaced (2-5 cm) "fractures". In the external zone, S2 develops as a macroscopic schistosity defined by an anastomosing network of finer grained olivine, stable with chlorite, antigorite and tremolite.

- Shear zones at various scale

  D2 structures are developed from macroscopic to mesoscopic scale throughout the peridotite body and clearly overprint D2 fold structures. Macroscopic shear belts are exposed in the northern and southern edge of the KSP (Appendix 1). Such zones are

characterized by the incremental development of a very fine-grained matrix composed by re-crystallised olivine This fabric is termed olivine "mortar structure" (Calon, 1979) and its morphological characteristics and origin are discussed in detail in chapter 5.3.

D3

D3 structures predominate in the outer margin of the peridotite and are defined by folds (F3) and related axial plane foliation (S3). Deformation is mainly related to the incipient development of crenulation cleavage (parallel to axial plane F3) in a 30 m thick zone (Fig.10), situated along the rim of the body. D3 folds hinges vary in style depending on the lithology in which they develop. In fact dunite is characterized by the occurrence of parallel folds (F3) with rounded hinges, whereas chevron type hinges more characteristic in harzburgite layers where there was a better developed S2. The intensity of the D3 deformation strongly decreases towards the inner zones of the body

5.2.3 Metamorphism

M1

A stable M1 assemblage is inferred from a study of a few coarse grained olivine relics within the olivine foam microstructure (D2). Highly strained porphyroclasts of olivine and orthopyroxene represent the oldest elements recognizable. Inclusions of Chromite within olivine porphyroclasts display rounded grain corners and straight grain boundaries.

Stable M1 assemblage inferred: Olivine + Orthopyroxene + Chromite

M2

During development of D2, an M2 stable mineral paragenesis is formed by tremolite (amphibole) grains in chemical equilibrium with recrystallized olivine and orthopyroxene, whereas tabular chromite grains are generally surrounded by idioblastic chlorite. The assemblage is well preserved in the core of the body and only the orthopyroxene is partially replaced by talc when D2 is developed.

Stable M2 assemblage is Olivine + Orthopyroxene + Tremolite + Chlorite/Chromite

M3

M3 paragenesis is defined by contemporaneous stability of olivine, chlorite, tremolite, and talc/antigorite. This assemblage is developed with both D2 folds and M3 shear zones. The metamorphic gradient varies from core to rim and it has been subdivided in three distinct metamorphic areas (Fig.10):

Enstatite zone

Represent the interior part of the body where the M2 assemblage is still preserved. Enstatite is not stable during M3 because is always replaced by talc.

Talc zone

50-100 m wide zone along the margin of the body (Fig.10) in which all orthopyroxene are replaced by talc.

Antigorite zone

An area of less than 50 m, along the external contact of the body, in which antigorite is the dominant mineral in association with minor tremolite and chlorite.

Stable M3 assemblage is: Olivine + Talc/Antigorite + Tremolite + Chlorite

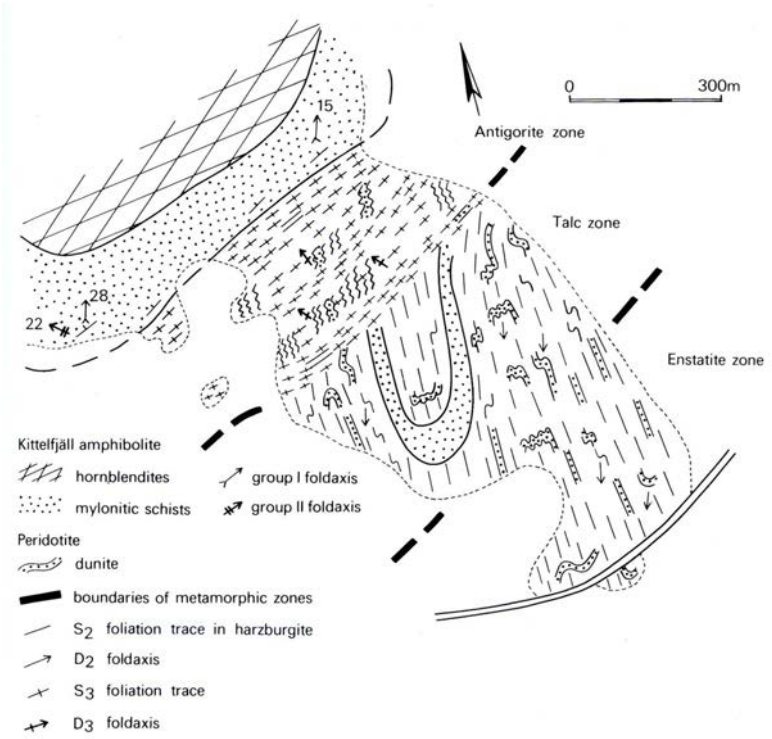

Figure 10: Geological map of Lebnjesnuone outcrop showing relationship between D2 and D3 at the rim of the peridotite body (after Calon, 1979)

M4

M4 mineral assemblage generate exclusively where D3 folds forms. Generally, most of the mineral, with olivine above all, are replaced by antigorite. Tremolite is always replaced by aggregates of asbetiform antigorite.

The stable M4 assemblage is: Olivine + Antigorite + Chlorite

5.1.5 Metamorphism-deformation interaction

The structural and metamorphic evolution of the body has been subdivided in four groups on the basis of overprinting and stable mineral assemblages in relation to main structures (Calon, 1979). Every deformation event is related to different and specific metamorphic conditions summarized in Table 2, except for D2 structures. In fact, even though D2 shear structures clearly overprint D2 fold structures, they must be considered as one single progressive deformation event because the stable mineral paragenesis does not vary. In fact stable mineral assemblage changes (antigorite to talc stability) depends only on the structural position within the KSP (Fig.10).

Structural group	Structures	Metamorphism	Stable paragenesis
pre-D1		M1	Ol + Opx + Chr
D1	Isoclinal Folds	M2	Ol + Opx +Tr+ Chl/Chr
D2	Folds/Shear zone	M3	Ol + Tc/Atg + Tr + Chl
D3	Crenulation cleavage	M4	Ol + Opx + Chr

Table 2: Summary of the metamorphic-structural evolution of the KSP body highlight by the relationship between structures and stable metamorphic mineral assemblages.

5.2 Bulk rock and mineral chemistry

5.2.1 Mineral chemistry

5.2.1.1 EMP analysis

Major elements mineral compositions were determined by EMPA at the Utrecht University using a JEOL JXA8600N super probe, equipped with five wavelength dispersive spectrometers, an acceleration voltage of 15 kV and a beam current of 20 nA. Fe3+ is calculated based on charge balance for anhydrous minerals (olivine, orthopyroxene, spinel) and with specific techniques for hydrous minerals like amphibole and chlorite. The procedure for classifying rock-forming chlorites of Zane and Weiss (1988) has been adopted for microprobe data iron balancing. The formula is based on 28 oxygen and all iron is considered bivalent. For amphiboles, cation calculations is on the basis of an anhydrous formula with 23 oxygen rather than 24 (Leake et al, 1997). The ideal cation-sums in the amphibole formulae are not fixed, but can vary between 15 and 16 cations (per 23 oxygen). Fe3+/Fe2+ ratio can be inferred adjusting the sum (Si + Al + Cr + Ti + Fe + Mg + Mn) to 13 (Leake et al, 1997).

5.2.1.2 Results

Olivine

The KSP is characterized by the presence of various textural types of olivine, namely olivine M1 porphyroclasts, olivine M2 foam microstructure and olivine M3 microstructure. EMPA of major oxides reveal an homogeneous composition for olivine M1 porphyroclast core to rim (Appendix 2). No sensible major element oxides differences observed with respect to olivine M2 and M3 grains (Table 3-4; Appendix 2). All types of olivine are defined by a very high Mg# (>91) and a constant NiO content (0,34-0,45 wt%) independent of texture (Fig.11; Table 3). Olivine Mg# is strongly correlated to the rock type, with a range of 92,5-93,6 in dunite and 91,2-92,5 in harzburgite (Fig.11).

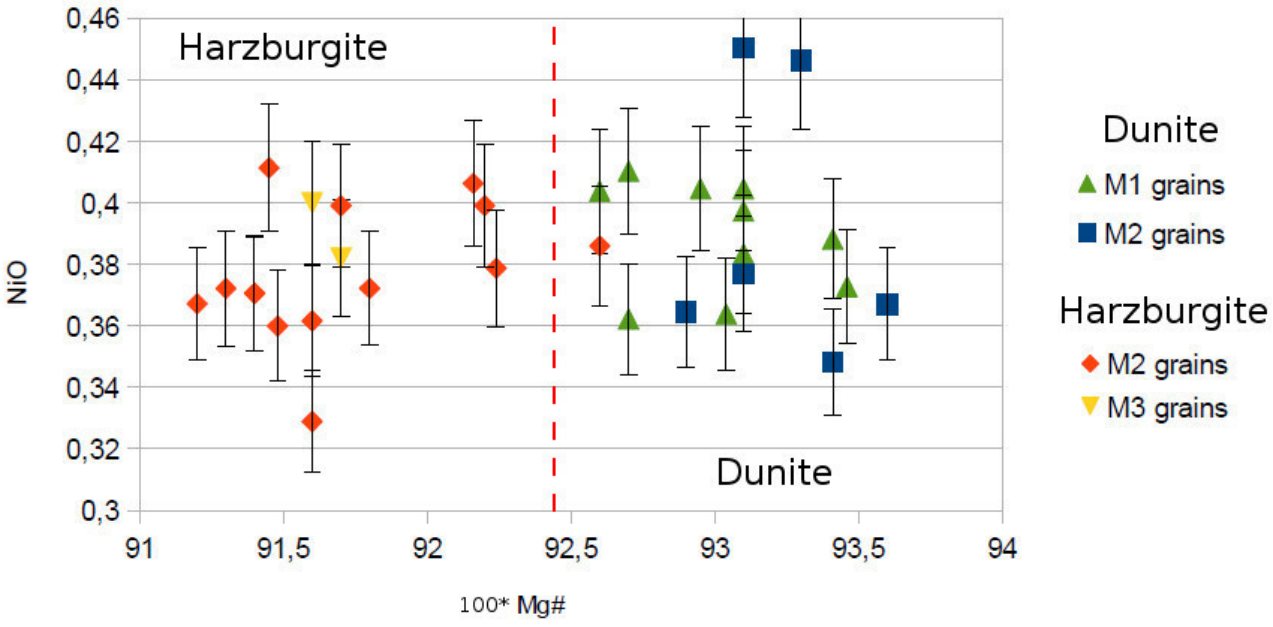

Figure 11: NiO vs (100*)Mg# for olivine in different textures and rock types: olivine M1 porphyroclasts, olivine M2 foam microstructure M2 and olivine M3 Mortar structure. A clear distinction can be seen between 100*Mg# for Dunite (92,5-93,5) and Harzburgite layers (91,2-92,5). Vertical bar represent the margin of error (+/- 5%) of the EMPA for trace elements like NiO.

5.2 Bulk rock and mineral chemistry

Lithology	DUNITE											
Sample	K3											
Type	porphyroclast (M1)			foam microstructure (M2)			Porphyroclast inclusion			Eq. with Foam structure		
Mineral	Olivine			Olivine			Chromite			Chromite		
SiO2	41,31	41,10	41,44	41,25	41,29	41,18	0,04	0,01	0,01	0,01	0,07	0,00
TiO2	-	-	-	-	-	-	0,07	0,11	0,13	0,06	0,07	0,15
Al2O3	-	-	-	-	-	-	1,78	4,17	4,76	12,44	13,17	10,05
Cr2O3	0,00	0,00	-	0,01	-	-	62,30	58,71	56,42	52,81	53,41	51,36
FeO	7,43	7,59	7,18	7,50	7,33	7,40	28,03	28,37	31,22	25,33	23,97	30,19
MnO	0,10	0,11	0,10	0,07	0,09	0,08	1,09	1,05	1,10	0,76	0,75	0,79
MgO	51,59	51,65	51,84	51,75	51,64	51,53	4,54	5,51	5,07	8,10	8,37	6,61
CaO	-	-	0,01	-	-	-	-	-	-	-	-	-
Na2O	-	-	-	-	-	-	-	-	-	-	-	-
K2O	-	-	-	-	-	-	-	-	-	-	-	-
NiO	0,37	0,39	0,40	0,35	0,37	0,38	0,05	0,03	0,06	0,02	-	0,08
TOTAL	100,80	100,84	100,96	100,93	100,72	100,57	97,91	97,96	98,77	99,53	99,82	99,24
100*Mg#	93,46	93,41	93,10	93,41	93,6	93,1	95,91	90,42	88,83	74,00	73,11	77,40
100*Cr#	-	-	-	-	-	-	25,25	30,51	27,58	41,00	41,00	34,00

Table 3: Representative major elements mineral compositions in dunite (Sample K3).

Lithology	HARZBURGITE											
Sample	K9											
Type	porphyroclast (M1)		Foam (M2)		Foam (M2)		Foam (M2)		Foam (M2)		Sp incl.	
Mineral	opx1		opx2		olivine		chromite		tremolite		chlorite	
SiO2	56,10	56,63	56,55	56,56	40,70	41,03	0,00	0,00	57,36	57,65	31,80	31,55
TiO2	0,03	0,01	-	0,01	-	-	0,06	0,05	0,02	-	0,01	0,04
Al2O3	1,97	1,90	0,89	1,22	-	-	10,14	11,40	0,79	0,13	12,50	13,59
Cr2O3	1,31	0,79	0,25	0,64	0,01	0,01	51,67	51,03	0,33	0,06	3,66	4,01
FeO	6,37	6,32	6,40	6,36	8,97	8,81	28,60	26,30	1,84	1,73	2,61	2,82
MnO	0,14	0,14	0,13	0,15	0,11	0,10	0,92	0,92	0,07	0,06	0,03	0,06
MgO	34,34	34,60	34,69	34,60	49,74	50,47	6,94	7,48	23,82	23,83	33,53	33,42
CaO	0,36	0,32	0,21	0,14	-	-	-	-	12,02	12,71	0,00	0,02
Na2O	0,04	0,04	0,01	0,03	-	-	-	-	0,86	0,09	0,01	0,01
K2O	-	-	-	-	-	-	0,04	0,05	0,04	-	-	-
NiO	0,10	0,09	0,05	0,07	0,37	0,38	-	-	-	-	-	-
TOTAL	100,76	100,85	99,19	99,77	99,90	100,79	98,35	97,23	97,15	96,25	84,16	85,52
100*Mg#	92,20	92,00	91,80	92,02	91,40	91,70	77,36	75,00	99,58	97,85	98,96	99,96
100*Cr#	-	-	-	-	-	-	36,43	39,64	17,24	21,43	16,56	11,12

Table 4: Table 1: Representative major elements mineral compositions in Harzburgite (Sample K9).

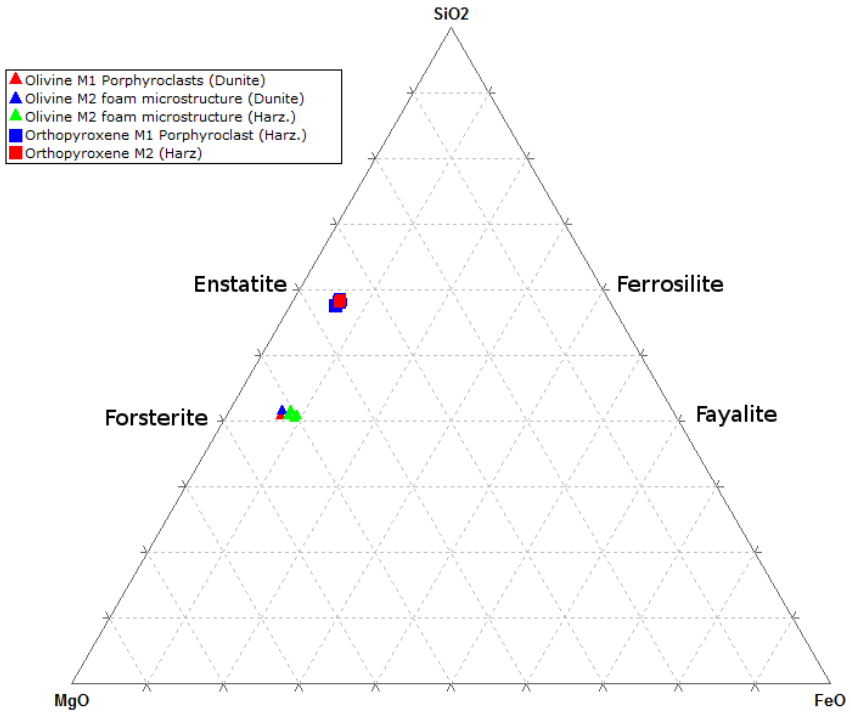

Figure 12: Triangular MgO-SiO2-FeO diagram indicating olivine (Forsterite-Fayalite) and orthopyroxene (Enstatite-Ferrosilite) composition in different microstructure and lithology.

Orthopyroxene

Representative mineral compositions of Opx are given in Table 4. Harzburgite is characterized by two different orthopyroxene textures: an M1 porphyroclasts (Opx1; 4-20 mm) and M2 neoblasts (Opx2; 200-400 um) in equilibrium with olivine M2 foam structure and amphibole. Both orthopyroxenes are Enstatite in composition (Fig.12) with high 100*Mg# (91,2-92,5) (Fig.11). Mg# of opx and olivine shows a positive correlation (Table 3-4).

The Al_2O_3 content is not constant over a linescan in the orthopyroxene M1 porphyroclasts (Opx1) in harzburgite, ranging between 0,89 and 2,2 wt% (Appendix 3). The fluctuating Al_2O_3 trend (Appendix 3) is most likely related to the incipient presence of exsolution lamellae throughout the orthopyroxene porphyroclast (Fig.13B). The Cr_2O_3 and CaO content are relatively high (respectively 0,79-1,31 wt%;0,19-0,40 wt%) and constant on a line profile (Appendix 3; Table 4)

There are generally positive correlations between grain size and Al_2O_3 - Cr_2O_3 contents of the orthopyroxene, the coarser the grain size, the higher the contents of these components (Table 4). In fact the neoblastic Opx in the matrix (Opx2) has lower Al, Cr and Ca contents than the porphyroclasts (Opx1) in the harzburgite (i.e. Al_2O_3 0,89-1,88 wt %; Cr_2O_3, 0,22-0,64 wt %; CaO 0,19-0,22 wt%). Interesting to note is the total absence of exsolution lamellae in M2 orthopyroxene grains (Fig.13)

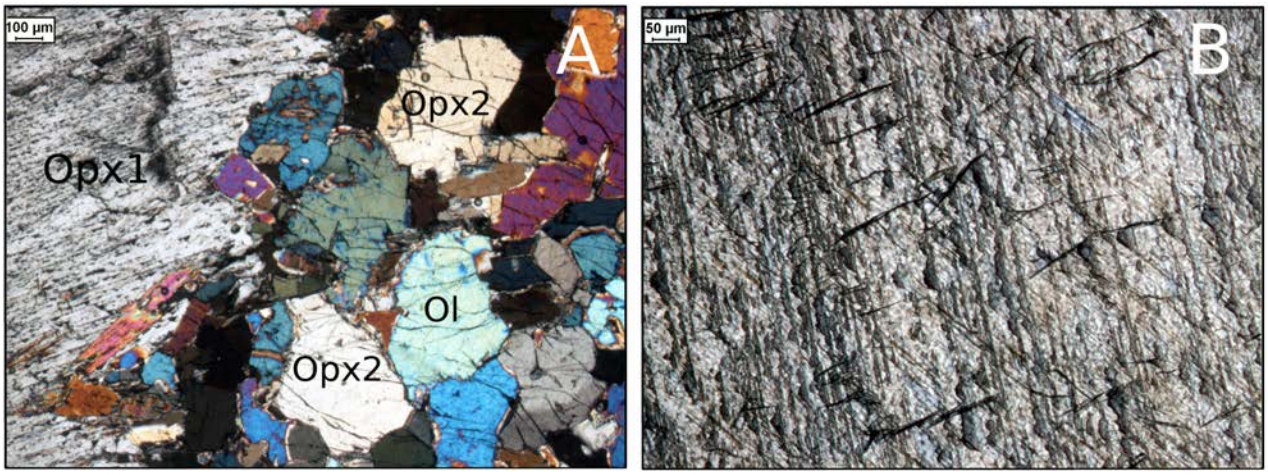

Figure 13: Optical microscope (XPL) micrographs (K9): A) Grain size differences between Opx1 and Opx2. Note the absence of exsolution lamellae in the M2 orthopyroxene neoblasts (Opx2); B) M1 Orthopyroxene porphyroclast is characterized by the incipient development of exsolution lamellae.

Spinel

Representative mineral analyses of spinel are given in Table 3-4 and the compositional variability is illustrated in Fig.14. On the basis of Cr# and Mg#, all measured spinel are defined as chromites (Fig.14). Chromite chemical composition is strongly influenced by textural position and rock type (Table 3-4). In dunite, chromites inclusions (50-300 um) within olivine porphyroclasts (M1) show preferential alignment (S_i) and in few cases are in close "association" with chlorite (Fig.15A-B). Composition is fairly constant, with an extremely high Cr# (89,3-96) and low Mg# (21-28,3) (Fig.14; Table 3-4). Chromite grains (50-300 um) in equilibrium with olivine in the M2 olivine foam microstructure have lower Cr# (72-79) and higher Mg# (34-43) (Fig.14; Table 3-4).
Harzburgite layers are characterized by larger chromite grains up to 1mm (Fig.15A) that have similar compositions to chromite grains in dunite layers. These chromite grains are characterized by Cr# 76-81 and Mg# 31-33 (Fig.14). Spinel is always associated to chlorite, either along oriented lamellae or randomly distributed inclusions (Fig.15). In rare cases the cubic chromite shape is still preserved despite the rim being destabilized by new chlorite growth (Fig.15C).

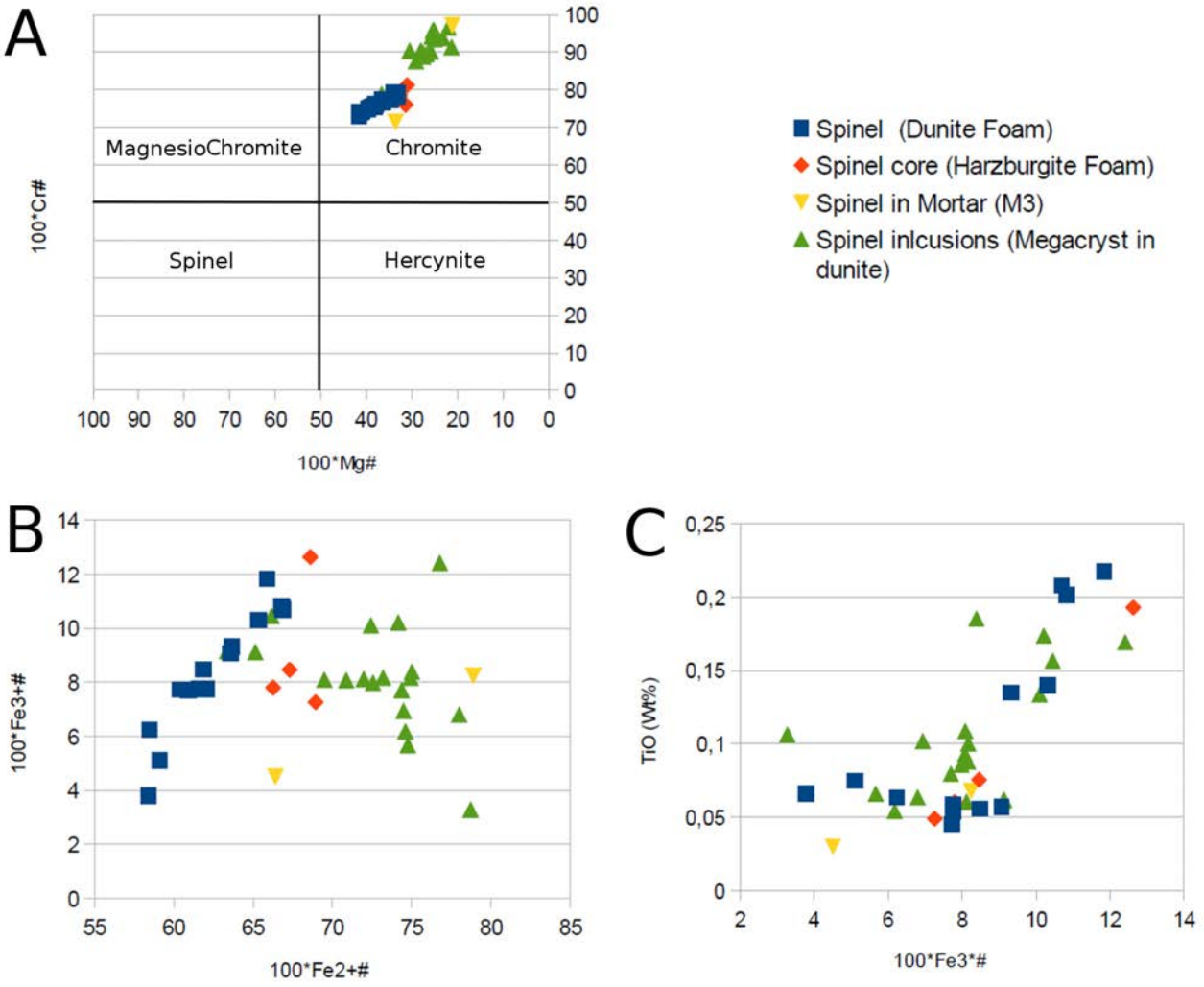

Figure 14: EMPA spinel composition plotted in: A) Cr# vs Mg# diagram + spinel classification. All spinels are chromite with high 100*Cr# (>70) and low 100*Mg# (<40); B) Diagram showing 100*Fe^{3+}# (3-14) vs Fe^{2+}# (60-80) relationships; C) TiO wt% vs Fe3+# diagram displaying the independence of TiO from texture and lithology.

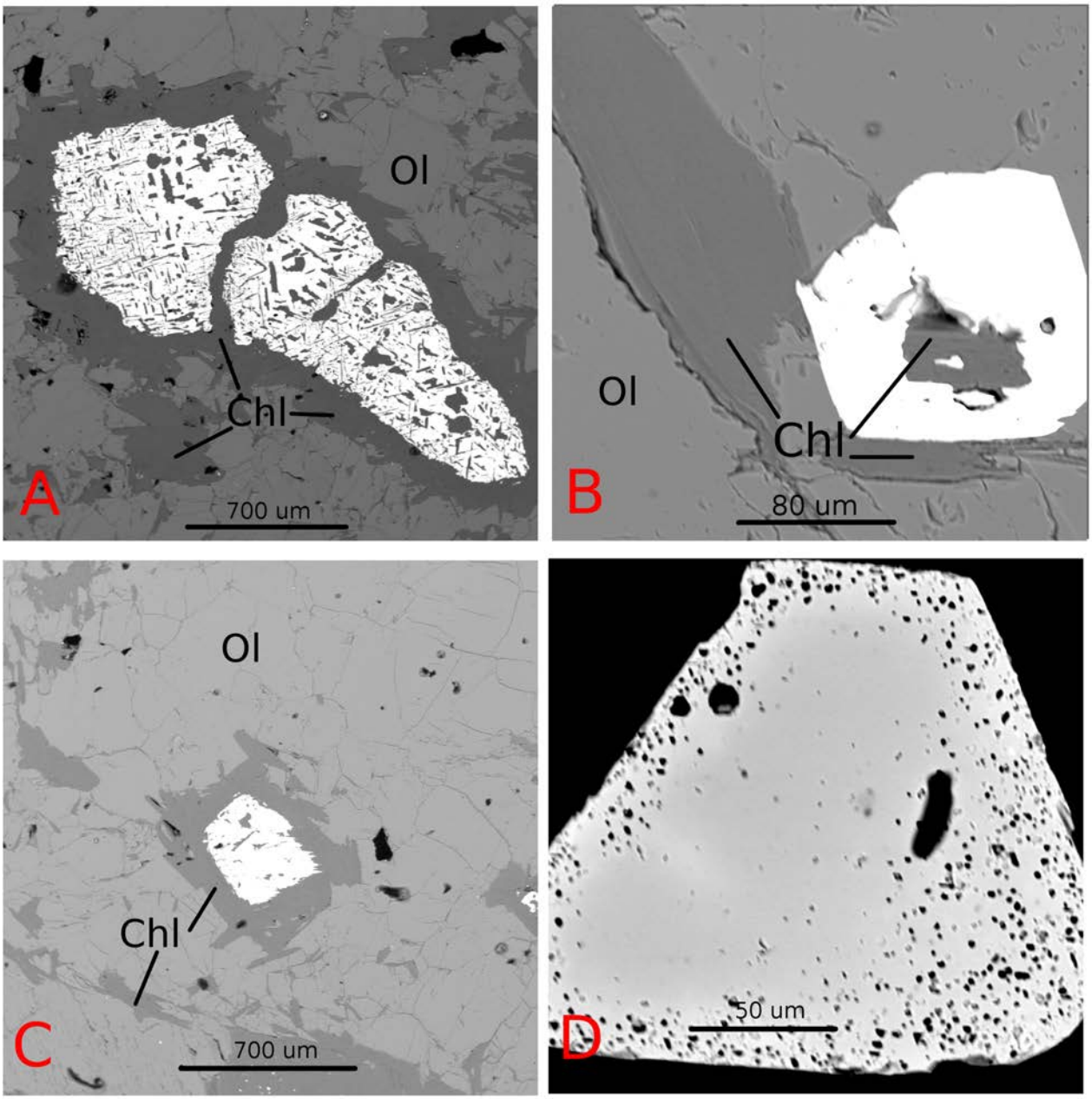

Figure 15: Electron microprobe micrographs of representative chromite grains in sample K3 (B-D) and K9(A-C): A) Microstructure of a strongly retrograde chromite grain with incipient formation of secondary chlorite along boundaries and well oriented lamellae inside chromite grain; B) Euhedral spinel inclusion in olivine porphyroclast (M1) characterized by extremely high Cr# (95,91) and low Mg# (25,25) (Table 4); C) Replacement of spinel by chlorite. To note the preservation of the original chromite grain cubic shape; D) Spinel in equilibrium with olivine M2 olivine foam microstructure is characterized by uniform composition, with Cr# (74) and Mg# (41).At the rim, another unknown phase develops, which could not be measured because was beyond the resolution power of the EMP.

Chlorite

EMP compositions of representative chlorite grains are listed in Table 5B and Appendix 4. Particular for chlorite, more specifically Penninite (Table 5B), is a general enrichment in Cr (2,8-5 Cr_2O_3 wt%). This is interpreted because they generate from the breakdown of the Cr-rich spinels (Fig.15-16).

Amphibole

EMP compositions of representative amphiboles are listed in Table 5A and Appendix 4. Due to the high MgO (21,22-23,93 wt%) and CaO (11,88-12,56 wt%) content the amphiboles all are classified as Tremolite (Table 5A).

Tremolite grains within orthopyroxene porphyroclast (M1) (Fig.17) are irregularly shaped and characterized by high Cr_2O_3 (0,3-1,2 wt%), MgO (23,82-23,94 wt%) and Al_2O_3 (0,5-0,8 wt%) content (Appendix 4). On the other hand, forming part of the olivine foam microstructure (M2), tremolite appears as elongated euhedral grains in chemical equilibrium with olivine (M2) and orthopyroxene (Opx2) (Fig.17). Their chemical composition of is very similar to tremolite inclusions within orthopyroxene porphyroclast, except a slight depletion in Cr_2O_3 (0,13 wt%), MgO (21,22-21,52 wt%) and Al_2O_3 (0,06 wt%) content (Appendix 4).

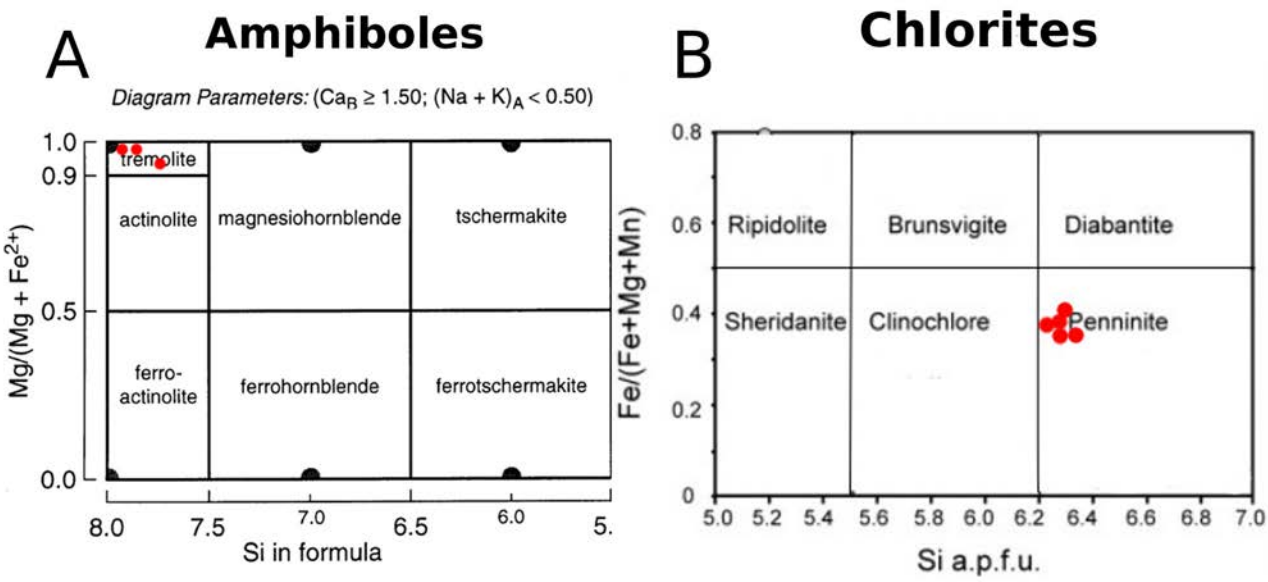

Table 5: A) Table for the nomenclature of amphiboles indicating Tremolite composition for the amphiboles in the KSP (Leake et al, 1997); B) Table for the nomenclature of chlorites indicating Penninite composition for the chlorites in the KSP.

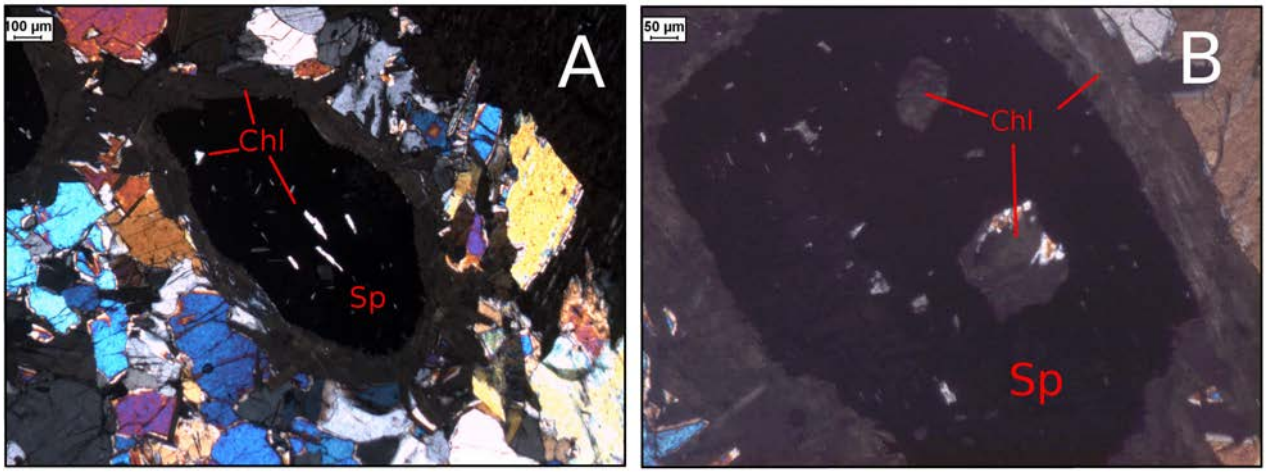

Figure 16: Cr-rich elongated spinel with incipient destabilisation to Chlorite (Chl). Note the concurrent presence of chlorite both as inclusions and along spinel rims.

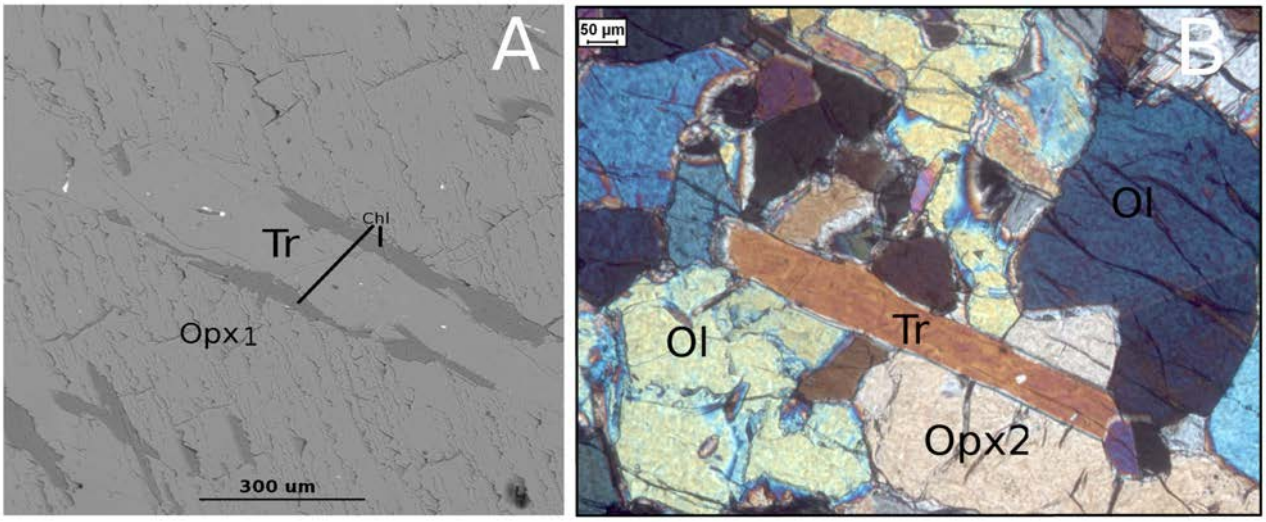

Figure 17: A) EMP image showing tremolite (Tr) and chlorite (Chl) growing together within a orthopyroxene M1 porphyroblast (Opx1); B)Optical microscope micrograph (XPL) showing elongated tremolite grain (Tr) in equilibrium with olivine and orthopyroxene (M2).

5.2.1.2 Discussion

Anomalous chromite composition

The chromium number of spinel (Cr#) is an important geochemical parameter for giving constraints about the degree of partial melting, equilibration or re-equilibration temperatures, and protolith provenance type in peridotites. In fact during progressive partial melting, Cr and Mg are strongly partitioned in the solid phase defining the restite, whereas Al and Fe preferentially go into the melt. As a result the Mg# of olivine and the Cr# of spinel will increase proportionally to the degree of partial melting defining a linear relationship Cr#-Mg# (Fig.18). Therefore establishing the chemical relationship between M1 olivine and M1 spinel grains will result as an invaluable tool to reconstruct the geodynamic setting of the protolith (Chapter 6.2).

Chemical composition of chromite (Cr#89-90;Mg#21-27) inclusions in olivine M1 porphyroclasts (Mg#~93) has been analysed in detail. In fact cr-rich spinels, forming oriented inclusions (s_i) within olivine M1 porphyroclasts, can reveal important information about the early M1 assemblages because the crystals were less affected by retrograde processes (i.e. break down in magnetite and/or chlorite) because of the impossibility to exchange Cr and Al with the surrounding olivine. Complications arise due to the anomalous spinel composition, characterized by high Cr# (89-96) and an extremely low Mg# (21,3-27,4) (Fig.18; Table 7). Normal depletion trends are expected to have an olivine with Mg# 92,5-93,5 coupled with a spinel Cr# 89-96 and Mg# 45-55 spinel (Fig.18, Red oval)(Dick et al, 1984). The observed chemical composition of M1 spinels match with empirically extrapolated compositions only for the Cr# but not for Mg# (). Such inconsistency lead to the formulation of two hypothesis:

1. Mg-Fe2+ partitioning during cooling of the rock, at decreasing temperature, cause a net Mg-Fe^{2+} transfer, with Mg preferably partitioned in olivine and Fe^{2+} in spinel. Therefore Cr# does not change but Mg# strongly decrease, causing a shift of spinel compositions towards lower Mg# (Fig.18), proportional to the modal spinel-olivine ratio (Dick et al, 1984). For instance, in massive chromitite (high Sp/Ol ratio) little Mg# change occur , but in dunite layers with disseminated spinel (i.e. KSP) with low Sp/Ol ratio, large and uniform drop in Mg# may occur. The Fe-Mg content of spinel is easily re-equilibrated but it is not possible to observe similar variations in olivine because modal abundances of chromite grains (~1 %) is too low to significantly influence olivine Mg#. In this scenario, the population of spinel inclusions within olivine porphyroclasts are extremely important because their Cr# represent the original Cr/Al ratio immediately after partial melting.
2. The rock equilibrated or precipitated from melts abnormally rich in iron

The first hypothesis is preferred because the presence of iron rich melt is not consistent with the high Mg# of olivine and the constant chemical composition of the peridotite all along the exposed area (Calon, 1979).

	Cooling effect	**Partial melting trend**
M1 Olivine Porphyroclast	Mg# 92,5-93,6	Mg# 92,5-93,6
M1 spinel inclusions	Cr# 89-96 ; **Mg#21-27**	Cr# 89-96 ; **Mg# 45-55**

Table 6: M1 olivine porphyroclasts Mg# and spinel Cr# and Mg# define a linear trend (Fig. 18) during partial melting. Olivine Mg# (92,5-93,6) positively correlate with spinel Cr# (89-96) but not Mg#. In fact is expected a spinel Mg# of 45-55 but M1 spinel in equilibrium with M1 olivine porphyroclasts is characterized by Mg# 21-27. The Mg# shift is attributed to cooling effects, in particular to a preferential partitioning of Mg in olivine.

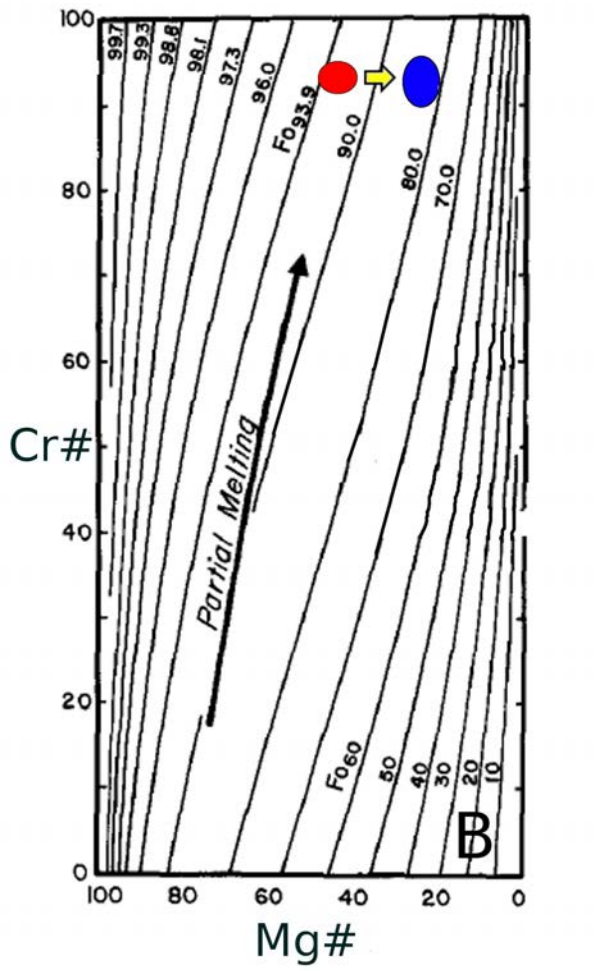

Figure 18: Spinel composition field in a Cr# vs Mg# diagram. Fo= Mg/Mg+Fe ratio in olivine crystals co-existing with spinel during partial melting. Red oval represent the spinel composition (Cr# 89-96 ; Mg# 45-55) in equilibrium with Olivine with Mg# = 92,5-93,5. Blue oval is the measured composition of spinel inclusion (Cr# 89-96 ; Mg#21-27) within M1 olivine porphyroclasts (modified after Dick et al, 1984).

Spinel-chlorite relationship

Chlorite inclusions represent up to modal 5-20 % of chromite grains (Fig. 15A-16) and are irregularly distributed or aligned along well oriented lamellae. The chlorite inclusions are considered as lamellae oriented parallel to one of four { I I I } planes of the host chromite (Fleet et al, 1993). Maximum number of chlorite orientations for each set of planes is three, therefore a maximum of 12 individual different orientations are possible in every chromite. Such structure is considered as an inter-growth in the spinel + chlorite field when the system was affected by infiltration of fluid phases (Fleet et al, 1993).

5.2.2 Bulk rock chemical composition of KSP

5.2.2.1 Bulk rock major element analysis

The Bulk rock chemical analysis of sample K7 and K9 are obtained by XRF analysis has been calibrated for typical elements of the ultramafic system (Mg, Fe, Si, Ca, Cr, Ni, etc..).

The element oxide analysis had to be carried out under dry conditions, therefore all samples were heated up in several steps. All elements eliminated during heating were measured and quantified as LOI in Table 7.

Sample	Lithology	SiO2	AlO3	TiO2	FeO	Fe2O3	MnO	CaO	MgO	Na2O	K2O	P2O5	TOTAL	Mg#
K7	Dunite	39,92	0,09	0,01	7,45	1,66	0,11	0,11	50,64	0,00	0,01	0,00	100,00	92,40
K9a	Harzburgite	42,10	0,43	0,01	8,26	2,01	0,14	0,46	46,60	0,00	0,01	0,00	100,00	91,10
K9B	Harzburgite	42,60	0,57	0,01	7,78	2,15	0,14	0,70	46,02	0,03	0,01	0,00	100,00	91,70

Table 7: Illustrating the results of XRF analysis performed on dunite (sample K7) and harzburgite (sample K9a and K9B) expressed as major oxides. The analysis are recalculated to 100% and are used to calculate pseudosections with the software Theriak Domino. Original analysis are plotted in Appendix 5.

All samples are characterized by an extremely high content of MgO > 46% and SiO_2 < 43% coupled with extreme low amount of Al_2O_3 and CaO. Mineral modal abundance is calculated from XRF analysis in Table 8 and is plotted in Fig.19.

		MODAL (%)		
Sample	Lithology	Ol	Opx	Tr-Chr-Chl
K7	Dunite	96	3	1
K9a	Harzburgite	85,6	13,1	1,3
K9b	Harzburgite	84,3	14,2	1,5

Table 8. Modal percentage of major minerals for dunite (K7) and harzburgite (K9a – K9B) calculated from XRF analysis in table 7.

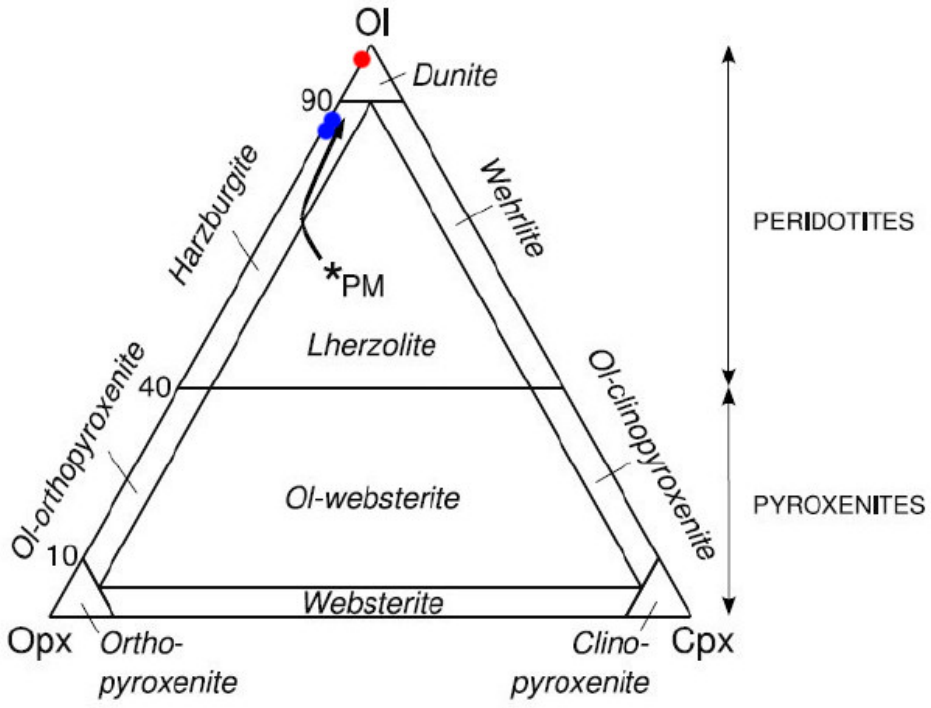

Figure 19: Classification for ultramafic rocks on the basis of mineral mode (Ol-Opx-Cpx). Black arrow indicates residual trend of peridotite during partial melting from primitive mantle composition (PM). Mode composition of dunite (Red dot) and harzburgites (Blue dots) plot on the lower end of the depletion trend.

5.2.2.2 Theriak domino

The Bulk rock composition of sample K9a (Table 7) has been used to produce phase diagrams using the PT software Theriak Domino. For simplicity it has been assumed that the fluid phase is exclusively H_20 at lithostatic pressure (Fluid pressure=total pressure). Such assumptions do not influence the position of phase boundary lines for Chlorite and Tremolite-in reactions (Fig.20-21) at moderate to high temperature (> 600°C). At lower temperature fluid effects is more important because antigorite (Atg) and talc (Tc) formation are fluid pressure dependent. In fact at lower water fugacity (i.e. water content), talc is more stable than antigorite (Fig.20-21).

In chapter 5.2.3 the validity of Grt-Sp phase boundary and the application to mineral assemblage characterizing M1, M2 and M3 for the KSP will be discussed.

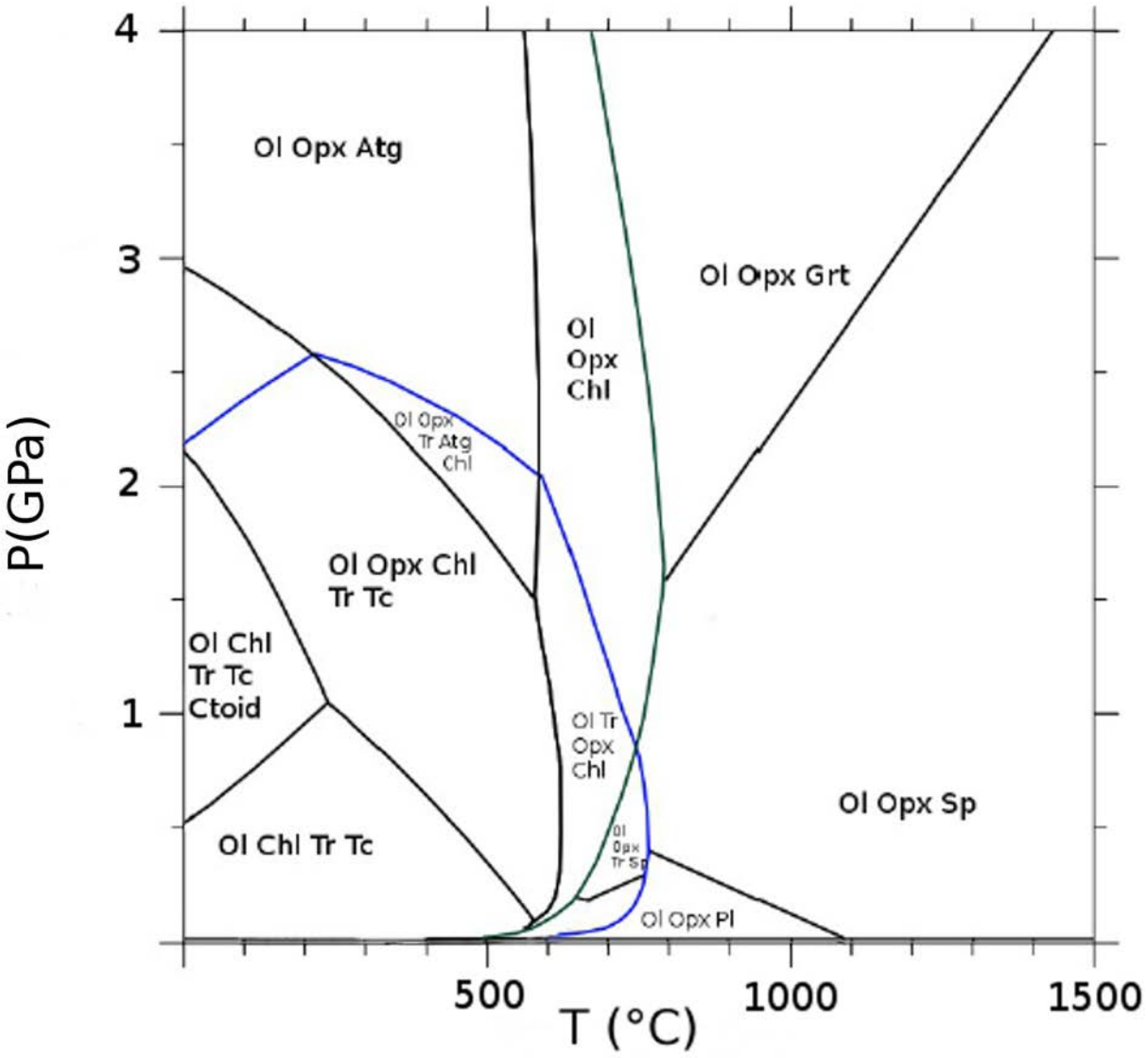

Figure 20 Calculated pseudosection for a Kittelfjäll Harzburgite bulk rock composition for H_20 = 4 % (Wt%). Highlighted Tremolite-in (Blue line) and chlorite-in reaction lines (Green line).

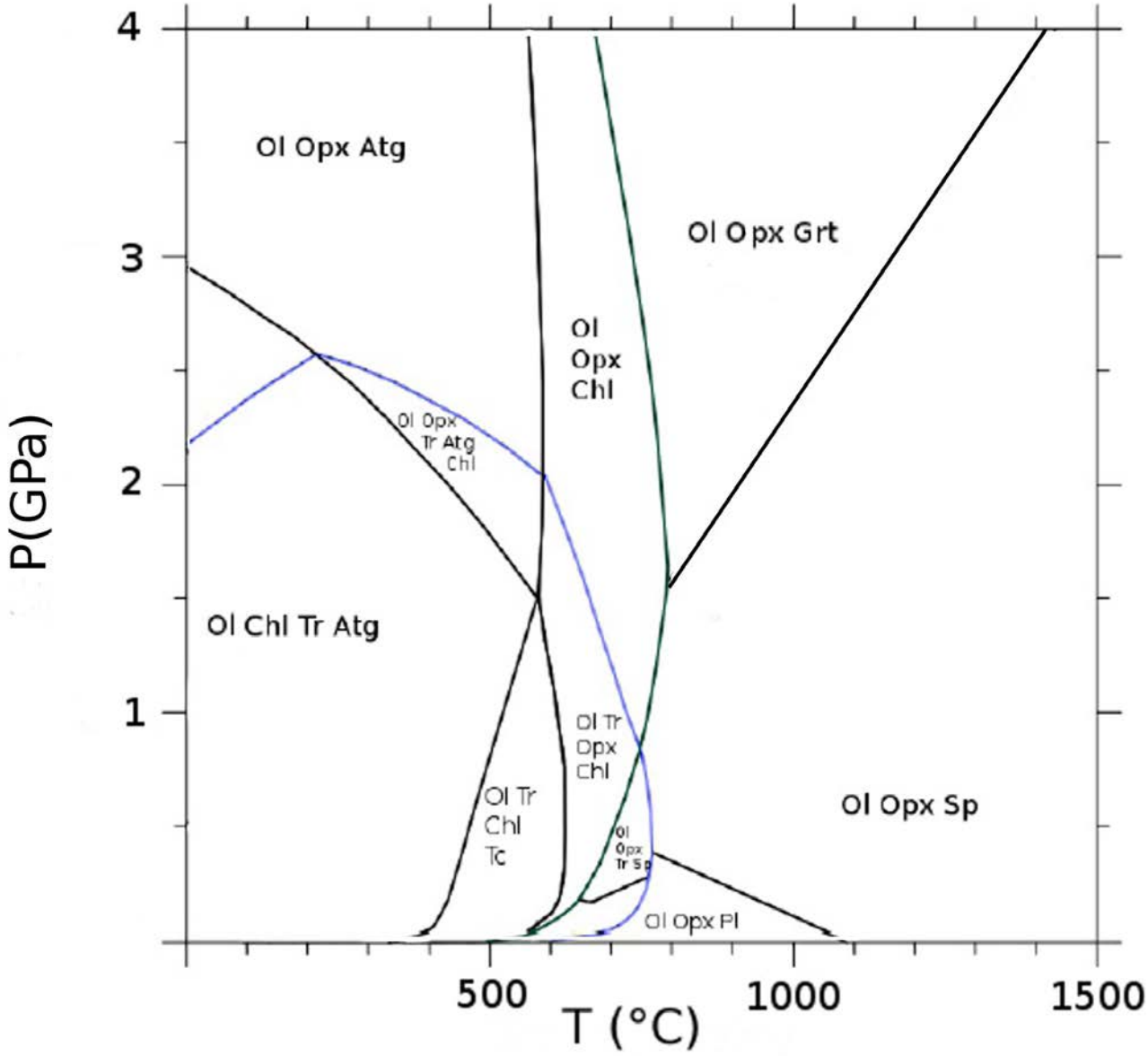

Figure 21.Calculated pseudosection for a Kittelfjäll Harzburgite bulk rock composition for H_20 = 10 % (Wt%). Highlighted Tremolite-in (Blue line) and chlorite-in reaction lines (Green line).

5.2.3 Geothermobarometry

5.2.3.1 Introduction

Geothermobarometers applicable to ultramafic rocks are often based on inter-crystalline Fe–Mg exchange between any anhydrous Fe–Mg phases like Ol–Spl, Ol–Grt, Opx–Cpx or Cr-Al exchange between spinel and Opx. Most of the geothermobarometers can only be used for PT estimates of ultramafic rocks equilibrated in the eclogite or granulite facies. However, when metamorphic re-equilibration occurs within greenschist or amphibolite facies, reliable geothermometers are lacking because of the presence of fluids. In fact, the activities of volatile species, their compositions (i.e. CO2/H2O) and quantities are parameters that deeply influence the PT position of reactions, but are generally difficult to estimate (Bucher, 2011).

For these reasons, classic geothermobarometry can be used on the KSP only for M1 assemblage as M2 and M3 are characterized by hydrous minerals, as tremolite, chlorite, talc and antigorite. Therefore the PT estimate must be inferred through the correlation between the M2-M3 stable mineral assemblagess and petrogenetic grids produced with a specific software: Theriak Domino (Chapter 5.2.2.2).

5.2.3.2 Geothermometry

Olivine-Spinel Mg-Fe exchange thermometer

The olivine-spinel Fe-Mg exchange thermometer (Ballhaus et al, 1991) has been tested on olivine M1 porphyroclast ($M1_b$) and chromite inclusions. Equilibration temperature give a temperature of 870-890° +/- 60° (0-3 Gpa) and can be considered as a re-equilibration temperature. The same thermometer has not been tested on olivine and spinel in the olivine foam microstructure (M2) because spinel is in equilibrium with chlorite, consequently Fe-Mg exchange does not occur with olivine but preferably with chlorite crystals.

Orthopyroxene-Spinel Cr-Al exchange thermometer

Application of the Al–Cr in opx thermometer of Witt–Eickschen and Seck (1991) to M1 orthopyroxene porphyroclast compositions listed in Appendix 2, gave values between 1052 °C and 1158 °C, with an average around 1094°C.

5.2.3.3 Geobarometry

The Garnet-Spinel reaction is extremely important for giving barometric constraint about the upper stability field of the Kittelfjäll spinel peridotite. In simple chemical systems (i.e CaO–MgO–Al2O3–SiO2) the univariant spinel-garnet transition range from 1,5 up to 3 GPa depending on temperature (Fig.22A). Such system is clearly a simplified system and can be considered reliable only for fertile mantle compositions as lherzolites. Strongly depleted peridotites are particularly enriched in Mg and Cr, therefore they require more complex calculations taking into account the influence of minor elements (Webb and Wood, 1986).

Klemme (2004) experimentally proved the importance of Chromium for the stability field of spinel and garnet (Fig.22B). For fertile mantle composition with Cr#< 0.1 there is a positive correlation with experiments in simpler system (Fig. 22A), whereas in depleted peridotites as harzburgites and dunites the stability is radically modified depending on Cr/(Cr + Al). In fact, Cr# plays a major role, expanding enormously the spinel stability field towards exceptionally high pressure. For instance, a Cr-rich spinel might be stable up to 7 Gpa (Fig. 22B). An additional remarkable feature for spinel with Cr# > 0.2 is the spreading out of the divariant garnet + spinel stability field in a broad range of pressure (Fig. 22B; Klemme, 2004).

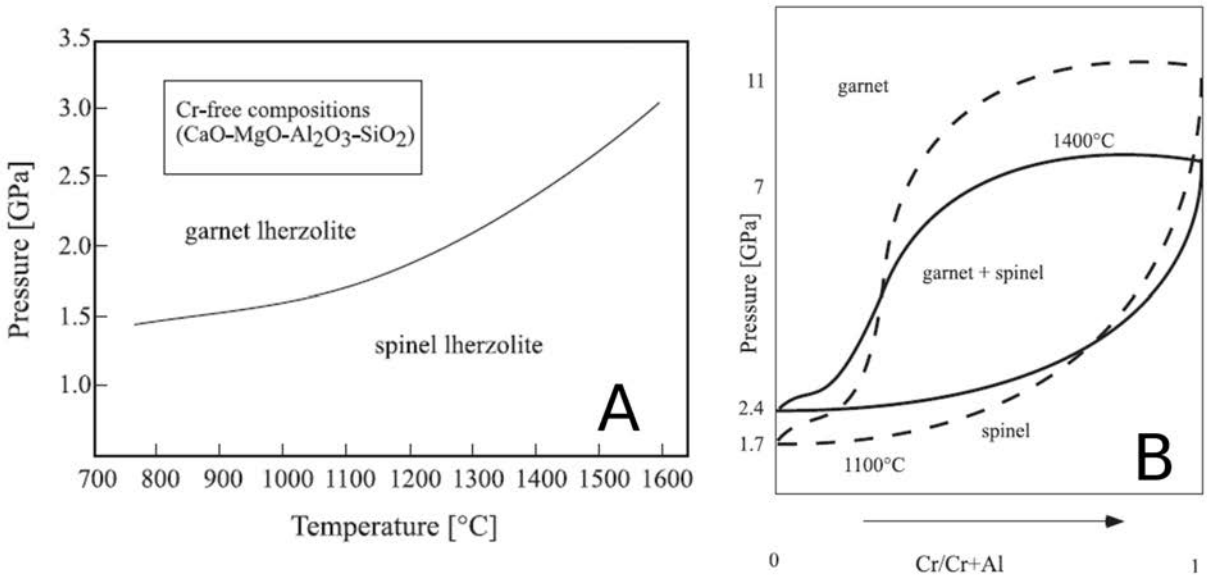

Figure 22: A)Transition from garnet lherzolite to spinel lherzolite in Cr-free (fertile) mantle (Klemme, 2004). The curve shown is based on experimental data in the system CaO–MgO–Al2O3–SiO2. B)The effect of Cr on the stability of garnet and spinel, based on thermodynamic models in the system MgO–Al2O3–Cr2O3–SiO2. The width of this garnet + spinel stability field is strongly dependent on Cr/(Cr + Al). The solid lines show coexisting garnet and spinel compositions at 1400°C, whereas the dashed lines depict their compositions at 1100°C (Modified after Klemme, 2004).

5.2.3.4 Discussion

$M1_a$ and $M1_b$

Geothermometry on coarse grained assemblage (M1) is characterized by different temperatures, respectively ~870 °C and ~1094 °C for M1 olivine porphyroclast and M1 orthopyroxene porphyroclasts (Chapter 5.2.3.2). The latter value can not be considered as the temperature affecting the peridotite during partial melting because higher temperatures, in the order of ~1300 °C (Mesozoic) to ~1800 °C (Archean) are then required. Hence, both temperatures are interpreted as indicative of thermal re-equilibration that followed initial partial melting.

Based on these assumptions, the M1 assemblage is subdivided in two categories, in order to better specify different moments of the cooling history (Table 9). $M1_a$ is indicative of subsolidus processes affecting the orthopyroxene porphyroclast (M1) chemical composition (i.e. exsolution lamellae) at ~1100 °C. Instead $M1_b$ represents re-equilibration of the Olivine-Spinel system at lower temperature, ~870 °C.

The M1a and M1b equilibration pressure cannot be precisely determined because of a lack of applicable geobarometers and anomalous Cr-rich spinel. In fact spinels (Chromite) inclusions within olivine porphyroclasts (M1) are characterized by a Cr/(Cr + Al)~0,9 (Chapter 5.2.1.2). As a result, the inferred upper limit for the stability of spinel in the KSP, during the formation and/or re-equilibration of the M1 coarse grained assemblage can be inferred from Fig.22B. Cr# in M1 assemblage (~0,9) an M2 assemblage (~0,7) indicate an upper stability of respectively, 6 and 4 Gpa.

M2 and M3

M2 and M3 stable mineral assemblages can be inferred from petrogenetic grid produced with the software Theriak Domino. M2 is defined by the mineral assemblage Ol + Opx + Chl/Sp + Tr , stable at 600-760 °C and 1-2 Gpa (Table 9; Fig.23). Amphibole has been observed to be stable only in relation with type II grains in the olivine foam microstructure (Chapter 5.3.2) and not with coarser type I grains. Possibly, the onset of deformation began when tremolite was not stable and, therefore, the inferred PT conditions are related exclusively to the final part of deformation when Type II grains developed.

The Lower limit of stability, during M2, is deduced exclusively considering the stable assemblage of the surrounding rocks. KSP is considered to be part of the Central Belt, which is composed by the Kittelfjäll amphibolite and the Marsfjället gneisses (Chapter 2.3), two unit characterized by the stable association kyanite-Kfeldspar during M2 event. Therefore the lower limit is defined by the kyanite-in reaction, approximately at 1 Gpa (Fig.23).

The M3 mineral assemblage for inferring PT conditions cannot be applied because of the transition reaction between antigorite and talc is entirely depending on fluids content and fugacity, two parameters difficult to estimate. Thermodynamic calculations of the software Theriak-Domino are here considered not reliable. For the purpose of this thesis the exact determination of the M3 metamorphic conditions is related to initial estimate of Calon (1979), at 550-600°C and 0,45-0,6 Gpa.

	M1a	M1b	M2	M3	M4
Olivine	$Ol_{megacryst}$	$Ol_{megacryst}$	Ol_{foam}	Ol_{mortar}	
Orthopyroxene	Opx 1	Opx1	Opx2		
Chromite	x	x	x		
Antigorite				$X_{high\ pH20}$	x
Talc				$x_{medium\ pH20}$	x
Tremolite			x	x	
Chlorite			x	x	x

Table 9: Paragenetic diagram for the Kittelfjäll spinel peridotite.

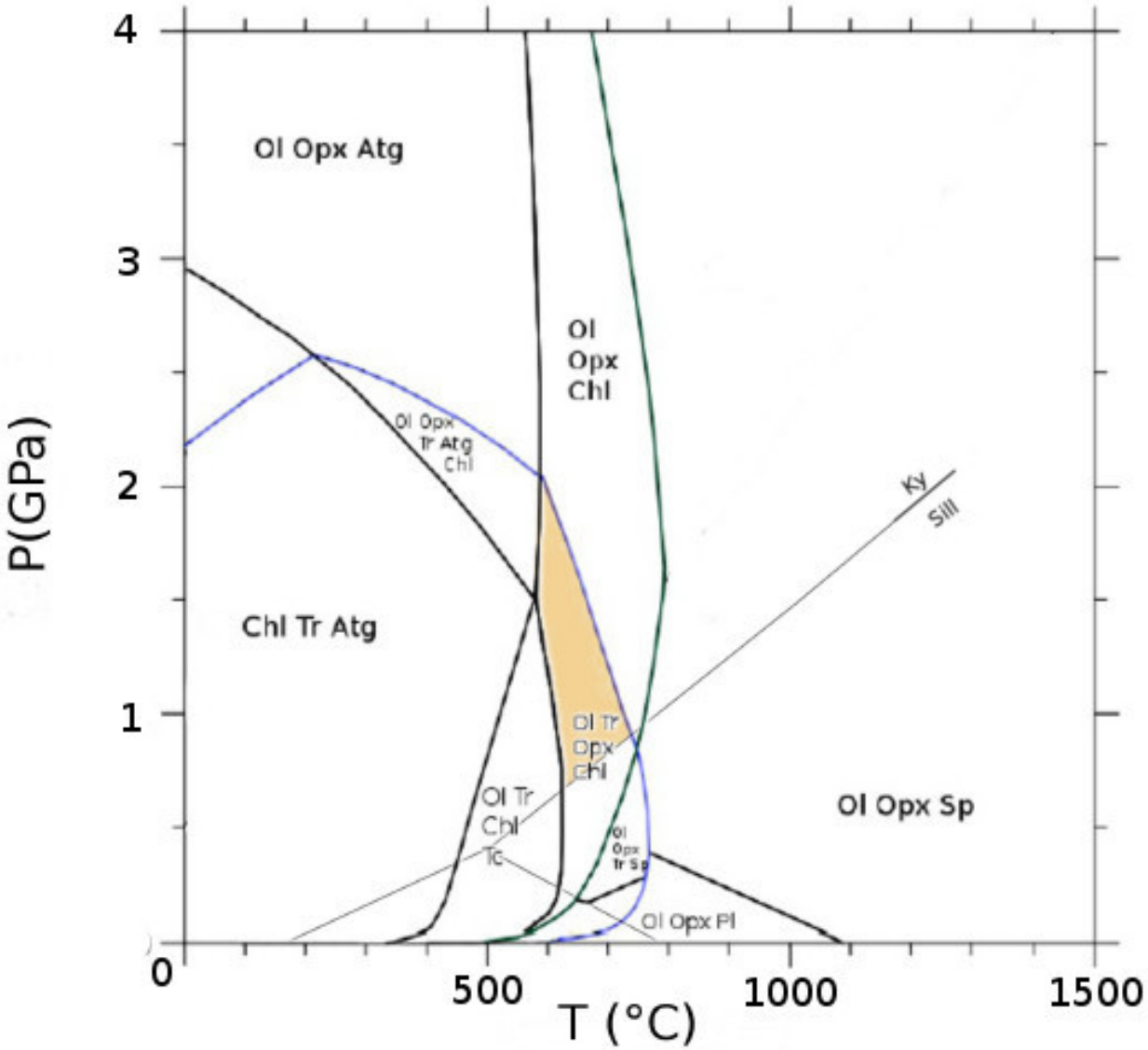

Figure 23: The M2 assemblage is defined by the mineral assemblage Ol + Opx + Chl/Sp + Tr (orange area), stable at 600-760 °C and 1-2 Gpa. The lower limit is indicate by the stability of the Kyanite-in the surrounding pelitic rocks during coeval development of M2.

5.3 Olivine fabric analysis

5.3.1 Introduction

Olivine forms one of the most important minerals of the Earth's upper mantle . As such the rheology of olivine plays a fundamental role in physical processes like mantle convection and/or dynamics of lithospheric fragments during plate collisional/extensional processes (orogenesis). This is clearly expressed by the ever increasing number of scientific publications that has appeared in the recent literature dedicated to the rheology of olivine since the development of plate tectonics theory. In fact, a better understanding of the deformation behaviour of olivine is of capital importance in defining the role of the lithospheric mantle during plate collisional processes.

The Kittelfjäll spinel peridotite provides an unique opportunity to investigate the dynamic structure and evolution of a subcontinental lithospheric mantle fragment during the formation of the Scandinavian Caledonides. In terms of bulk rock compositions the studied samples can be regarded as a mono-mineralic dunite. This is because the additional minerals like orthopyroxene, spinel, chlorite and amphibole can be considered as "accessory" minerals in the rock, implying that the presence of these minerals is interpreted not to influence the rheological behaviour of the dunite/olivine.

The peridotite is characterized by three contrasting olivine microstructures, formed in response to different metamorphic and deformation conditions. The latter were studied for the first time by Calon (1979), who summarized the olivine microstructural evolution as follows: coarse grained, highly strained olivine crystals (up to 20 cm; called M1 porphyroclasts) surrounded by dynamically recrystallized olivine grains (200-2000 um mm) that define a characteristic olivine "foam" microstructure (called M2 grains). The latter olivine microstructure forms a penetrative fabric extended throughout the Kittelfjäll peridotite. In strongly localized shear zones M1 and M2 olivine microstructures are overprinted by a finer grained (1-20 um), dynamically recrystallized, M3 olivine microstructure, called the olivine "mortar" texture (M3).

To investigate the deformation mechanisms that have formed the olivine microstructures described above, an olivine fabric analysis is performed and presented in this chapter. This optical investigation involves the study of the olivine crystallographic preferred orientations (CPO's), the deformation-induced dislocation slip systems and substructure(s), as well as a detailed study of the associated olivine microstructures (grain size, grain boundary geometry).

Special emphasis is paid to the deformation conditions (i.e. stress, strain rate, temperature, water content) operating during formation of the M2 olivine foam microstructure. Implications concerning strain localisation and state of stress will be discussed and related to lithosphere or crustal deformation.

5.3.2 Deformation-induced olivine microstructures

In this section the results of optical observations performed on the M1, M2 and M3 olivine microstructures are described.

5.3.2.1 Porphyroclast (M1)

In the field coarse grained olivine crystals (5-20 cm) are rare and when present, they are inhomogeneously distributed in dunite layers. Good examples are found within the quarry close to the hill of Lebnjesnuone (Appendix 1) where they appear as strongly elongated crystals with an exceptional grain size up to 20 cm (Fig.24).

In the optical microscope the M1 olivine porphyroclasts form elongated and highly deformed crystals with a characteristic internal microstructure that consists of well developed kink bands. Crystals are characterized by two sets of regularly spaced kink bands. One set is parallel to (100) and has large spacing (100-200 um)(Fig.25B). The other set of kink bands, rare and not uniformly developed in every porphyroclasts (M1), is parallel to (001) and has a smaller spacing (50-100 um) (Fig.25B). The first set is clearly foregoing because the sequence of formation is indicated by neat cutting relationships (Fig.25B). Grain boundaries of M1 olivine porphyroclasts are strongly irregular (Fig.25B-26A) abruptly passing over into a fine-grained matrix of optically strain free, polygonal olivine defined below as the M2 olivine foam (Fig.24). M1 porphyroclasts contain well oriented chromite crystals, lined up in a parallel array, defining an internal olivine foliation (S_i).

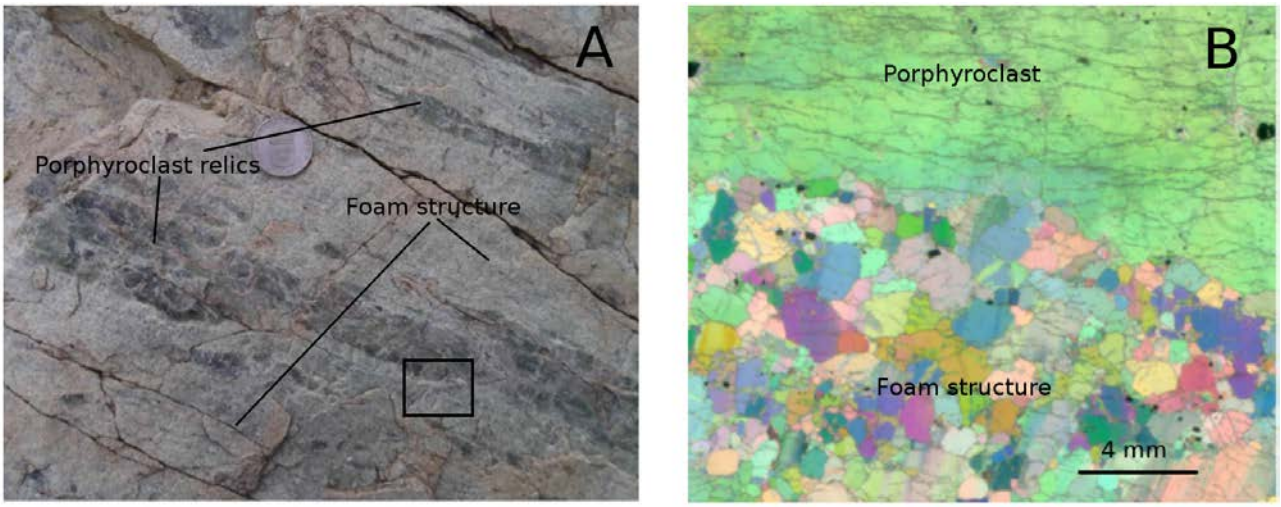

Figure 24: A) Field micrograph illustrating elongated porphyroclasts (M1) of olivine embedded in a matrix of finer olivine grains characterizing the olivine "foam microstructure" (M2). The black box is the area magnified in Fig.24B; B) Optical micrograph (crossed polarized light (XPL)) displaying the large grain size transition between a megacrystal at the top and the olivine foam microstructure at the bottom .

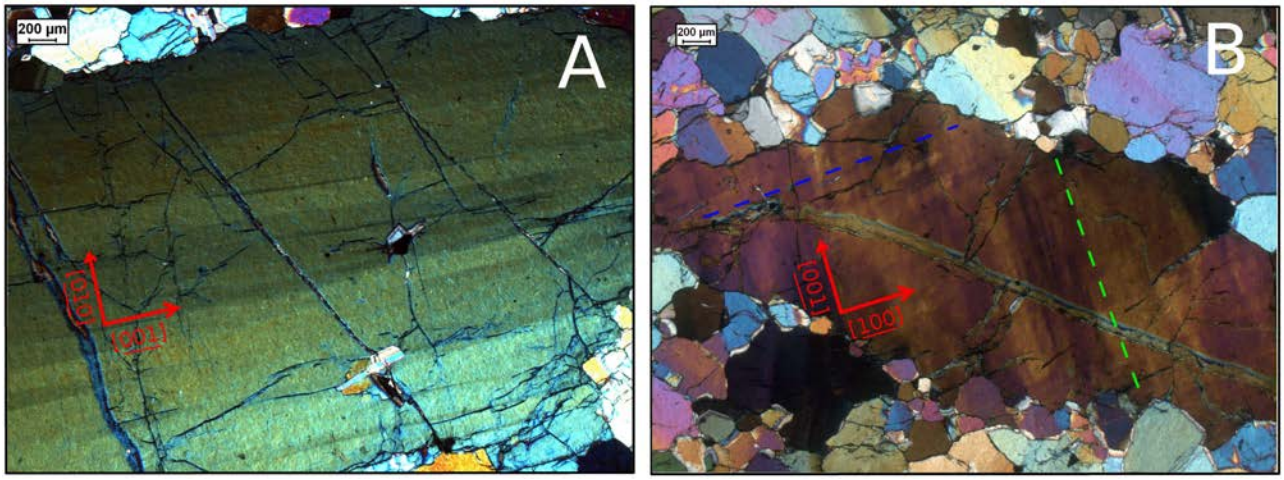

Figure 25: Optical microscope (XPL) pictures of the section K8C (A) and K7 (B): A) Straight Kink bands (100-200 um) parallel to [001] in a olivine porphyroclast (M1) ; B) Cutting relationship between two sets of kink bands. The set parallel to [100] (blue dotted line) clearly postpone the formation of the larger spaced kink bands (green dotted line) aligned along the crystallographic direction [001].

5.3.2.2 The olivine foam microstructure (M2)

In the field the olivine foam microstructure forms a penetrative fabric element that is developed throughout the entire peridotite body but is best preserved in the innermost structural areas, where later deformation-overprints are less intense. In dunite layers, the S2 foliation is really difficult to define due to the absence of elongated minerals and for the granoblastic nature of M2 olivine grains. Only in harzburgite layers a weak preferential elongation of porphyroclasts of orthopyroxene is helpful to trace a clear S2 foliation plane.

In the optical microscope the olivine foam microstructure is strongly inhomogeneous, which can be related to preferential development of one of the two typologies of olivine grains, here called Type I and Type II (after Calon, 1979):

Type I Grain

Type I matrix grains (Fig.26A-27) form the coarsest olivine grains within the olivine M2 matrix. They occur as isolated olivine crystals within smaller sized type II matrix grains (Fig.28) and/or occur along rims of M1 olivine porphyroclasts (Fig. 26A). Only few domains are characterized by the predominance of type I olivine grains (Fig.27) defining a foam texture. In the neighbourhood of M1 olivine porphyroclasts, type I olivine grains are characterized by a coarser grain size, up to 2 mm, whereas in distal areas they may have similar sizes but can also drop to grain sizes as small as 0,5-1 mm.

Type 1 olivine grain boundaries appear irregularly shaped when associated with highly deformed M1 crystals (Fig.26A), whereas in more distal areas M2 olivine grains are characterized by straight grain boundaries interconnecting in triple point junctions defining an annealed structure (Fig.27).

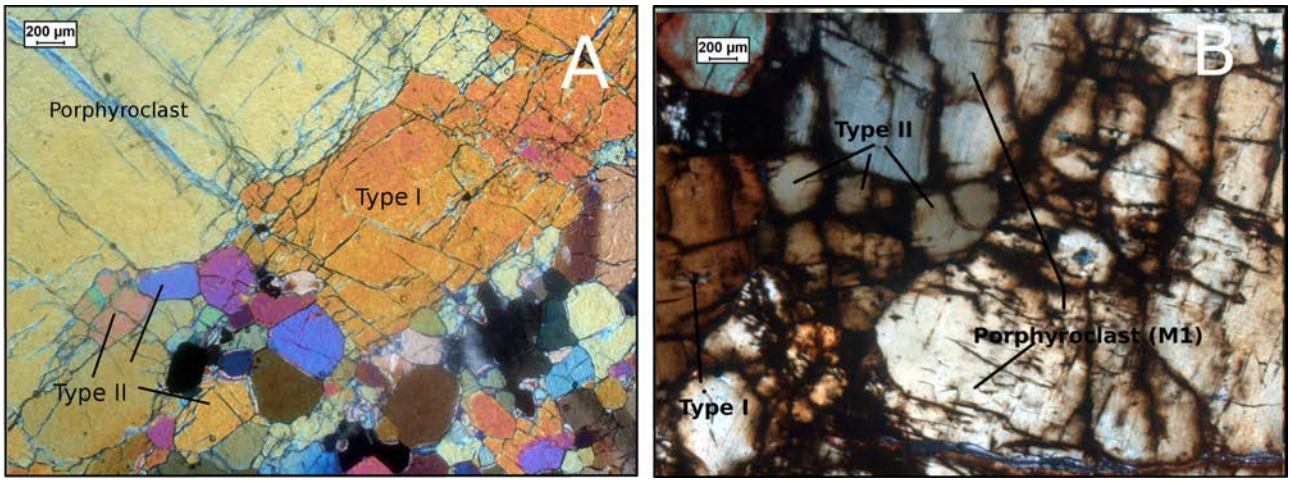

Figure 26: Optical micrographs (XPL) showing : A) Transition zone from M1 olivine porphyroclast (top left) to a type 2 grains olivine foam texture (bottom right side). Note the occurrence of olivine type I grains at the interface between the two olivine microstructures. B) Foam neoblasts (M2) with extinction angle of 10°-40° with respect porphyroclast (M1).

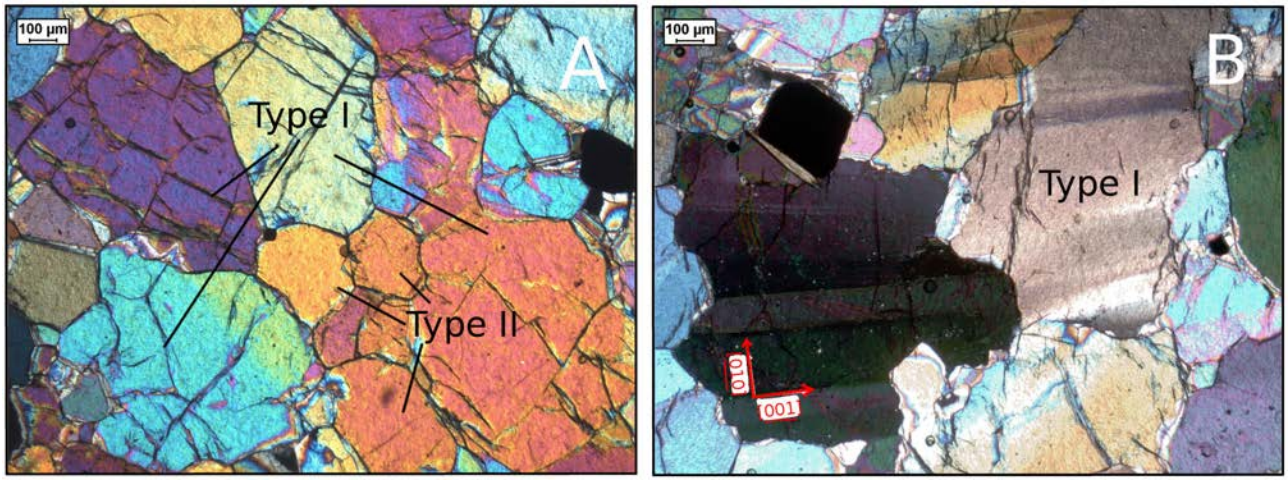

Figure 27: Optical micrograph (XPL) of sample K8d showing A) matrix domain dominated by olivine type I grains with minor type II grains. Characteristic triple point junctions and straight grain boundaries can be seen defining an annealed micro-structure; B) Well developed kink bands in olivine type 1 grains. Note that the spacing between the kink bands is in the order of 100 um . Red arrows represent main crystallographic direction measured with Universal Stage

Type II Grain

Type II matrix grains form the main constituent of the matrix (= foam micro-structure sensu stricto). Type II crystals are generally equidimensional and strain-free. Their grain boundaries are "straight" and meet in triple point junctions defined by angles of 120° between olivine-olivine grain boundaries (Fig.28-29). Grain size is highly variable, with a major distribution around 200-400 um (without considering tabular shaped olivines.

Strain free type II grains preferentially form either from highly deformed type I olivine grains (Fig.26A) or directly from M1 porphyroclasts (Fig.26A). Clear morphological differences and similarities can be recognized between type I grains proximal to porphyroclast (Fig.30A) and within well developed type 2 olivine foam microstructure (Fig.30B). Their grain size is comparable (~ 200 um) but with strong differences in their grain boundary configuration. In fact Type 2 grain boundaries of crystals in contact with M1 porphyroclasts (Fig.30A) are scalloped and irregularly shaped, whereas the olivine type 2 grain boundaries appear straight when surrounded by other type II grains (Fig.29-31B).

Tabular shaped olivine crystals (Fig.29) are rare and randomly distributed but always present in every sample analysed. Tablet grains differ from the other polygonal crystals for their pronounced elongation along [001] and because the majority of grain boundary crystallographic planes seems not casually oriented, but are interpreted to be sub-parallel/parallel to low index faces.

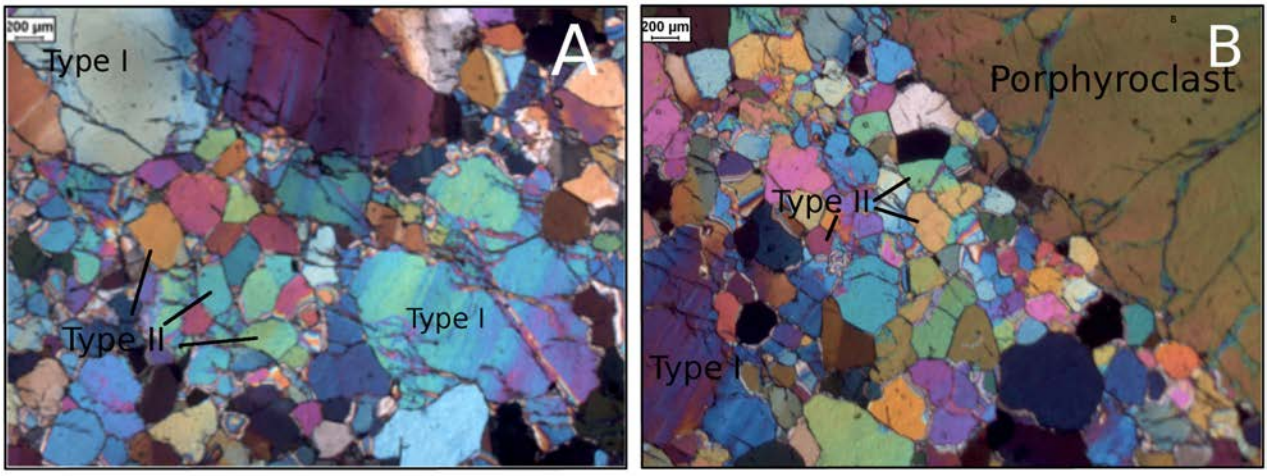

Figure 28: Optical micrograph (XPL) of sample K8a showing microstructural relationships between olivine M1 porphyroclasts and olivine type I & II grains. A)Highly strained Type I grains in a matrix composed of Type II grains (straight boundaries and triple point junctions); B) Type II grains form either from large porphyroclasts (top right) or from highly strained Type II grains.

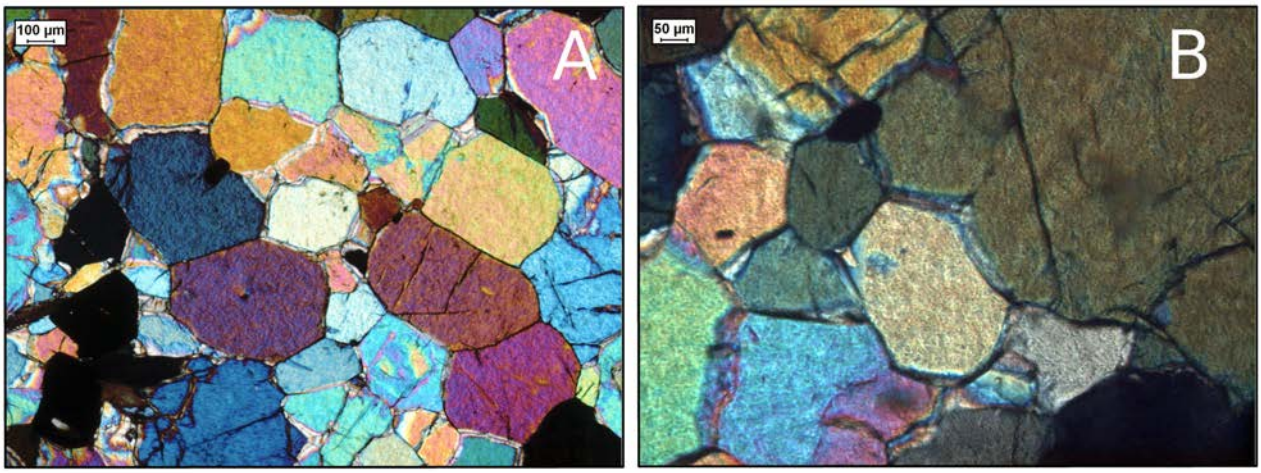

Figure 29: Figure 31: Optical micrograph (XPL)of sample K8a: A) Olivine foam microstructure in which optical strain free grains display straight grain boundaries meeting in 120° triple point junctions. Grains are generally equidimensional but tabular shaped olivine grains are randomly distributed in every sample analysed; B) Tabular shaped olivine with straight grain boundaries meeting in triple point junctions.

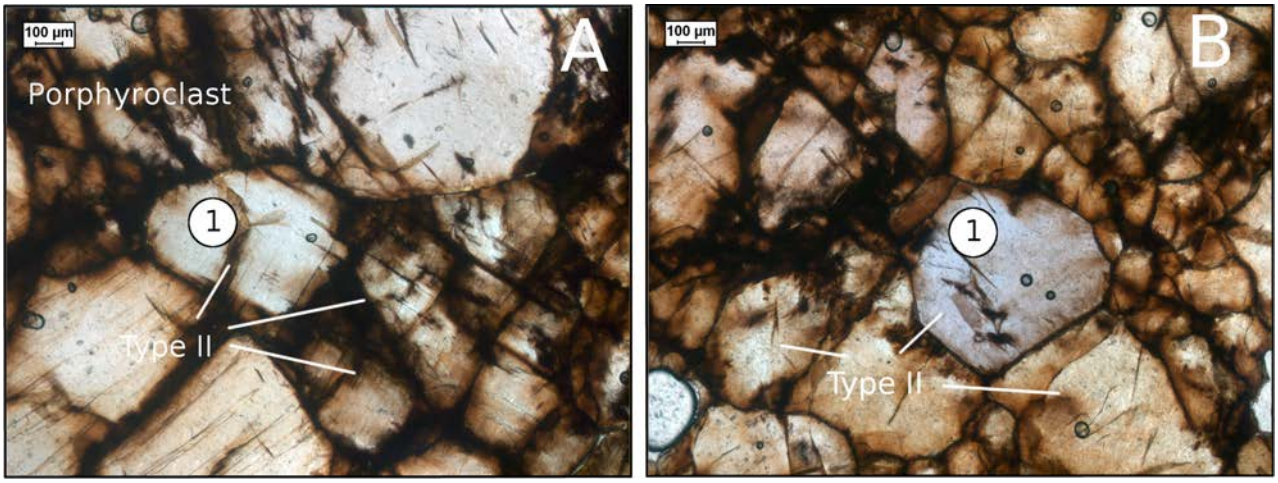

Figure 30: Optical micrographs (plane polarized light=PPL) of a decorated thin section (K8e). illustrating type II grains in two different textures: A) Showing Type II olivine grain (1) in contact with olivine M1 porphyroclast (top side). Grain boundaries of crystals in contact with M1 porphyrocla are scalloped and irregularly shaped B) Matrix composed exclusively of type II olivine grains. Grain boundaries of type II grains (1) are in this case straight and well defined triple point junctions.

5.3.2.3 The olivine mortar microstructure (M3)

In the field the olivine mortar structure appears as a non penetrative, irregularly distributed structure related to the D2 shear event (Chapter 5.1.3). The olivine mortar structure is only strongly localized and pervasive in narrow micro- and mesoscopic shear zones in the outer part of the ultramafic body (Appendix 1).

In the optical microscope the mortar structure is characterized by a very fine-grained matrix (1-20 um) defined by equant, optically strain-free olivine grains surrounding and occurring within coarser grained, heavily strained relics of a pre-existing M2 olivine foam microstructure (Fig.31-32B). The olivine mortar fabric is highly heterogeneous, showing a wide range of microstructures dependent on the intensity of the deformation within the shear zone.

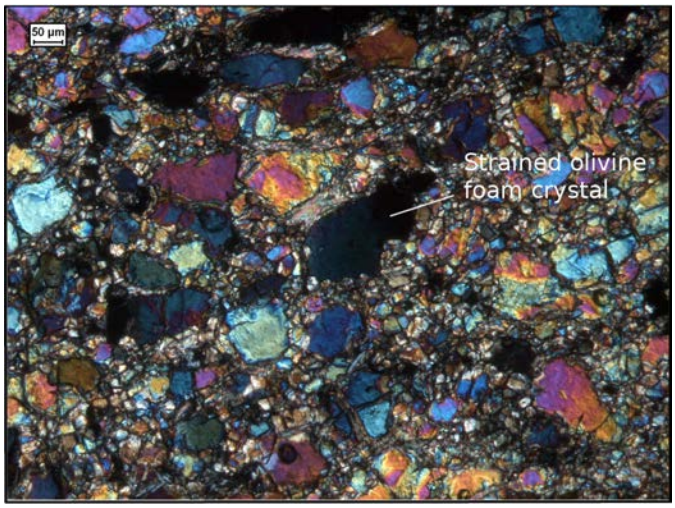

Figure 31: Optical micrograph (XPL)of sample K4 showing transitional stage leading to the formation of Olivine Mortar structure (M3). Deformed and strongly strained crystals of olivine foam microstructure (M2) are surrounded by strain free and finer olivine grains.

Outside the margin of the M3 shear zone boundaries margins the olivine foam microstructure is perfectly preserved (Fig.32A). Within the shear zone it is possible to observe a series of incremental microstructures defining transitional stages from olivine foam microstructure (M2) to olivine mortar structure (M3). In fact in the neighbourhood of the shear zone, original sharp grain boundaries (Fig.32) are blurred by the formation of fine grained new olivine crystals (1-50 um) while olivine foam crystals display undulatory extinction

(Fig.31-32B). A strong grain size reduction occurs at the edges of crystals with progressive deformation blurring the grain boundaries. Towards the core of the M3 micro-meso shear zone the amount of deformation increase, leading to the development of a mortar structure in sensu stricto. In such areas, olivine foam grains are completely re-crystallized in a finer olivine microstructure. This characteristic fabric develop in a anastomosing network of fine grained olivines (M3) surrounding lentiform relics of the olivine foam microstructure (Fig.32C). A well developed olivine mortar structure is defined by irregularly shaped olivine grains in equilibrium with antigorite crystals (Fig.32D). In few cases triple point junctions develops at the interface between olivine mortar grains. When this microstructure develops it is associated with irregular rather than straight grain boundaries like in the olivine foam microstructure (M2).

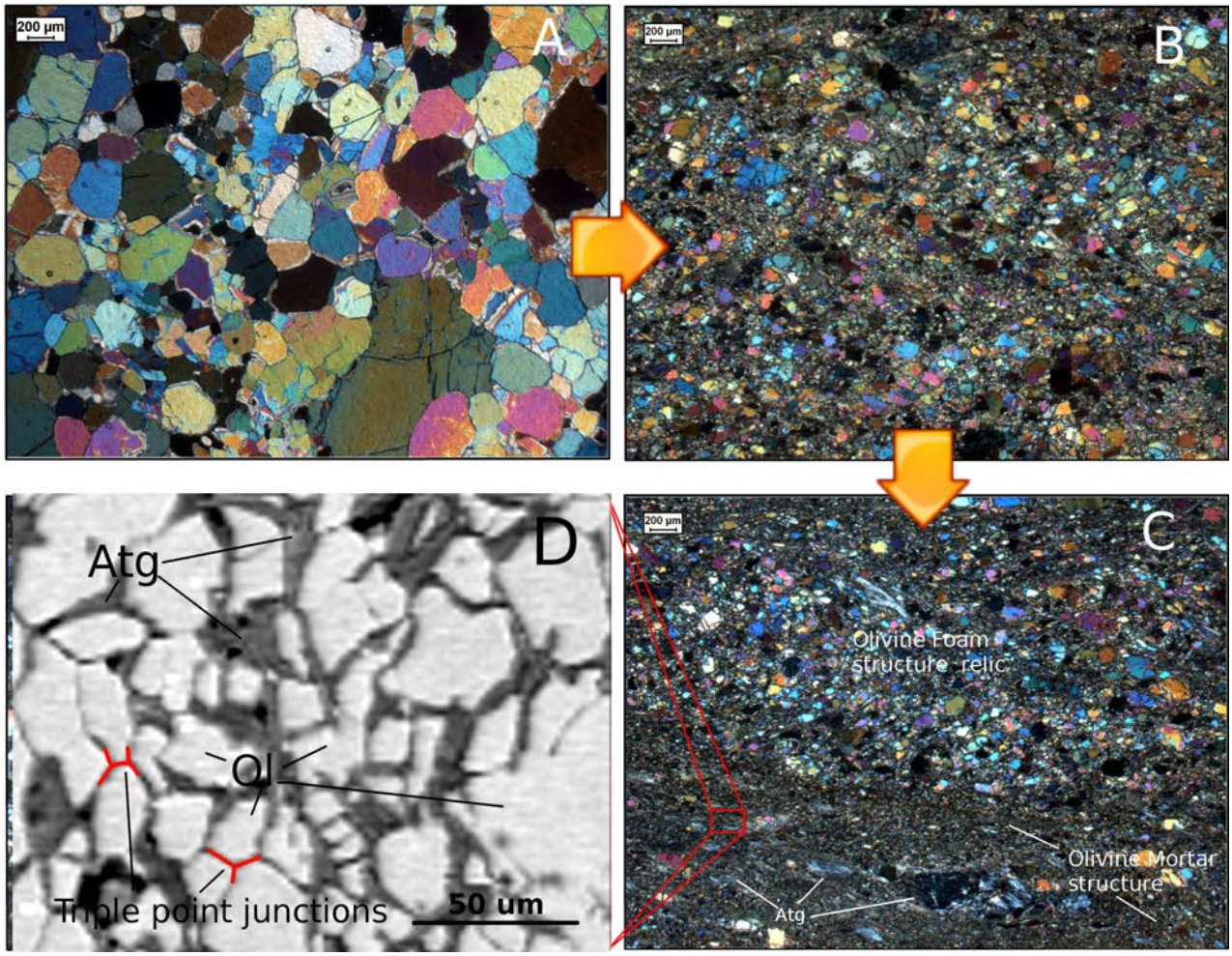

Figure 32: Optical micrograph (XPL) of sample K4 showing incremental development of olivine mortar: A) Perfectly preserved olivine M2 foam microstructure (M2) outside M3 shear zone; B) Original straight grain boundaries of the foam microstructure are strongly deformed and blurred by the formation of new fine grained M3 olivine crystals (1-20 um); C) Anastomosing network of fine grained olivines (M3) surrounding lentiform domains characterized by olivine foam microstructure (Fig. 11C); D)EMP micrograph showing a well developed mortar microstructure in equilibrium with crystals of antigorite (Atg). Note the development of triple point junctions when the olivine crystals are in contact with each other. Grain boundaries appear scallopped and only rarely, straight.

5.3.3 Dislocation substructures

5.3.3.1 Introduction

Deformation in natural rocks is controlled by processes operating on the scale of individual grains (Passchier and Trouw, 2006). The most common deformation mechanism in shallow mantle/deep crust, is plastic deformation through production, propagation and annihilation of dislocations within grains. Dislocations are stress-induced linear defects in the crystal lattice, usually generated around impurities in the crystal. Generation and movement of dislocations occur at high temperature by slip+climb and at low temperature by glide along. For instance, in 2D the slip system [001](100) is defined by the slip plane (100) and the magnitude of the lattice displacement (B = Burgers vector [100]). In 3D the displacement vector [B] pro duces a linear defect, here called the dislocation line (L). The relationship between L and B define the typology of dislocations. If L and B form an angle of 90° the dislocation is called "edge dislocation", whereas when the angle is 0° is a "screw dislocation". During deformation, a concurrent recovery of the stress-induced "defects" might occurs. Such process aims to restore a lower energy configuration within the crystal lattice through annihilation or migration of dislocations. As a result, High Temperature (HT) deformation can be seen as the result of an equilibrium situation between dislocations production and recovery (Passchier and Trouw, 2006). The predominance of one mechanism over the other is dictated by the interlocking of many factors, like temperature, pressure, strain rate, fluids etc... Studying dislocations substructures might, therefore, furnish important constraint on the operating slip system produced by the deformation.

Dislocations cannot be directly observed in normal thin sections with an optical microscope, but TEM is required. However, dislocations can be made visible by an etching technique. In this chapter, results will be presented from an analysis of one decorated sample (K8e), produced by heating in an oxidizing environment (Kohlstedt et al. 1976). This process is particularly useful for olivine, because oxidation causes precipitation of iron oxides dislocations lines, making them visible in the optical microscope.

5.3.3.2 Observations

The decoration method of Kohlstedt (1976) appear to be ineffective on M1 porphyroclast of olivine. Results indicate that crystals belonging to the olivine M2 foam microstructure display well defined patterns of dislocation substructures, whereas relics of porphyroclast (M1) appear dislocation free (Fig.33). This is interpreted to be due to an insufficient time of sample heating, causing iron diffusion and oxidization only in smaller crystals. The reason for this difference decoration microstructures must lie in some intracrystalline defect features or defects because it is not related to a difference in the iron content between the olivine of the two microstructures. Therefore it is possible to describe dislocation microstructures only in olivine M2 foam Type I an II grains . Both typologies of grains share the same internal dislocation sub-structure, putting sever constraints on their petrogenesis.

The most stunning feature is the total absence of equant subgrain structures, in favour of linear structures. The presence of subgrains was expected at least in olivine M2 type I grains because they are mother grains for some of the type II grains (5.3.2.2). Nevertheless, dislocations are mainly clustered in organized walls parallel to (100) (Fig.33). The formation of these intracrystalline dislocation sub-structure is highly irregular and can be divided into three sets of sub-structure:

1. Well developed subgrain walls parallel to (100). The spacing between the subgrain walls is 1-3 um (Fig.34A) and further characterized by a low dislocation density in between the walls
2. Some olivine grains develop dislocation arrays and line directions oblique with respect to the main crystallographic directions (100, 010, 001) (Fig.34B-35B). The latter are formed by equally spaced (1-3 um) subgrains walls sub-parallel to [110] , often interrupted by sudden clusters of tangled dislocations (irregular, long and curvilinear) (Fig. 35B)
3. areas dominated by tangled dislocations in which subgrain walls are not developed (Fig. 34B-35B)

Sub-grains walls parallel to (100) are rare. The (100) subgrain walls are mutually connected by parallel arrays of dislocations, sub-parallel to [100] and interpreted to lie in the plane (001). Additionally, a relevant number of grains does not display any dislocation substructure but it is not know if this feature must be attributed to insufficient time of heating or for other unspecified reasons.

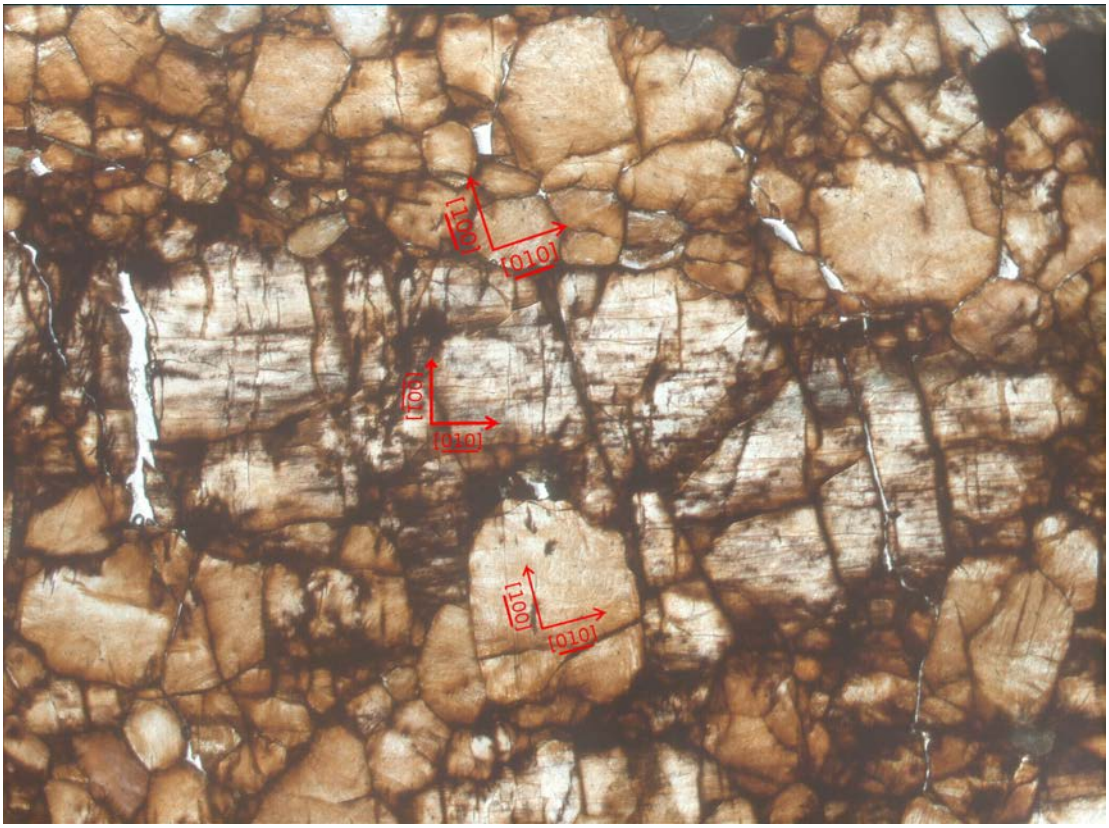

Figure 33: Optical micrograph (XPL) of decorated sample K8e. Red arrows represent main crystallographic directions measured with the Universal Stage. Note the differences in decoration microstructures between M1 olivine porphyroclast and M2 olivine olivine foam microstructure.

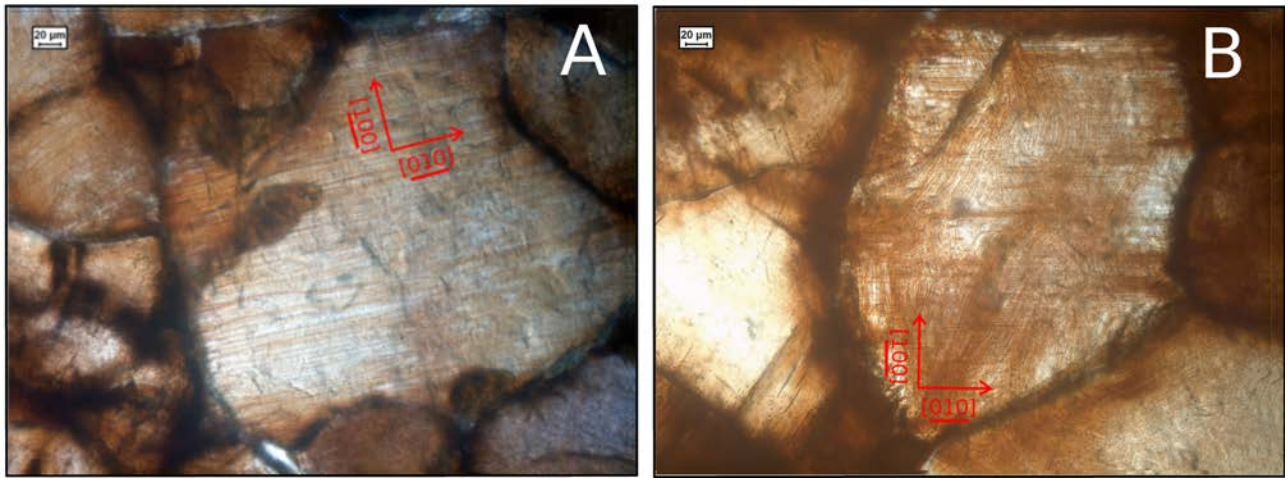

Figure 34: Optical micrograph (XPL) of decorated sample K8e. Red arrows represent main crystallographic directions measured with Universal Stage: A) Olivine crystal characterised by dislocation organized in subgrain walls parallel to (100) ; B) Example of a crystal in which subgrain walls parallel to (100) intersect with an oblique set of dislocations defining walls sub-parallel to [110]. Where the structure is not developed it is possible to observe a low dislocation density.

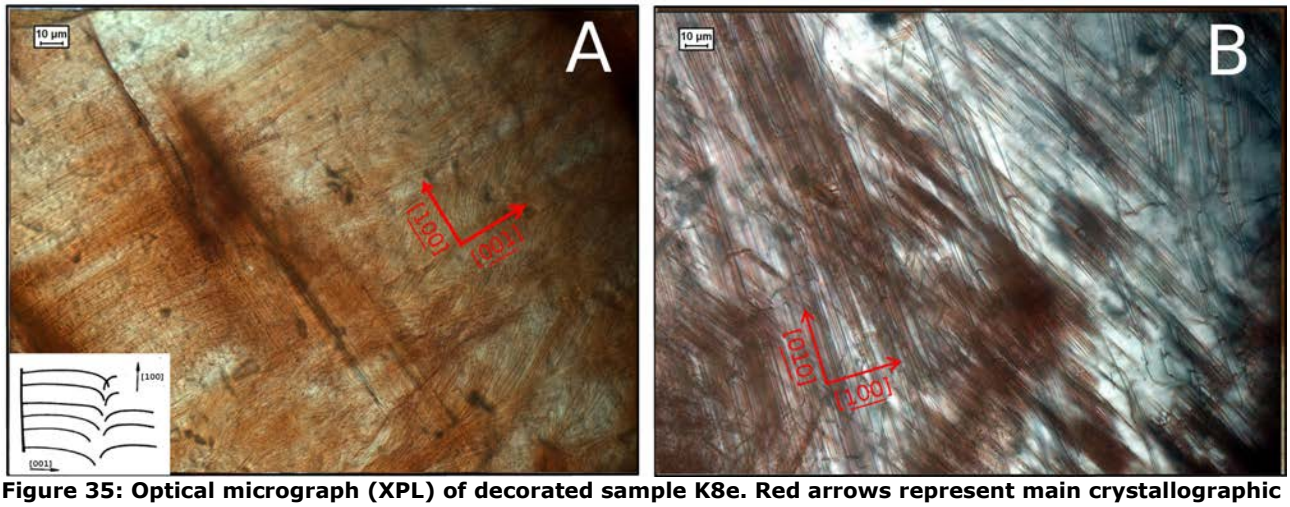

Figure 35: Optical micrograph (XPL) of decorated sample K8e. Red arrows represent main crystallographic directions measured with Universal Stage: A) Rare grains display subgrain walls in (100) connected by parallel running dislocation lines sub-parallel to [100] interpreted to lie in (001); B) Detailed micrograph highlighting relationship directions [100] and [010] and the oblique set of dislocations forming walls sup-parallel to [110]. On the right side it is possible to observe clustering of tangled dislocations.

5.3.3.3 Discussion

During deformation new dislocations nucleate and propagate within the deforming crystal lattice. This causes an increase of the internal strain energy of the crystal. However, at high temperature the occurrence of recovery processes enhance the crystal to lower the dislocation density (i.e. crystal internal strain energy) by reorganising or annihilating dislocations.

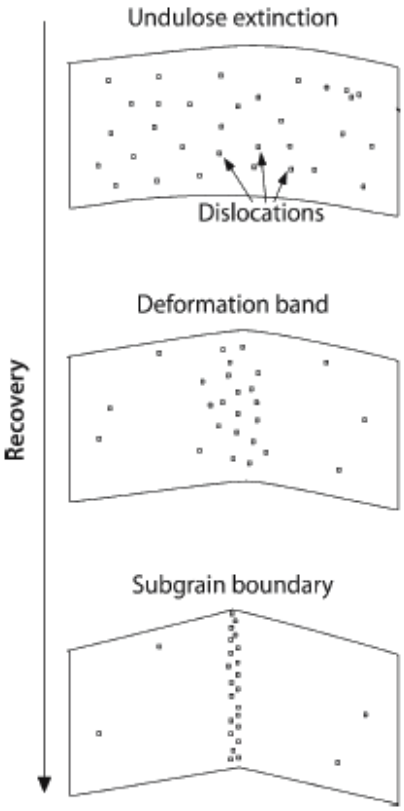

Figure 36: Schematic illustration of the recovery process syn/post deformation. Dislocations are initially randomly distributed over the crystal producing undulate extinction. Increasing amount or recovery re-set dislocations in more organised sub-structures, inclined to reduce the internal energy of the deformed crystal. Recovery occurs by annihilation or dislocations migration in well organised structures called deformation bands and subgrain boundary (tilt wall) (modified after Passchier and Trouw, 2006)

One of the most typical processes, leading to recovery of the crystal lattice, is the migration of dislocations into well organised planar networks. This process can be active during and after deformation, addressing free dislocations (usually irregular, long and curvilinear) into subgrain walls (organised structures formed by straight dislocations) (Fig.34).

Dislocation substructures, described in chapter 5.3.3.2, can be interpreted as the result of recovery processes that were active and/or after deformation. Type I and type II grains share the same style of dislocation substructures, characterized by the presence of 1-3 um spaced dislocation walls parallel to (100) and surrounded by strain free areas (i.e. areas free of dislocations). Reduced spacings between dislocation walls might be the consequence of annealing processes that occurred when temperatures were still high enough to permit dislocations slip and climb. In fact, at HT dislocation creep is expected involving dislocations to glide + climb, whereas at "low" temperature dislocation mobility is strongly limited, allowing dislocation only to glide.

The regular structure (i.e. regular spacing) of the (100) tilt boundaries is in favour of an origin by climb and slip of [100] edge dislocations, during or after deformation. In rare cases olivine M2 foam type II grains develop a subgrain pattern parallel to (001) (Fig.35A) interpreted to be a clear indication of [001] slip-climb direction. From the dislocation sub-structure it appears that the olivine foam microstructure formed (and deformed) by major dislocation glide of [100] dislocation and by a minor component of [001] dislocations. (100) dislocations are clearly predominant and characterized by low dislocation densities in the slip planes (Calon, 1979). These characteristics indicate the importance of climb-controlled processes during the development of the olivine M2 foam microstructure. The extensive migration of dislocations can be seen as a microstructure due to recovery processes by climb/slip of dislocations (Fig.36).

Results are in agreement with the work of Calon (1979), which performed a detailed TEM study on dislocation substructures on dunite of KSP. He found a similar substructure also in M1 porphyroclast , where the dislocation substructure is defined by 1-3 um spaced (100) array of [100] edge dislocations and by rare (001) dislocation arrays (Calon (1979). The intersection of the two dislocation array create equant, tabular subgrains, with sizes measured by Calon (1979): Olivine type I grains have larger subgrains (10-50 um) with respect type II grains (10-20 um). This information can be used in the application of specific paleopiezometric techniques (Chapter 5.3.5.3).

5.3.4 Crystallographic Preferred Orientations (CPO)

5.3.4.1 Introduction

An alternative way to study dislocation motion during plastic deformation is to determine the dominant slip plane and direction from a study of the crystallographic preferred orientation (CPO's). Dislocations propagate preferentially along well defined crystallographic planes and directions depending on specific characteristics of the deformed minerals in combination with the external conditions (T, P, strain rate , fluid pressure etc..) during deformation. An important effect of plastic deformation is the development of Crystallographic Preferred Orientations (CPO) of crystals. Hence, the determination of CPO gives the possibility to infer Burger's vector, slip plane and creep regimes (dislocation vs diffusion) directly from a study of preferred crystallographic orientation of crystals. Common notation to denominate slip systems is : [slip direction](slip plane), where the slip direction is the Burger vector. For more information concerning olivine slip systems, the reader refers to the work of Jung et al (2006).

In order to infer the dominant operating slip system during the formation of the olivine foam microstructure (M2) the olivine CPO has been measured in thin section K8c (Appendix 6) with an Universal Stage mounted on a optical microscope. A discrete number of 200 grains (only olivine foam type II grains) have been measured. Raw data from the Universal Stage have been converted with specific software (MSc thesis Gilio, 2013) in order to be coherent with an E–W lineation (L) and a N-S pole of the foliation that define the M2 foam texture (external reference of the CPO). Result are illustrated in Fig.37.

5.3.4.2 Result

The Universal stage measurements of the type II olivine foam microstructure shows a clear and strong CPO (Fig.37). The main slip direction during deformation can be determined from the axis parallel to the lineation (L). Figure 37, clearly displays a symmetric [100] axis maxima parallel to the E-W lineation (L), implying a dominant [100] Burger's vector. The [010] axes are oriented perpendicular to L, minor scatter occurs in a girdle subnormal to the the lineation. [001] axes show biaxial distribution with a dominant orientation normal to the foliation and a minor parallel to the L. As a result, the CPO of olivine foam microstructure can be interpreted by the activation of the following 2 slip system:

- **[100](001)** is the main operating slip system. A CPO formed by the activation of this slip system is called **E-type CPO** by (Jung et al, 2006)
- **[001](100)** is a minor slip system, termed **C-type CPO** (Jung et al, 2006)

Interesting to notice is the connection between the olivine foam neoblasts and the adjacent parental porphyroclast (Fig.37, Appendix 6). In fact maximum concentrations of M2 crystallographic olivine directions in every plot fall in close proximity with the crystallographic orientation of the main olivine porphyroclast (M1) from which the neoblasts (M2) are interpreted to have formed.

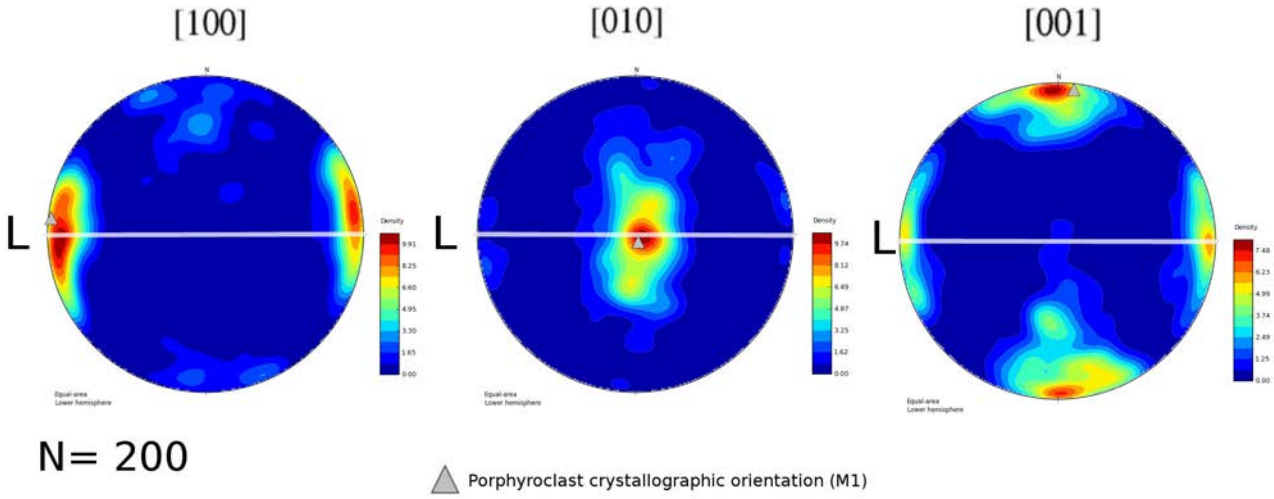

Figure 37: Crystallographic Preferred Orientations (CPO's) of olivine measured in an olivine foam microstructure formed by type II grains (M2) in thin section K8c. The full microstructure is illustrated in Appendix 6. N is the number of discrete grains measured (N=200). Figures (equal area, lower hemisphere projections) are oriented in order to have an E–W lineation(L) and a N-S pole of the S2 foliation (White horizontal line). Crystallographic orientations of 200 grains was manually measured with an Universal Stage applied to an optical microscope and plotted in comparison with porphyroclast. (M1) crystallographic direction (Grey triangle). The CPO displays [100] axes maxima concentration parallel to the E-W lineation, and [001] perpendicular to the foliation indicating [100](001) slip system (E-type). A subordinate maximum is aligned along [001] within the (100) plane, this configuration defines a minor operating [001](100) slip system (C-type). As a result the olivine M2 foam is a microstructure formed by the action of two different slip systems: [100](001) and [001](100).

5.3.4.3 Discussion

The stereographic plots of the olivine M2 foam type II grains reveal a strong CPO's (Fig.37), which define the activation of two sets of slip systems during deformation. The majority of deformation is related to development of an E-type fabric, defined by [100](001) slip. The final microstructure is related also to the formation of [001] dislocations, as indicated by minor slip along [001](100) (C-type slip). CPO is clearly symmetric with respect the foliation and lineation (Fig.37). Lacking of a shear sense, is an indication of deformation under pure shear conditions that are usually related to the development of uniform fabric within peridotites (i.e tectonite). In this regard the CPO's is coherent with observations in the KSP. In fact the olivine foam microstructure (M2) is developed throughout the body without any strain localisation.

E-type slip is interpreted (Jung et al, 2006) to be related to deformation that occurred in coexistence with a fluid. Indeed, experimental deformation studies proved the preferred development of an A-type fabric in a dry environment, whilst E-type CPO's (Fig.38), indicate that deformation took place in the presence of moderate amounts of water (Katayama et al., 2004). Interesting to notice is that Katayama (2004) suggests to relate an E-type fabric to the combined action of A and C-type slip (+ climb).

Other evidences for the activation of E-type and C-type slip during M2 deformation is recorded in olivine M1 porphyroclasts (Fig.25) and in the dislocation sub-structures (chapter 5.3.3.3). In fact, some porphyroclast relics are highly strained and characterized by the occurrence of two sets of regularly spaced kink band boundaries. A first regularly spaced (100-200 um) set is parallel to (100) and is cross-cut by a second set of kink bands (50-100 um) parallel to (001) (Fig.25). Fig.38 is a simplified sketch illustrating relationships between slip system and related kink bands. The slip direction indicated by the Burger's vector and the

slip plane the surface along which the dislocations preferentially move. In order to define in which crystallographic plane the kink bands boundaries (KBB) generate, it is necessary to understand in which plane edge dislocations propagate. The resulting plane can be considered as the KBB. In this regard, E-type slip can form KBB's parallel to (100) and C-type slip parallel to (001) (Fig.38), coherently with deformation structure in M1 olivine porphyroclasts. Another important implication is related to the propagation of screw dislocations on a common plane (010) for both slip systems. This characteristic is extremely important because it allows rotation of tabular subgrains (Fig.25) generated by the intersection of the two kink band systems.

In the last decade several debates and controversies arose around the interpretation of the development of an A-type (or E-type when “wet”) vs C-type fabrics. Most of the discussion circulates around the mechanism that induced the switch from A-type, the most common under mantle conditions, to C-type . As a results olivine C-type fabrics are attributed either to high water fugacity during deformation (Jung et al, 2006) or to UHP conditions with a high confining pressure effect (Jung and Green, 2009). In this master thesis I do not want to discriminate between the two contrasting environmental conditions during the formation of the olivine M2 foam microstructure in the KPS body. That is due to the limited CPO data available in my thesis.

Several future studies might be realized on the KSP, regarding CPO's analyses. Firstly, I suggest to carry out more CPO's analyses, to test the validity of the results obtained with the Universal Stage, possibly on the same typology of rocks (i.e. dunite) and from different locations throughout the KSP body. Secondly, dunite layerS are defined by the typologies of olivine grains, in descending size order, M1 porphyroclasts (5-20 cm), M2 Foam Type I (500-2000 um) and M2 Foam Type II (200-400). Olivine CPO'S has been performed only on foam type II crystals and, therefore, it should be realized on the other typologies of grains, in order to have a broader overview concerning style of deformation.

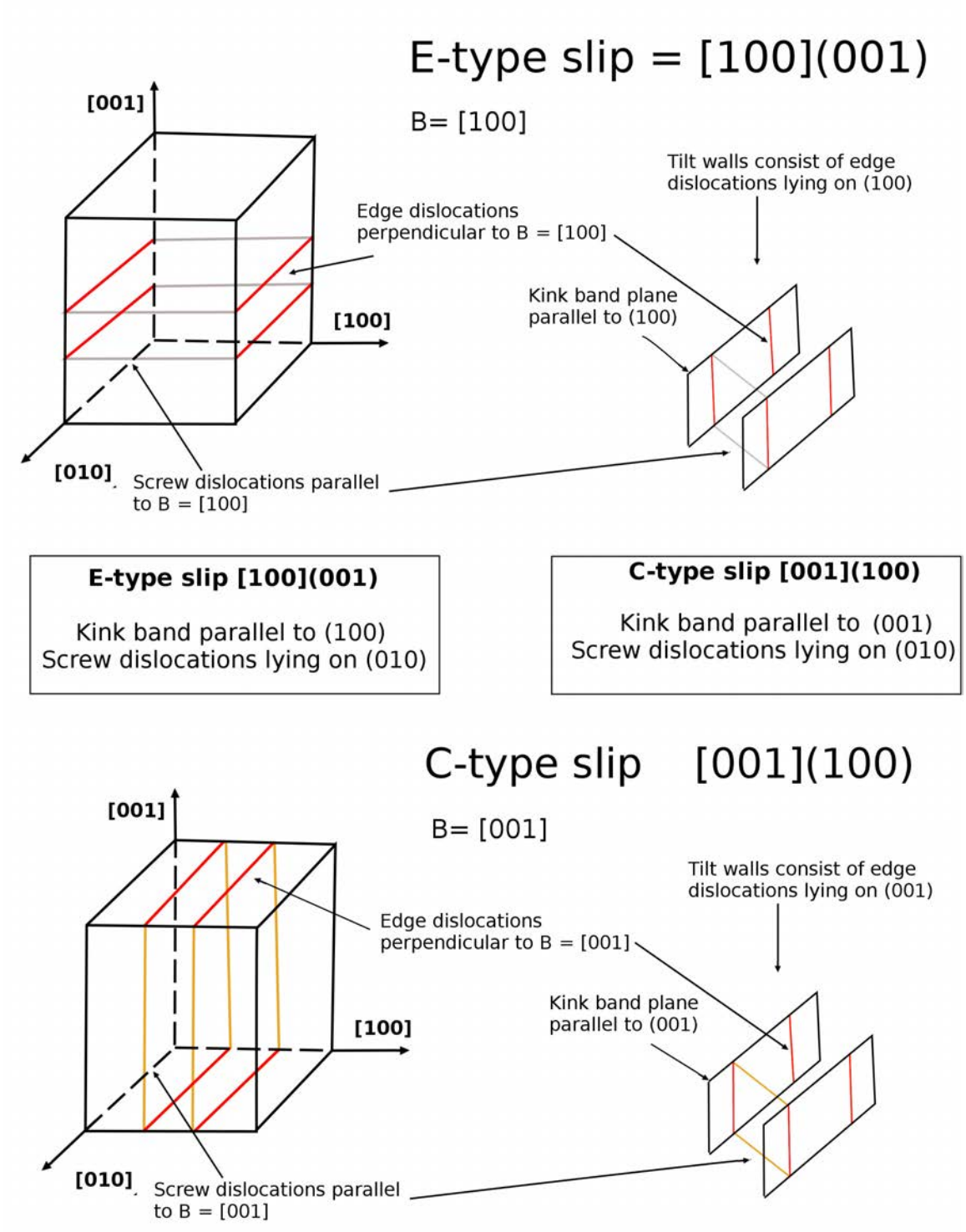

Figure 38: Graphic three-dimensional representation of the two main slip systems operating during M2 deformation in relation to the olivine orthorhombic crystal symmetry. Every slip system is defined by : [slip direction](slip plane). On the right side is presented a sketch of the relationship between dislocations (edge and screw) and KBB. The olivine foam (M2) microstructure main slip system is (001)[100], termed as E-type CPO. [001](100) slip (C-type), has minor influence on the final structure (terminology after Jung et al, 2006).

5.3.5 Discussion

5.3.5.1 Recrystallisation mechanisms

Deforming crystals can reduce their internal strain energy by (1) annihilation and migration of dislocations (chapter 5.3.3.3), (2) by the production of neoblasts having lower internal energy, (3) by the migration of grain boundaries or by (4) a combination of the mentioned processes (Fig.39). Process (2), termed dynamic recrystallization (DRX), is caused by a stress-induced re-crystallisation process. During DRX two end-member processes are responsible for the formation of new grains: subgrain rotation (SGR) and grain boundary migration (GBM) (Passchier and Trouw, 2006).

SGR (Fig.39) involves progressive crystallographic rotation of subgrains within grains without significant migration of the grain boundary. During deformation an increasing number of dislocations migrate, through the deforming crystal, towards subgrain walls accommodating part of the strain. Such process induces a progressive lattice rotation between the subgrains and the host parental grain. When the misorientation is > 5-10° a new grain is formed (Passchier and Trouw, 2006). Furthermore, characteristic orientation relationships between the starting grain and the new grains can be recognized when SGR (or dislocation creep) is the main process of deformation (Lloyd et al., 1997).

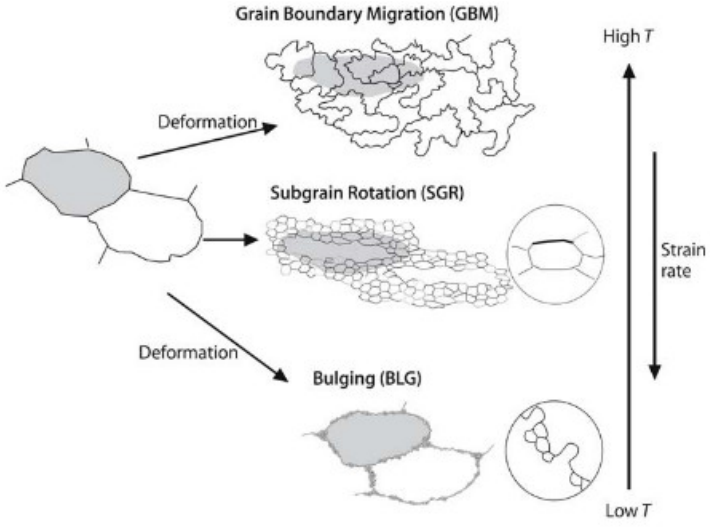

Figure 39: Three main mechanism of dynamic recrystallisation: GBM, SGR and BLG. Grey shaded area defines relationship between microstructures domains, before and after deformation. The SGR microstructure can be correlated with the olivine M2 foam microstructure (Appendix 6). BLG microstructure is similar to mortar structure (Fig.31). (modified after Passchier and Trouw, 2006)

During GBM (Fig.39) the thermodynamic driving force is the reduction of the stored strain energy related to dislocation density inside old and new grains. In fact grains with lower internal strain energy grow at the expense of those with larger dislocation density (Fig.39-40). This mechanism is particularly effective at high temperature (>T_m). At low temperature the deforming mechanism is slightly different because grain boundary mobility is strongly reduced but grain boundaries can locally bulge into crystal areas characterised by higher dislocation densities. Isolation of the bulge is achieved by the development of subgrain walls, followed by increasing deformation causing progressive misorientation of the bulge area leading to the formation of new grains (Fig.40A). This process is generally named grain boundary bulging (BLG). The final product of BLG are new small grains, internally strain-free and clustered along the former boundaries of coarser crystals (Fig.39-40). GBM and BLG are mainly driven by diffusive processes (Diffusion creep). Often coupled with DRX, annealing processes actively influence the final microstructure. The presence of intracrystalline or inter-crystalline fluid/melt accelerate the annealing processes.

The Olivine M2 foam microstructure

Clear decrease in grain size, from the starting M1 olivine porphyroclast sizes (5-20 cm) to type I (500-2000 um) and II (200-400 um) foam grains, is attributed to incremental DRX. This hypothesis is supported by microstructural observations and a strong M2 olivine foam

CPO'S (Fig.37). The majority of deformation is related to development of an E-type fabric, ([100](001) slip) but the final microstructure is also influenced by C-type slip ([001](100)). Both fabric are interpreted to be formed by HT dislocations creep processes. The deformation mechanism can also produce the observed KBB's in olivine M1 porphyroclasts as well as the olivine M2 foam microstructure (Chapter 5.3.3-5.3.4). As a result olivine M2 foam grains are interpreted to have formed mainly by HT dislocation creep mechanisms ([100](001) and [001](100) slip) but with a strong component of diffusion creep related to annealed structure

Mortar structure (M3)

The olivine mortar structure (M3) is morphologically different from the above described olivine foam microstructure (M2). The fined grained (10-50 um) M3 neoblasts preferentially form along grain boundaries of strained M2 olivine foam crystals. The microstructure thus clearly indicate high strain gradients at grain edges, which contrasts with the low strain gradient inside the cores of the deformed grains. Consequently new grains can be produced either by SGR and/or BLG. Further investigations are required in order to define which recrystallisation mechanism was the most t dominant during deformation.

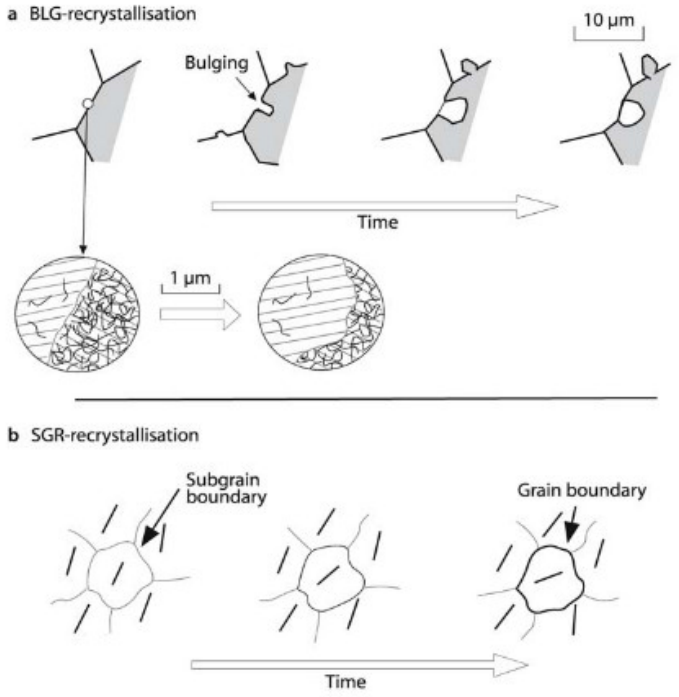

Figure 40. Cartoon illustrating the two recrystallisation mechanism that can form new grains: a) Bulging recrystallisation (BLG). Bulging is triggered by a gradient in dislocation density and subsequently develops into new grains. b) Subgrain rotation (SGR) recrystallisation. Dislocations progressively migrate into subgrain walls causing rotation until new grains are formed (misorientation >5-10°). *Bars* within grains represent lattice orientation (after Passchier and Trouw, 2006)

5.3.5.2 Water content

The size of dynamic recrystallized grains is considered as one of the best tools to reconstruct paleostress magnitudes. Direct correlation between the state of stress, and grain size is extensively studied, but several recent studies demonstrate the importance of a new parameter: water (Shimizu, 1998; Jung and Karato 2001). In fact experiments have demonstrated that water may affect dynamic recrystallisation mechanisms and the size of grains. On one hand, experiments (Jung and Karato, 2001) have demonstrated that "dry" samples preferentially deform through SGR, with widespread formation of well developed subgrain boundaries, whereas "wet" samples subgrain development is slowed down and assisted by GBM. A high water content accelerates dislocation recovery processes and GBM, preventing accumulation of high amounts of strain within grains (i.e. lowering dislocation density and related subgrain wall formation).

On the other hand, recrystallised grain size is strongly related to water fugacity (Fig.41A). At constant stress but variable water contents grain size can thus vary several order of magnitude. Hence, it becomes necessary to justify the amount of water present during deformation in order not to over or underestimate the effective deviatoric stress during deformation.

Olivine foam microstructure (M2)

In the KSP multiple indicators can demonstrate a moderate amount of water during development of the olivine foam microstructure (M2):

- Amphibole and chlorite belong to the stable mineral assemblage that is associated with olivine Foam type II grains (Fig.17)
- Tabular shaped olivine grains, present in the microstructure (Fig.29), are related to presence of water along grain boundaries, which triggered preferential growth parallel to low index directions (Chapter 5.3.2.2)
- The olivine foam microstructure is characterized by the presence of a strong [100] (001) fabric, called E-type (Fig.37). Its development is inferred to be related to moderate quantities of water (Katayama, 2004)

The experiments of Jung and Karato (2006) were performed at a constant temperature of 1200 °C. Attention should be paid because the inferred temperature for the formation of the olivine foam microstructure (M2) is ~800°C (Chapter 5.2.3) and a direct correlation cannot be made. Despite this limitation, I assume that a quantitative water estimate for E-type fabrics can be equally used at 800°C, because deformation structures described in the experiments of Jung and Karato (2001), perfectly match the fabric observations decribed in this thesis (Chapter 5.3). The authors denote that E-type fabrics are characterized by the formation of linear dislocation structures organized into tilt walls parallel to the (100) plane, with rare subgrain boundaries development in other directions. Such observations are consistent with the olivine foam microstructure dislocation substructures, mainly organised in subgrains walls parallel to (100) (chapter 5.3.3).

As a result, it is inferred that the olivine foam microstructure (M2) developed in the presence of a fluid phase. Future research may define the origin of the fluids (intracrystalline or external source) with detailed REE analysis.

Mortar structure (M3)

The mineral assemblage of the olivine mortar microstructure consist of olivine, antigorite, talc, tremolite and chlorite (Chapter 5.1). Such minerals are a clear indicator of high water fugacity during deformation.

5.3.5.3 Paleo-piezometer

The olivine microstructure described in the previous chapter (5.3.5.2) can be used for paleopiezometric analysis. In fact the dunite layers are characterized by extremely high mass volume of olivine (>95%) and can be considered as monomineralic rocks in which olivine rheology is not influenced by secondary phases. The KSP microstructure provides special opportunities to estimate paleo-stresses based on the induced recrystallized grain sizes (Van der Wal, 1993). The reader must be conscious that the recrystallized grain size does not only depends on imposed paleo-stresses, but is also dependent on other processes like annealing and GBM. In the following section, the measured grain size for M2 (200-400 um, Chapter 5.3.2.2) will be used as originally measured because annealing processes did not significantly alter the size of M2 foam neoblasts (Fig.30).

Olivine porphyroclasts (M1)

No precise constraint can be made concerning the magnitude of the flow stress and PT conditions for the M1 coarse-grained assemblage. Their incredible large M1 grain size (up to 20 cm) clearly indicate a mantle rock developed (or recrystallized) under low deviatoric stress (<1MPa) and the presence of an internal chromite foliation (S_i) implies a tectonic origin.

The onset of porphyroclasts deformation is assumed to start at a maximum temperature of 870±20 °C, inferred by Al-Cr exchange thermometer for Ol-Sp (Chapter 5.2.3).

Olivine foam microstructure (M2)

The re-crystallized grain-size has been used to give constraints about the magnitude of the differential stress during formation of the olivine foam microstructure (M2). Grain sizes (Table 10) relative to olivine M2 foam grain type I-II are used to infer paleostress, strain rate and temperature of formation in the following steps:

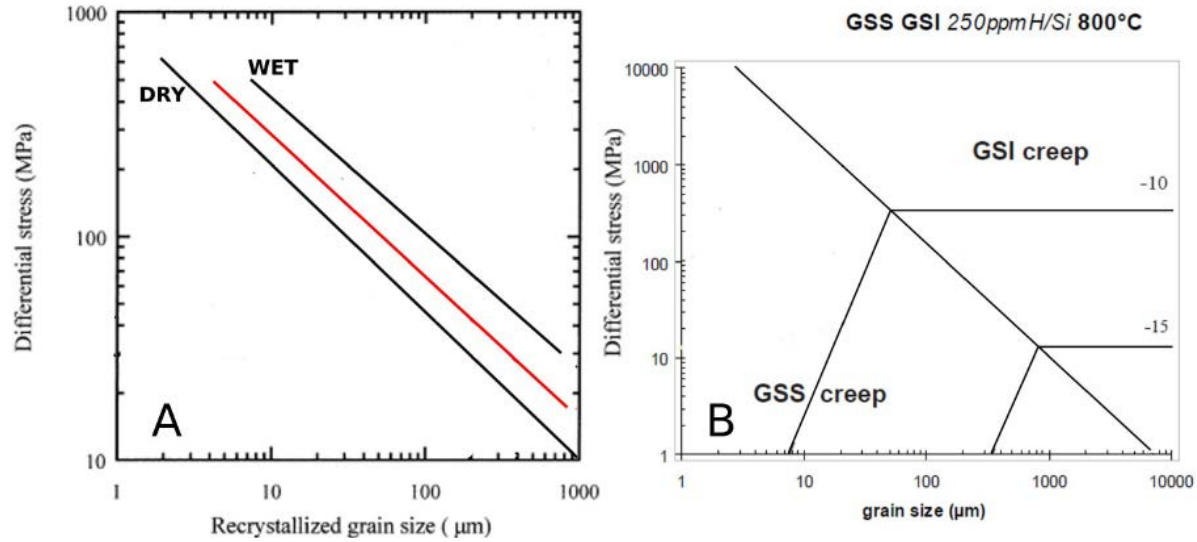

Figure 41: A) Stress vs recrystallized grain size diagram. Solid black lines representspiezometer for "dry" (van der Wal et al, 1993) and "wet" conditions (Jung and Karato, 2001).Red line is an intermediate piezometer, arbitrary located, representing deformation at mediumwater fugacity (modified after Jung and Karato, 2001). B) Deformation mechanism map forolivine in presence of medium amount of water (250 ppm H/Si) at 800°C (stress vs grainsize). Strain rate range from from 10^{-15} s-1 to 10^{-10} s-1 (modified after Palasse, 2008).

Type I olivine foam grains (Fig.27)	500-2000 um
Type II olivine foam grains (Fig.29)	200-400 um

Table 10: Grain size for olivine foam structure divided in Type I and II grains.

1. Typical piezometers for "dry" olivine (van der Wal et al, 1993) and "wet" olivine (Jung and Karato, 2001) can not be directly applied because they represent end member conditions and do not reflect the "moderate" water content of KSP. Therefore, an intermediate piezometer for moderate amount of water has been arbitrary constrained (Fig.41A) and applied to the olivine foam microstructure with the necessary precautions and approximations. Results indicate that Type I olivine foam grains (500-2000 um) and Type II olivine foam grains (200-400 um) were deformed with a differential stress of, respectively, 10-20 ± 5 Mpa and 30-42 ± 5 Mpa (data from Fig.41A). Good correlation can be traced with stress estimates (7-50± 5 Mpa) coming from application of an additional piezometer (Fig.42), based on subgrain size (10-50 um for olivine foam microstructure).
2. The paleostress values obtained are plotted in a deformation mechanism map computed for moderate water content (250 ppm H/Si) at 800°C (Fig.41B). As a result the strain rate occurring during formation of the olivine foam microstructure is in the order of 10^{-13}-10^{-14} s^{-1} (Fig.41B).
3. One of the greatest advantages of computer programs dealing with deformation mechanism maps is the possibility to graphically explore various options just by holding constant or vary main parameters, like temperature or strain rate. In this regard, stress estimates and related grain size were plotted in Fig.42 in order to explore temperature variability at constant strain rate of 10^{-13} s-1 (representative mean strain rate value for the formation of olivine M2 foam microstructure). From Fig.42 it can be seen that, Type II grains (500-2000 um) were deformed in relation to a stress of 10-20±5 Mpa at 830±20 °C, whereas Type II grains (200-400 um) stress estimates are in the order of 30-42±5 Mpa at 750±20°C (Fig.42). Also from Fig.42 it can be seen that olivine Type II olivine foam grains box (C in Fig.41) lies precisely at the boundary between dislocation creep and diffusion creep. Type II olivine foam grains are interpreted to have formed mainly by HT dislocation creep mechanism ([100](001) and [001](100) slip) but with strong diffusion creep component related to formation of the annealed microstructure.

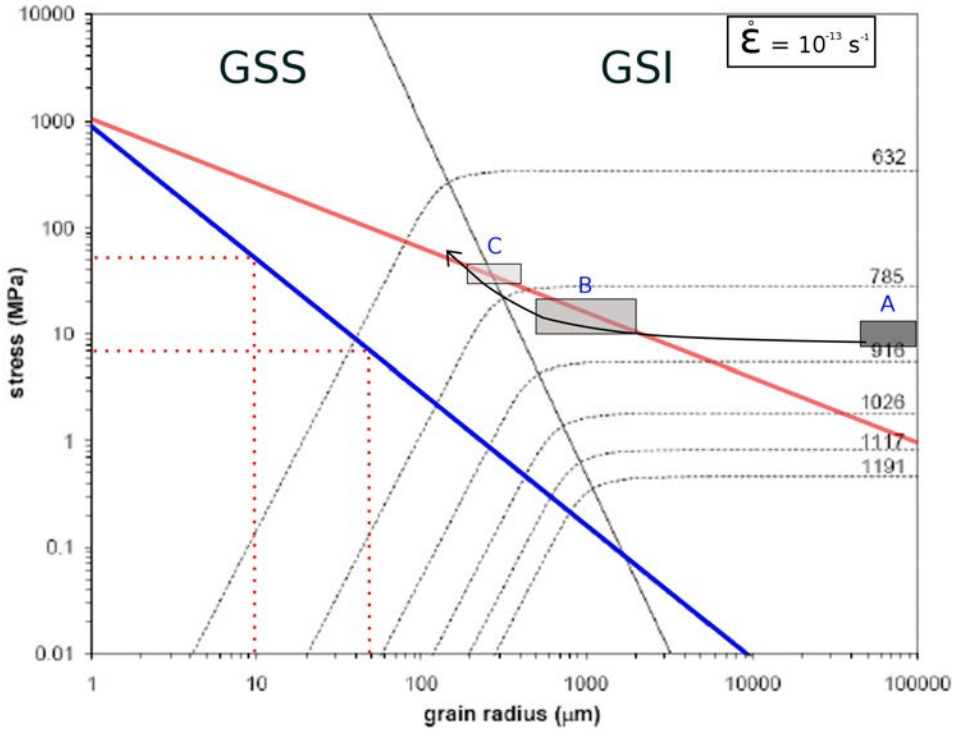

Figure 42: Deformation mechanism map for olivine (constant strain rate 10^{-13} s-1) exploring temperature variations (black dotted lines) between 630-1200°C. Black line is the mechanism boundary and the blue solid line is a piezometer based on subgrain size (den Hartog, 2008), whereas red solid line is a grain size piezometer for medium water content (Fig. 12A). Dotted red lines are size of subgrain in olivine foam microstructure (10-50 um) defining a stress of 7-50 ± 5 Mpa during M2 deformation. Grey areas are the inferred conditions during M2 deformation: A) Olivine M1 porphyroclasts were stable at minimum temperature of 870±60 °C before the onset of M2 deformation (Chapter 5.2.3); B) Type I grains (500-2000 um) deformed with a stress of 10-20±5 Mpa at 830±20 °C; C) Type II grains (200-400 um) deformed with a stress of 30-42±5 Mpa at 750±20°C (modified after MSc thesis of den Hartog, 2008).

Olivine mortar microstructure (M3)

The piezometer for "wet" conditions of Jung and Karato (2001) was applied to the olivine M3 mortar microstructure. Recrystallized M3 grain size (10-50 um) is related to paleostress of 150-300 Mpa. Concerning the validity of this stress estimate only speculations cab be made because in this thesis it has not been possible to define in detail which mechanism was responsible for the grain-size reduction. Field observations clearly indicate the development of an olivine M3 mortar microstructure in narrow shear zones but it is not known which mechanism was mainly responsible for the strain localisation (Chapter 5.3.5.1). The olivine mortar microstructure requires additional and specific studies before unravelling with certainty the dominant mechanism. Therefore I suggest further and more specific studies on the olivine M3 microstructure before considering the stress obtained reliable.

5.3.6 Conclusion

The main results of the microstructural study are summarized in Table 11 and lead to the following conclusions:

- Olivine M1 porphyroclasts grew over a tectonite foliation (S_i) under low deviatoric stress (σ <1MPa) and probably at high temperature
- The olivine M2 foam microstructure was formed in a Km-scale shear zone. The indicating physical conditions of: σ=7-42±20 Mpa; T=750-830°C; ε= 10^{-13}-10^{-14} s_{-1}. The dominant mechanism of deformation was HT dislocation creep that allowed new grain formation by SGR assisted by GBM. Olivine CPO, dislocation substructures and KBB orientations are consistent with a major development of an E-type slip and minor C-type.
- Mortar structure formed in a metric to centimetric-scale shear zone at 550-600°C in presence of high water content.

	M1	**M2**	**M3**
Fabric/Grain size	Coarse (5-20 cm)	olivine foam microstructure (200-2000 um)	olivine mortar microstructure (1-50 um)
T (°C)	>870	750-830	550-600
Deviatoric stress (MPa)	≤1	7-42	150-300??
Water content		Medium	High
Strain rate (S_{-1})	-	10^{-13}-10^{-14}	-
Shear zone scale		kilometric	metric

Table 11: Summary of conditions operating during the formation of olivine M1, M2 and M3 texture

6 DISCUSSION

6.1 Melting estimate

The extraction of mafic and ultramafic melts from fertile lherzolitic protolith produces a depleted restite, whose composition is strongly determined by the geo-tectonic setting, PT conditions and amount of melt extracted. In order to estimate the degree of partial melting it is necessary to compare the major elements and modal compositions with experimental residue trends (Fig.43A; Walter, 1998). In Fig.43A the Mg# of some Caledonian peridotites is plotted against modal olivine. It can be seen a distinct relationship between the bulk rock composition of Kitttelfjäll and Almklovdalen dunites. The latter is one of the most studied ultramafic bodies in the Western Gneiss Region (WGR) in Norway and it has been modelled as residues after very high degrees (>60%) of melt extraction at high pressure (5–7 Gpa) (Beyer, 2006).

The extreme refractory nature of dunites (Red dots, Fig.43A), with high Mg# (0,92-0,93) and modal olivine (96%), place the Kittelfjäll dunites at the extreme end of the pyrolite residue trend at depth of ~3 Gpa, with rough extrapolation of the degree of partial melting in the order of 50-60%. In contrast, Kittelfjäll harzburgite (Blue dots, Fig.43A) composition plots close to the oceanic trend at 2 Gpa and is characterized by roughly 35% of melting.

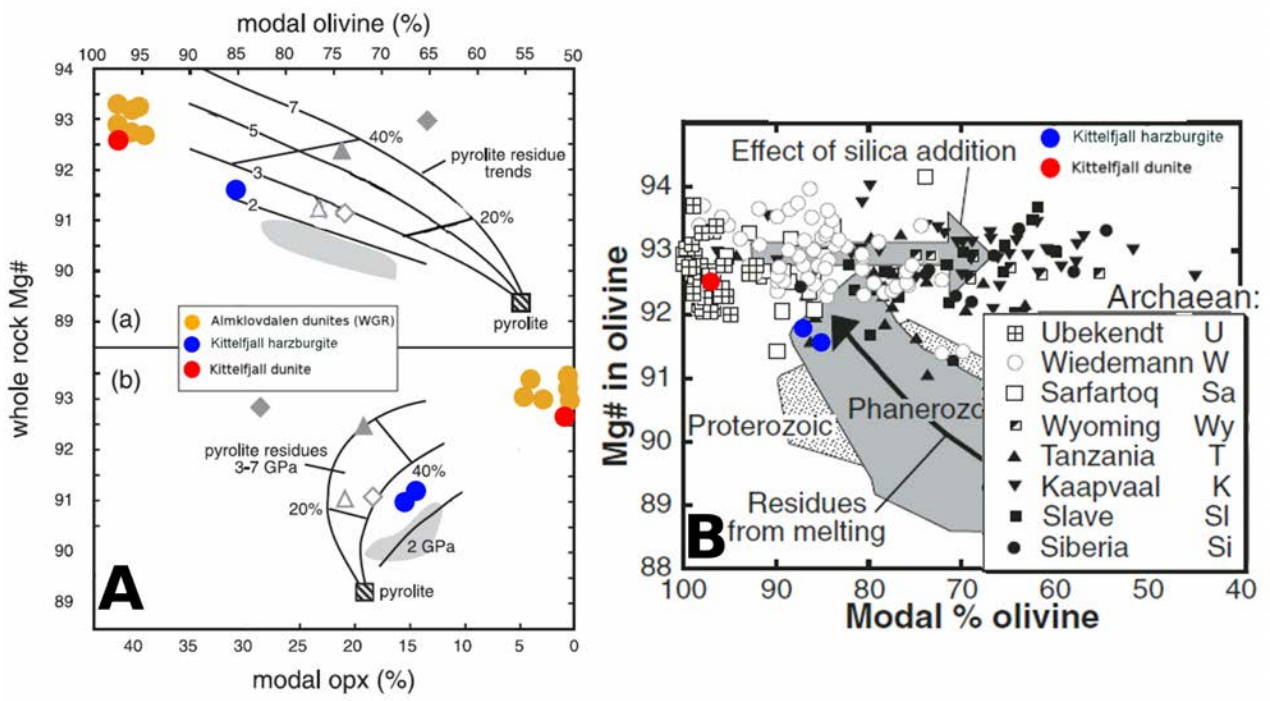

Figure 43: A) Whole rock Mg# vs modal olivine (a) and orthopyroxene (b) graphs showing residue compositional trends for various degrees of melting from pyrolitic mantle compositions (Walter, 1998). Number labelling each trend represents % of melt and pressure (Gpa). Triangles represent peridotites from Kaapvaal and diamonds peridotites from Siberia. Circles are indicative of peridotites from the Scandinavian Caledonides. Grey field is the area representative of ophiolites and oceanic peridotites. (Modified after Walter, 1998). B) Mg# vs modal olivine diagram illustrating effect of silica addition on ultra-depleted peridotites of Archean age for various cratonic peridotites. In this regard, Kittelfjäll harzburgite can be seen as the product of refertilization by Si-rich fluids/melts (modified after Bernstein et al, 2007).

Distinct differences in composition and degree of partial melting between harzburgite and dunite can not simply explained by a local differences in the amount of melt extraction. The most logical explanation is to consider an initial strong depletion, that already formed highly

depleted refractory dunites (Mg#~93), followed by re-fertilization by Si, Al, Fe and Ca rich melts or fluids. This hypothesis is supported by the similar contents of TiO (Table 3, Chapter 5.2.1.2) and NiO (Fig.11) in dunite and harzburgite. Ni and Ti are two elements that commonly are not transported in fluids or melts and therefore their contents are strongly connected to initial depletion. A 20-30% difference in degree of partial melting should result in a greater Ni and Ti depletion in dunite rather than in harzburgite. Hence, the compositional layering, alternating dunites and harzburgites, might be considered as the product of refertilization processes rather than a primary mantle feature. This hypothesis is fully supported by the work of Bernstein et al (2007) which interpret opx-rich peridotites in cratonic areas as the result of the interaction of Si-rich fluids/melts with ultra-depleted, opx-poor dunitic protolith (Fig.43B). Additionally, the idea of an Archean highly depleted peridotite, refertilized during Proterozoic has already been described in detail in the WGR. The Almklovdalen peridotite (Beyer, 2006) in the southern part of Norway (WGR) and the Friningen garnet peridotite (Brueckner et al, 2004; Janak et al, 2012) in the SNC are splendid examples. Both peridotites are characterized by layers of highly depleted dunites and re-fertilized garnet harzburgites/lherzolites (Table 11) formed during the Proterozoic by the intrusion of basic dikes. In these ultramafic rocks, compositional layering is generally interpreted as the result of melt/fluid percolation after initial high degree of partial melting.

In this context, Kittelfjäll spinel peridotite origin and evolution can be associated with the peridotites aforementioned, but further analyses are required. In order to fully prove this hypothesis, a detailed trace element study, with special emphasis on REE differences between dunites and harzburgites is necessary/required.

6.2 Protolith origin

6.2.1 Archean peridotite

The bulk rock composition of peridotites is strongly influenced by the degree of depletion which depends on the tectonic settings of origin (Arai, 1994). Hence it is possible to identify the peridotite protolith origin through a detailed chemical investigation and a comparison with known tectonic settings. Most useful indicators are forsterite content of olivine (Mg# = Fo content) and spinel Cr# because their variability is linked to the tectonic setting in which partial melting occurred (Fig.44 A-F). In this regard, Kittelfjäll dunite layers have an uncommon composition, only comparable with highly depleted cratonic peridotites of Archean age (Fig.44 F). Mg# of olivine (~ 93) and modal olivine (~ 96%) positively correlate Almklovdalen and Kittelfjäll dunites with mantle xenoliths coming from Greenland, Slave and Tanzanian Craton (Fig.45B).

The possibility that the KSP peridotite is an highly refractory restite, resulting from extensive partial melting in the Archean is confirmed by the high degree of partial melting. In fact, during the Archean, heat flow was about three times greater than in modern times, allowing massive melting (> 35%) at great depth (3-7 Gpa), with extraction of komatiitic and picritic melts from highly depleted mantle peridotites (Walter, 1998). During Proterozoic and Phanerozoic times, the earth heat flow of the earth steadily decreased causing a change in chemical composition (Fig.45A) due to lowered temperature conditions and minor melt extractions. As a result, the only way to justify 50-60% partial melting of peridotite is to consider extensive partial melting during Archean. This idea is reinforced by geochemical evidences illustrated in Fig.44 (G) and Fig.45, in which a positive correlation cab be seen between peridotites suites of Archean origin and the Caledonian Kittelfjäll and Almklovdalen dunites. Additionally, KSP bears surprising geochemical affinities (Fig.43-44-45; Table 12) with the Almklovdalen dunites in the WGR (Beyer, 2006), whose Archean origin is certified by Re-Os dating. In fact, dunites yield Archean model ages and Proterozoic re-fertilization ages that produced layers of garnet peridotites (Beyer, 2006).

Similar evolution can be proposed for the Kittelfjäll spinel peridotite, even though the final

confirmation should come from Re-Os dating on sulphide within M1 olivine porphyroclasts.

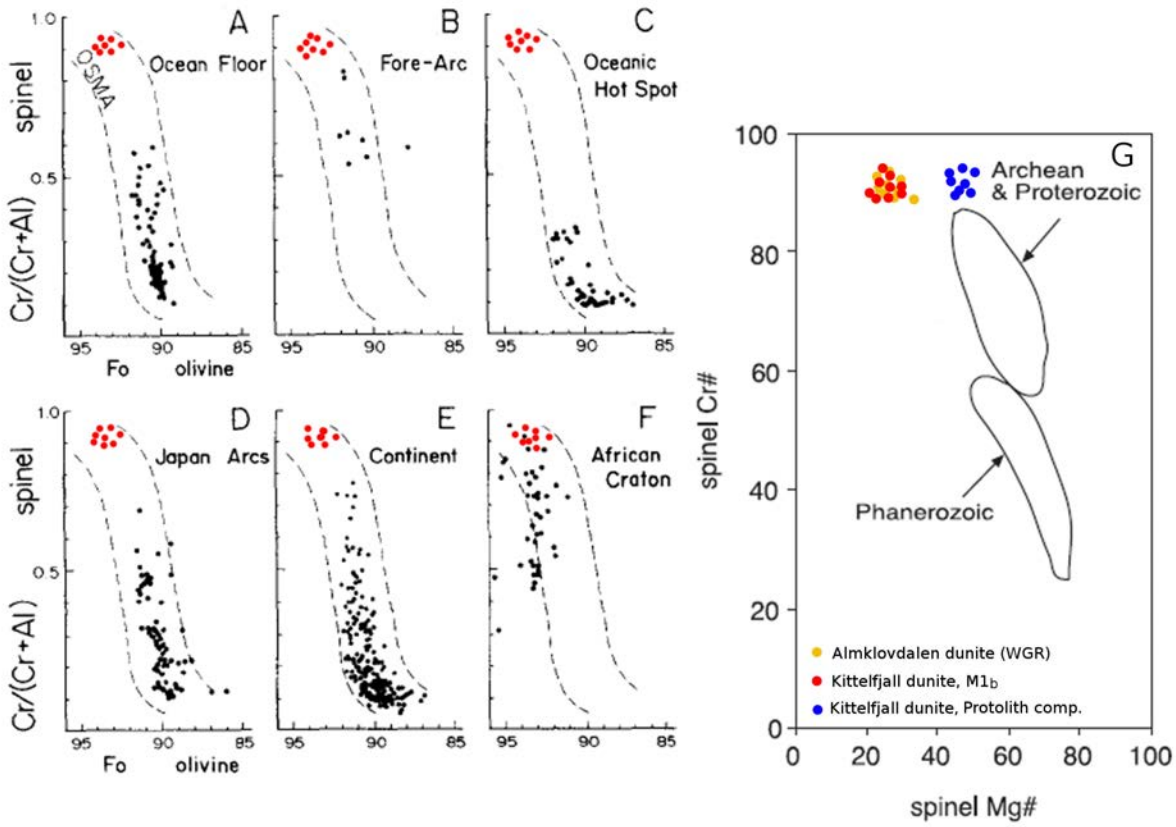

Figure 44: (A-F) Fo (olivine)-Cr# (spinel) relationships of different tectonic settings compared with Kittelfjäll spinel peridotite (Red) (modified after Arai, 1994). (G) Cr#-Mg#(*100) spinel compositional variation diagrams comparing spinel Cr# (89-94) and Mg# (20-28) of Almklovdalen dunites (Orange) with Kittelfjäll dunites spinel Cr# (89-96) and Mg# for M1a (protolith comp. 45-55) and M1b (21-27) assemblages (Chapter 5.2.1.2) (modified after Beyer, 2006).

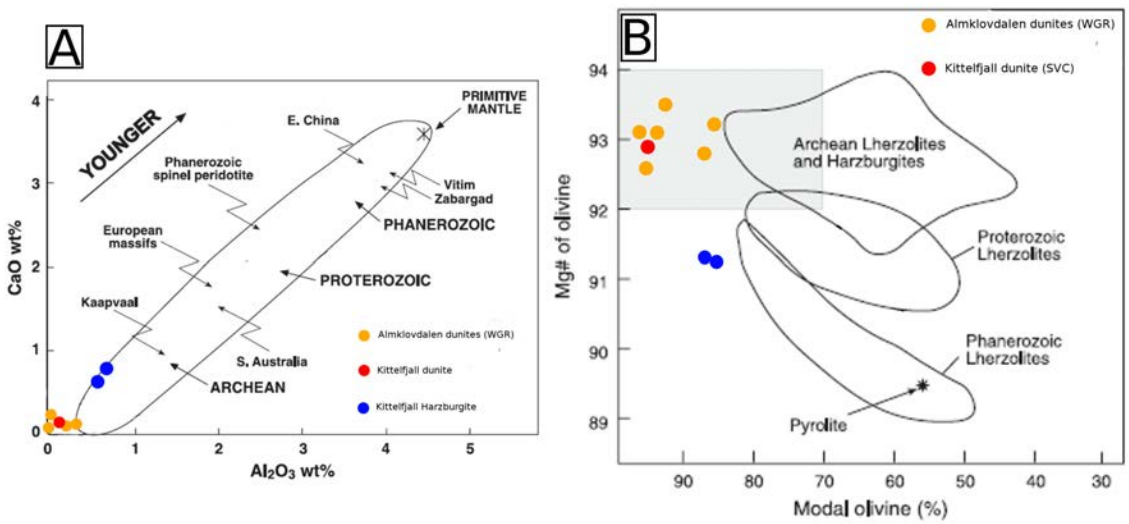

Figure 45: A) Plot of Al2O3 vs CaO showing a depletion trend varying in time (Archean-Phanerozoic). Plotted composition for Almklovdalen (after Beyer, 2006)) and Kittelfjäll dunites and harzburgite (Chapter 5.2.2) indicate a positive dunite correlation with Archean peridotites . B) Mg# olivine vs modal olivine plot showing Phanerozoic, Proterozoic and Archean fields. Grey area represents the field in which are plotted mantle xenoliths from Wiedemann Fjord (Greenland; Bernstein et al., 1998), the Slave Craton (Boyd & Canil, 1997), the Tanzanian Craton (Lee & Rudnick, 1999) and Greenland (Bernstein & Brooks, 1999). Plotted composition are from Almklovdalen (Beyer, 2006) and Kittelfjäll dunites (Mg# ol (~93); mode ol 96%)-harzburgites (Mg# ol (~91,5); mode ol ~85%) (modified after Beyer, 2006).

6.2.2 Sub-Continental affinity

Data presented in this thesis demonstrates that the Kittelfjäll spinel peridotite has sub-continental mantle affinity rather than sub-oceanic. This consideration is fully supported by the following observations and interpretations:

1. Chemical composition

A mutual comparison of chemical compositions of peridotite bodies throughout the world is a useful tool to infer their provenance. In this respect the chemistry of KPS can be compared to other ultramafic rock suites of widely accepted origin (Table 12). Fig.46 shows olivine Mg# and spinel Cr# ranges for a wide range of ultramafic rocks in different geological and tectonic settings (modified after Friend et al., 2002) in relation to the Olivine Spinel Mantle Array (OSMA) of Arai (1994). Two clear depletion trends defined by different olivine Mg#, neatly separate cratonic (sub-continental affinity Mg#>90) from abyssal (sub-oceanic affinity Mg#<90) peridotites. Fig.46 clearly illustrates that the spinel Cr# by itself can not used as a discriminant geodynamic indicator but it has to be coupled with olivine Mg#. The KSP are characterized by olivine Mg# 92,5-93,6 and spinel Cr# of 89-96 for M1 assemblages and 70-80 for M2 assemblages. Such numbers (Table 12) are comparable with cratonic peridotites, and more specifically with the orogenic peridotite massifs of Almklovdalen in the WGR (Beyer et al, 2006) and with a suite of ultramafic xenoliths representing ultra-depleted mantle underneath Greenland (Bernstein et al, 1998,2006). The positive feedback points towards a sub-continental origin of the KSP. In addition, olivine Mg# is a successful geodynamic indicator that can be used in future studies to discriminate between orogenic peridotite massifs (olivine Mg#>90) and ophiolitic peridotites (Olivine Mg# <90) (Fig.46; Iyver et al, 2007).

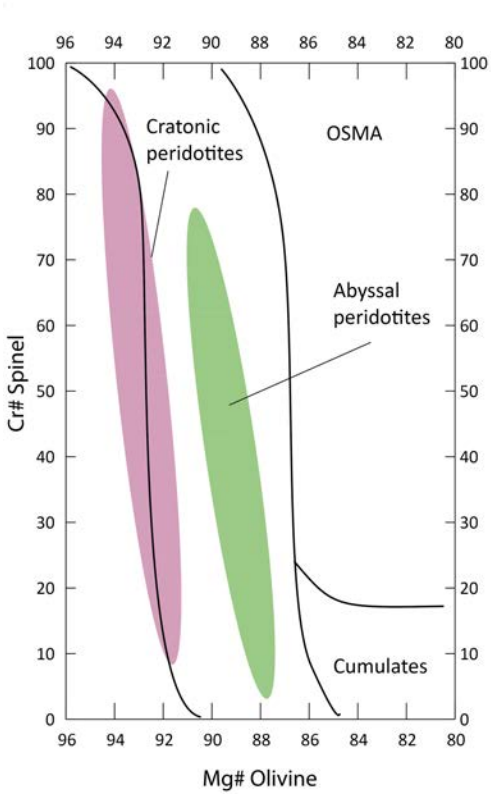

Figure 46: 100*Mg# olivine vs Cr# spinel diagram illustrating abyssal and cratonic peridotites chemical variation in relationship with the the olivine–spinel mantle array (OSMA) of Arai (1994). The compiled field for cratonic peridotites is composed by data from xenoliths (Bernstein et al. 1998, 2006) and orogenic peridotite massifs from the WGR (Beyer et al, 2006)(Modified after Friend et al, 2002).

Provenience	ROCK COMPOSITION	Mg# Olivine	Cr# Spinel	REFERENCE
Kittelfjal (Seve Nappe Complex)	HARBURGITE	91,2-92,2	76-81	
	DUNITE	92,5-93,6	89,3-96	
Friningen (Seve Nappe Complex)	GARNET PERIDOTITE	90-91	18-28	
	DUNITE	93	46-51	
Almklovdalen (Western Gneiss Region)	GARNET PERIDOTITE	90,6-91,7	57-67	Beyer et al, 2006
	DUNITE	92-93,6	89-94	
Xenoliths (Wiedermann Fjord Greenland)	UNDIFFERENTIATED	92,7	5-75	Bernstein et al, 1998
Xenoliths (Ubekendt Ejland, Greenland)	DUNITE	92-93,7	47-96	Bernstein et al, 2006
Leka (Koli Nappe Complex)	DUNITE	86-90	70-80	Iyer et al, 2007

Table 12: Olivine 100*Mg# and spinel 100*Cr# range for a wide range of ultramafic rocks in different geological and tectonic settings. Olivine Mg# for Friningen Garnet peridotite and Kitttelfjäll spinel peridotite is comparable to Archean sub-continental peridotite of Almklovdalen (Beyer et al, 2006) and xenoliths from the mantle underneath Greenland (Bernstein et al 1998, 2006). Olivine Mg#(*100) is a successful petrogenetic indicator that allow to discriminate between orogenic peridotite massifs (Mg# 90-94) clearly contrast with ophiolitic peridotites (Mg# 86-90) (Iyver et al, 2007).

2. Age constraints

KSP is interpreted as the result of Archean (>2500 Ma) partial melting followed by later re-fertilization event forming harzburgite (Chapter 6.2.1). Thus, age constraints are in favour of a subcontinental rather than sub-oceanic origin. In fact, the onset of the rifting which separate Laurentia (Greenland) from Baltica is dated around 750 – 800 Ma. This must be considered as a maximum age for the formation of a sub-oceanic mantle that could be actively involved in the Caledonian orogeny.

3. Rock association

The KSP lies in a rock envelope formed by gneisses (Kyanite-KFeldspar) and amphibolites (chapter 2.3). This is also the typical rock association for most of the orogenic peridotite massifs in the WGR and it is in clear contrast with rock associations of ophiolite complex. In fact peridotites emplaced by obduction are often associated with typical ophiolite sequences formed by ultramafic rocks, gabbros, basalt and oceanic sediments (see Leka ophiolite complex, Iyver, 2007; Fig.7). However, in areas of intense deformation the ultramafic rocks can be completely dismembered from the original sequence, therefore the rock association by itself is not a discriminant factor.

6.3 PT path estimate

6.3.1 Pre-Caledonian evolution (M1)

Early history of the peridotite is related to its evolution within the SCLM. Previous considerations lead to interpret the Kittelfjäll spinel peridotite as the product of an Archean partial melting, followed by refertilization, probably of Proterozoic age considering similar cases elsewhere in the Caledonides (i.e. Friningen (Brueckner et al, 2004) and Almklovdalen (Beyer, 2006) garnet peridotites). The simplest hypothesis which might explain such evolution is to consider an initial Archean adiabatic upwelling at ~1800°C (Fig.47A) with massive partial melting (>50%) (Fig.47B) of a fertile lherzolite. Depletion continued as long as astenopheric underplating continued at the lithospheric base, generally placed 100-150 Km (Spengler, 2006). At this point the rock was a highly depleted dunite with high olivine Mg# (~93) and a Cr-rich spinel (Cr# ~90). It is likely to suppose that the chromite foliation (S_i) formed during this early stage but this is a pure speculation which can not be supported neither by chemical analysis nor by microstructural observations. Peridotite partial melting was followed by fluid/melt infiltration, which re-fertilized the dunite and it is responsible for the compositional layering alternating dunites and harzburgites. The timing of the process it is not known but it clearly altered the original chemical composition. In fact Mg# was lowered in harzburgite layers from ~93 (Dunite layers) to ~91 (Harburgite layers) due to global enrichment of Si, Al, Fe and Ca (Chapter 6.2.1).

Several assumptions are necessary to define the geological evolution of the KSP after partial melting but before crustal emplacement because applied geothermometers (M1a ~ 1100 °C; M1b ~ 870 °C) give only temperature but no pressure constraints. Firstly, I assume (based on conclusions of Spengler, 2006) lithospheric formation by isothermal cooling towards stable continental geotherm during Proterozoic (Fig.47C). This phase is generally characterized by an isobaric cooling from high temperature at great depth (>100 Km) under low deviatoric stresses (<1 Mpa). Such conditions are the ideal kinetic and kinematic conditions for the formation of coarse porphyroclast of olivine and orthopyroxene (M1 assemblage) by selective growth of crystals with the lowest energy configuration.

Final decompression and crustal emplacement are related to the early Caledonian SNC subduction and eduction loop during Caledonian orogenic event. Interaction between the subducted plate and subcontinental mantle probably occurred during development of the M2 mineral assemblage (Chlorite-Tremolite stable) and related olivine M2 foam microstructure (Chapter 5.3.2.2) (Fig.47D). Possibly, the olivine M1 porphyroclasts were initially deformed in

the mantle before the Caledonian orogeny, perhaps during the Gothian (1,5 – 1,75) or Sveconorwegian-Greenvillian Orogeny (1,05-0.9 Ga) (Chapter 2.1). Further analysis are required to test this hypothesis.

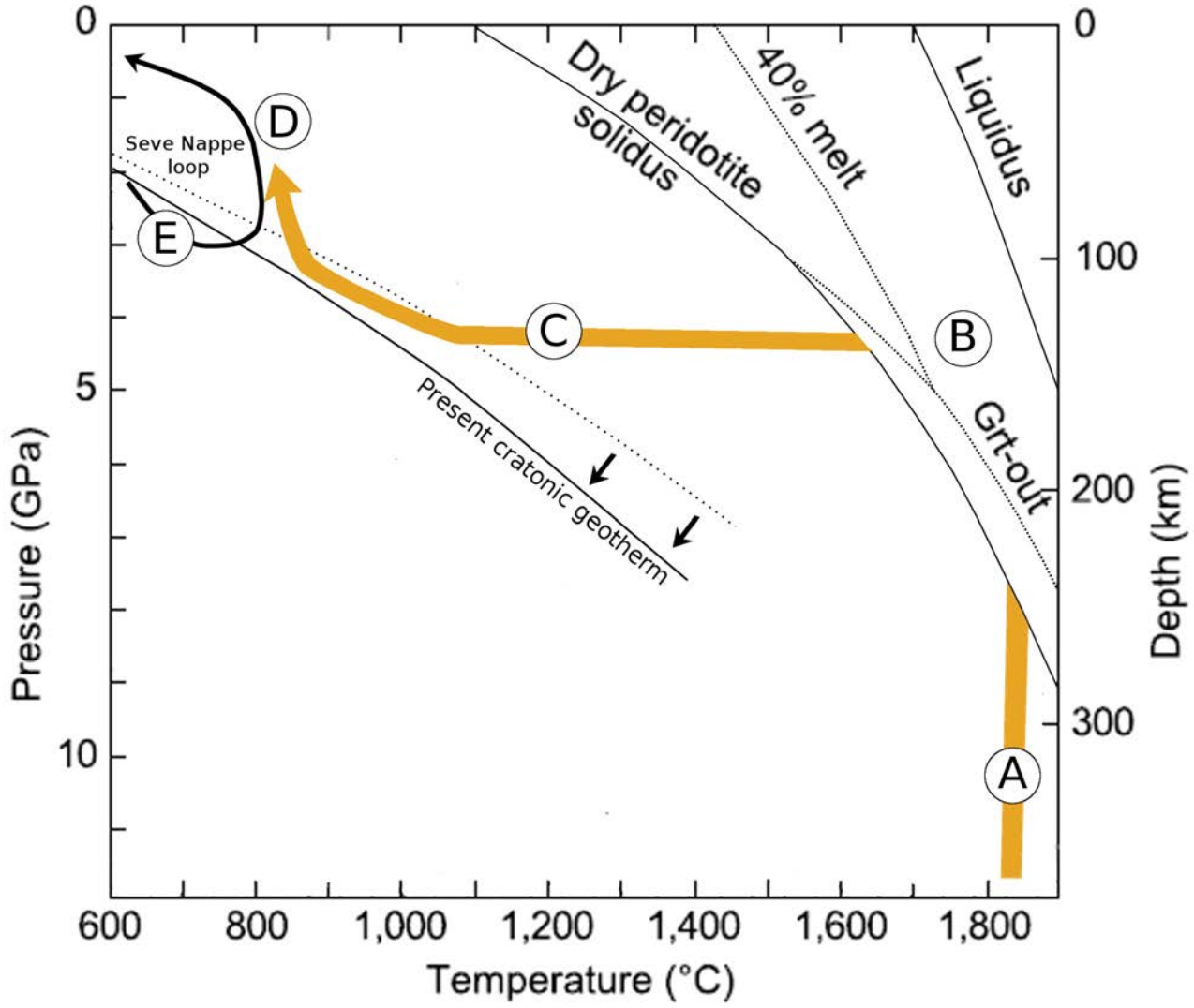

Figure 47: Schematic PT path for the Kittelfjäll spinel peridotite: A) Isothermal upwelling of astenospheric mantle is thought to occur at ~1800°C during Archean (Spengler, 2006). B) Fertile lherzolite underwent massive partial melting (>50%) at depth of 100-200 km. C). It followed an isobaric cooling towards stable continental/cratonic geothermal conditions during Proterozoic (Dashed line). Further cooling is recorded by Al content in orthopyroxene (M1a at ~ 1100 °C) and Cr-Al exchange in the system Ol-Sp (M1b at ~ 870 °C) During this stage PT conditions tend to evolve towards present continental geotherm (Solid line). D)Further decompression and crustal emplacement is related to the early Caledonian Seve Nappe Complex (SNC) loop (subduction + eduction). Interaction between subducted plate and subcontinental mantle occurred at temperature of 800±75 °C and pressure 2±1 Gpa. E) Early Caledonian Seve Nappe Complex PT "loop" with metamorphic peak recorded by pyroxenite dyke within Friningen garnet peridotite, metamorphosed under Ultra High Pressure (UHP) conditions , at 800 °C and 3 Gpa (Janak et al, 2013). (Modified after Spengler, 2006)

6.3.2 Early Caledonian evolution (M2-M3)

The structural and metamorphic evolution of the KSP is isofacial (i.e. same metamorphic grade an deformation history) for M2 and M3 with respect to the evolution of host-rocks of the Central Belt, the Marsfjället gneisses and the Kittelfjäll amphibolite (Trouw, 1973; Biermann, 1977; Chapter 2.3). The development of retrograde mineral paragenesis (M2-M3) and microstructures (Olivine M2 foam and M3 mortar microstructure) in the KSP is therefore associated with the early Caledonian orogeny. The presence of eclogites, garnet bearing-peridotites, zircons and pyroxenite with ages ranging from 445 Ma to 460 (Chapter 2.4) is clearly associated to early Caledonian subduction-eduction cycle of the SNC during the Jämtlandian phase (Chapter 2.5). This data indicate that crustal emplacement of the KSP occurred from the SCLM during eduction of the SNC.

M2 is defined by the development of an olivine M2 foam microstructure within the stability field of Ol + Opx + Chl/Sp + Tr , stable at 600-760 °C and 1-2 Gpa (Fig.48). However, temperatures estimated from the recrystallized olivine M2 Type I and Type II grains indicate that deformation occurred at 750-830°C (Chapter 5.3.5.3). The two ranges of temperatures overlap only in a narrow area around 750°C. The most likely hypothesis to explain the temperatures incongruence is to consider the olivine M2 foam microstructure as the result of a progressive deformation that crossed the tremolite-in phase boundary line (Fig.48). Onset of M2 occurred outside the stability field of tremolite at 830°C (Ol+Opx+Sp) with the generation of olivine M2 Type I grains (Chapter 5.3). Moreover, geothermometry on olivine M1 porphyroclasts is in agreement with this hypothesis because results indicate that a last coarse grained assemblage re-equilibrated at 870±60°C. Final part of the M2 deformation is related to the development of olivine M2 Type II grains just inside the stability field of tremolite (Fig.48) at 750°C. The drop in temperature is associated with increasing deviatoric stress (σ=7-42 Mpa) interpreted to indicate evolution from mantle (σ <1MPa) to crustal conditions (Chapter 5.3.6).

The olivine M2 foam microstructure pressure of formation can not be inferred neither with geobarometry nor with the help of petrogenetic diagram (Chapter 5.2.3) because of the absence of indicative minerals. In fact pressure is generally constrained by the phase boundary line of spinel-garnet. Unfortunately, this is not applicable for the KSP, due to the Cr-rich spinel (Cr#~90) that expands the spinel stability field up to 4 Gpa (Chapter 5.2.3.3). Upper pressure limits during development of olivine M2 foam structure can be assumed to be related to the last subsolidus re-equilibration experienced by the peridotite at ~ 870 °C (M1b). Such temperature is typically associated with pressures of ~3 Gpa in an average cratonic area (Fig.47). However, the idea of the emplacement into the subducted slab at similar depth seems remote, it will hereby be considered as the upper limit. Instead, the lower pressure limit is placed at ~1 Gpa, inferred from the Kyanite stability in the surrounding rocks during M2 phase (Chapter 2.3). As a result the pressure range in which the characteristic olivine M2 foam microstructure developed is 2±1 Gpa.

The olivine M2 foam microstructure formed at at 750-830°C – 2±1 Gpa by dislocation creep processes producing dominant E-type CPO's and subordinate C-type CPO's formed by the operation of the [100](001) and [001](100) slip systems. Even though the microstructure is strongly annealed by syn-to post diffusion processes a strong CPO is preserved (Chapter 5.3).

M3 deformation is associated with an olivine M3 mortar microstructure generated in strongly localized shear zones characterized by a stable assemblage Ol + Atg/Tc + Tr + Chl. PT conditions operating during M3 record progressive stages of exhumation, inferred to be at 550-600°C and 0,45-0,6 Gpa (Fig.46; Calon, 1979). M3 can be considered related to early Caledonian as well as to main the Caledonian phase (Scandian).

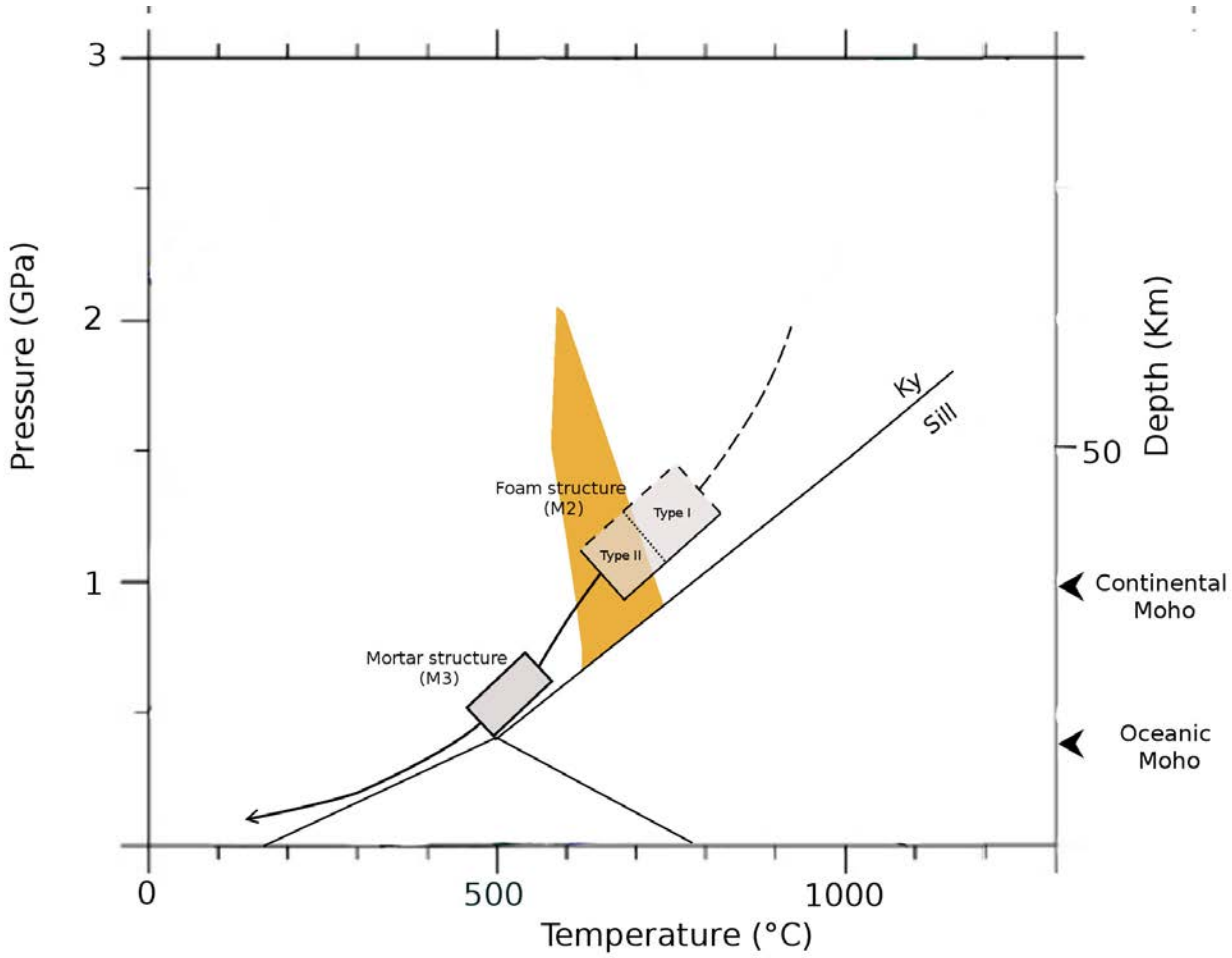

Figure 48: Retrograde PT path for the Kittelfjäll spinel peridotite. Grey boxes represent inferred stability area during M2 (defined by olivine "FOAM" microstructure) and M3 (defined by olivine "MORTAR" structure). M2 deformation event is characterized by a stable assemblage of Ol + Opx + Tr + Chr (Orange area) in equilibrium with Type II grains within the olivine foam microstructure. Lower stability field is inferred by the stability of kyanite during M2 in the surrounding rocks (Trouw, 1973; Biermann, 1979). Onset of M2 deformation occurred at 800±75 °C and pressure 2±1 Gpa, giving severe constraints on the subcontinental origin of the peridotite. Tremolite is stable only with olivine foam type II grains (Type II) in the final part of the M2 deformation event.

6.4 Geodynamic interpretation

The aim of this chapter is to link the tectono-metamorphic evolution of the Kittelfjäll spinel peridotite (KSP)with that of the Seve Nappe Complex (SNC) in order to obtain a better understanding about the geodynamic setting. For this purpose, structural (microstructures) and petrological (mineral chemistry) data -which were collected and analysed in previous chapters- will be combined together to reconstruct a (possible) geodynamic model of the studied area (Fig.49). This conceptual model is aiming to exclusively describe the tectono-metamorphic evolution of the SNC, without involving the general geodynamic regime of the Scandinavian Caledonides. The afore mentioned geodynamic model, is based on a comparison of two orogenic peridotite massifs: the KSP and the Friningen Garnet Peridotite (FGP), data for the latter body have been provided by the MSc student Mattia Gilio. In this chapter, the structure and the petrology of FGP will be briefly described and compered with

KSP. Further information concerning FGP is available by the work of Brueckner et al, (2004) and Gilio (2013) (MSc thesis).

The FGP belongs to the Ertsekey Lens of the Central Belt of the SNC. It consists of layers of different bulk rock compositions: Al-poor dunite, garnet-bearing harzburgite and garnet lherzolite, locally intercalated with eclogitic- and/or garnet pyroxenite layers/dikes. The oldest recognized mineral assemblage ($M1^F$a) in the FGP consists of coarse-grained olivine+opx+cpx+garnet with common break down of the $M1^F$ a garnet to a coarse grained amphibole+opx+spinel symplectite ($M1^F$b). A second assemblage ($M2^F$) overprints the $M1^F$ assemblages and consists of olivine(2) + opx(2) + cpx(2) + garnet(2) + spinel(2). The $M2^F$ assemblage is of early Caledonian age (Brueckner and Van Roermund 2004, 2007). The $M3^F$ assemblage consists of olivine(3) + opx(3) + chlorite + amphibole (3).

FGP and KSP are both interpreted as orogenic peridotite massifs with sub-continental affinity (similar olivine Mg# in Fig.46). Both peridotites share an early pre-Caledonian evolution in the mantle but deformation events linked to the Caledonian orogeny are different. The mantle evolution is related to an Archean partial melting event followed by refertilization, probably of Proterozoic age (Chapter 6.2.1). This early evolution is confirmed in the FGP by whole-rock Sm-Nd ages carrying Proterozoic re-fertilization ages of 1,1-1,2 Ga (Brueckner et al, 2004). KSP and FGP divergent PT path is related to the inferred subduction of the SNC during the Jämtlandian orogeny (Chapter 2.5), which metamorphic peak is dated ~450 Ma (Brueckner et al, 2004). During subduction FGP was tectonically transferred from the mantle into the subducted continental crust where the $M2^F$ prograde mineral assemblage and related olivine fabric was generated (MSc thesis Gilio, 2013). Peak conditions are inferred from a pyroxenite dyke within FGP, metamorphosed at 800°C and 3Gpa (Janak et al, 2013). The KSP is characterized exclusively by retrograde $M2^K$ olivine fabric and a mineral assemblage Ol + Opx + Tr + Chl (Chapter 5.2.3.4; 5.3.6). The same mineral assemblage develops during $M3^F$ in the FGP and is associated to an olivine fabric interpreted to be retrograde (MSc thesis Gilio, 2013). Both peridotites recorded regression histories to the chlorite peridotite, suggesting the emplacement of KSP into the crust as the slab returned back towards the surface (Fig.49).

The development of a prograde fabric indicate a clear hangingwall (or mantle wedge) provenance for the FGP (Chapter 3.3.1). Instead, complications arise whether or not KSP was emplaced during eduction from the Laurentian mantle wedge (hangingwall), or from the Baltic mantle lithosphere (footwall)(Fig.49). In fact, after slab break off the subducted slab down-going movement was reversed, causing fast eduction and reverse shear at the contact with the underlying Baltic mantle (Chapter 3.3.1; Fig.8b). In this tectonic context, peridotite emplacement occurs either from the hangingwall or footwall. Shearing along the lower boundary could allow peridotite transfer from the Baltic mantle into the SNC along its base. Some field characteristics seem to be consistent with a "basal shear model" (After Brueckner et al, 2010). In fact the KSP is emplaced in a rock envelope composed of gneiss and amphibolites equilibrated under granulite to upper amphibolite facies conditions. Such mineral assemblages are generally expected at the base of the crust. Additionally, the KSP lies at the lower boundary of the Central Belt (Fig.3-4), a favourable structural position in support to the emplacement by reversal shearing from the footwall.

However, there are important geochemical arguments that does not fully support the basal shear model. As a matter of fact KSP is characterized by a similar chemical composition with respect to FGP, the Almklovdalen garnet peridotite in the WGR and xenoliths from the mantle underneath Laurentia (Fig.46, Table 12). The scarcity of data concerning the Baltic subcontinental mantle does not allow to discriminate with certainty whether the KSP represents a lithospheric fragment belonging to Laurentia, Baltica or a possible microcontinent (Chapter 2.5). For simplicity and strong chemical affinity with Laurentia sub-continental mantle, the preferred interpretations by the present author is that KSP represents a mantle fragment that formed part of a mantle wedge during subduction of the SNC but further investigations in such directions are required.

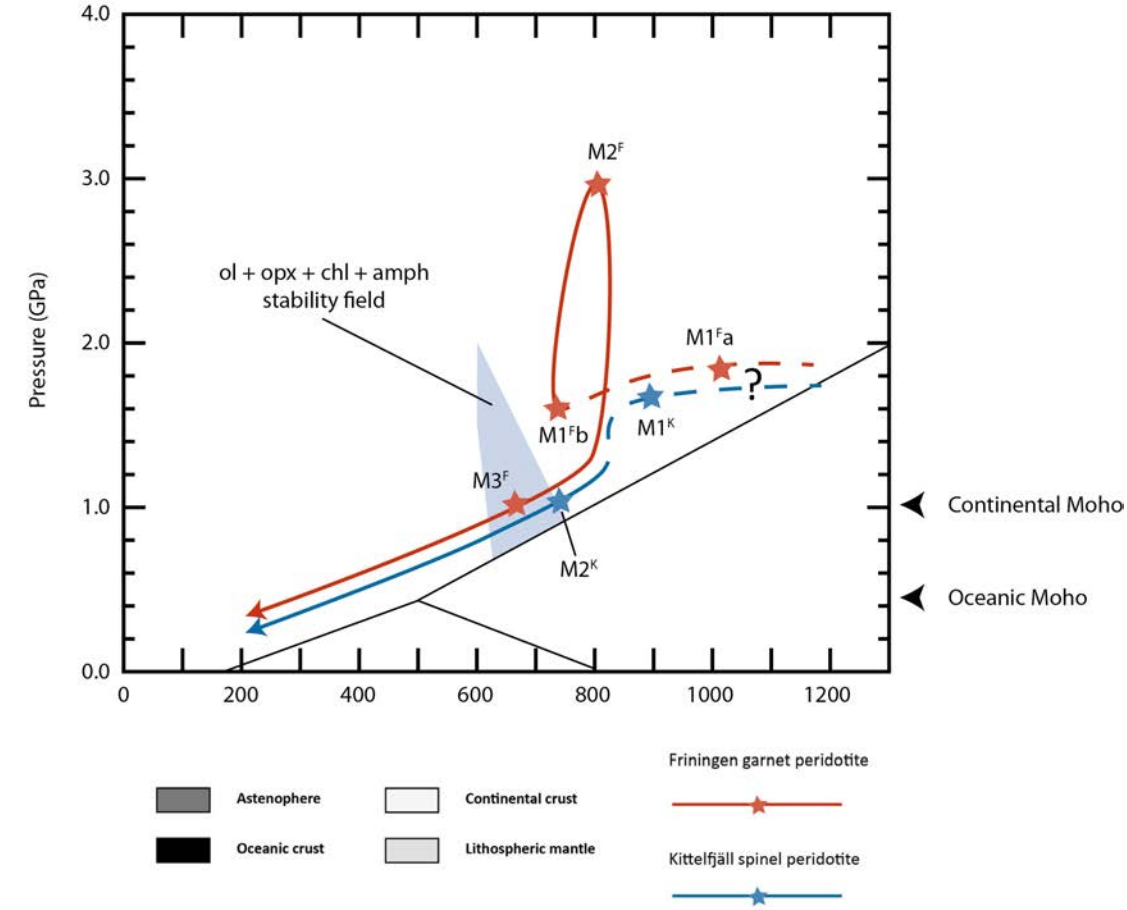

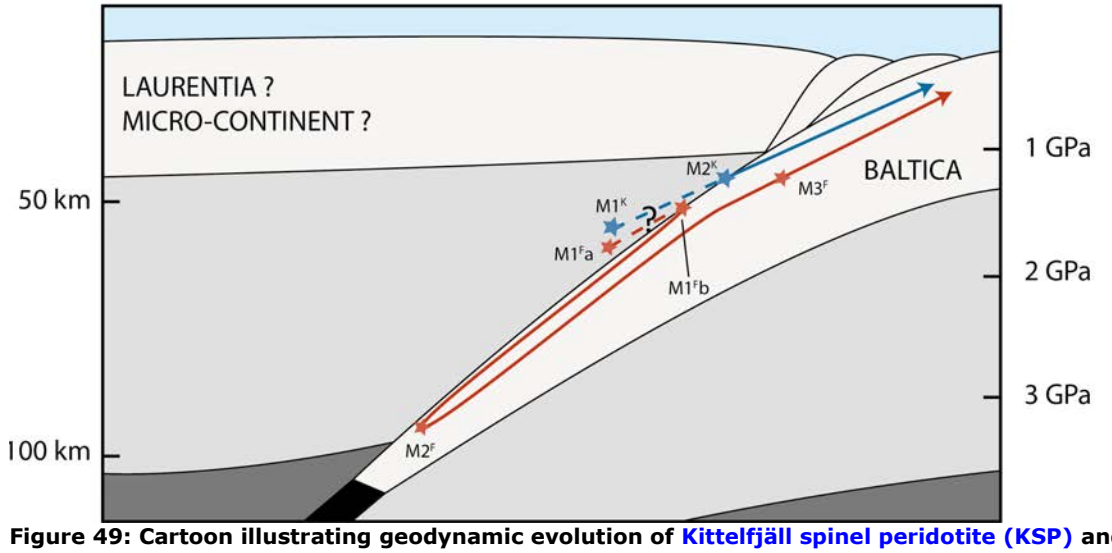

Figure 49: Cartoon illustrating geodynamic evolution of Kittelfjäll spinel peridotite (KSP) and Friningen Garnet peridotite (FGP). A) Contrasting PT path defined by retrograde conditions in the KPS and prograde in the FGP. Metamorphic peak is recorded by pyroxenite dyke within Friningen garnet peridotite, metamorphosed at 800 °C and 3 Gpa (Janak et al, 2013). M2 in the KSP and M3 in the FGP are defined by a stable assemblage ol + opx+ tr + Chl (Blue shaded area) developed during exhumation of the Seve Nappe Complex (SNC); B) Simplified cartoon illustrating geodynamic evolution of KSP and FGP in relation with the subducted SNC. FGP is emplaced in the down-going slab during subduction (Gilio, 2013) and KSP during eduction of the SNC (present thesis).

7 CONCLUSION

I. The geochemical and mineralogical data of the KSP is indicative for a "deep" SCLM origin, probably is of Archean age (partial melting >50%) followed by re-fertilization during Proterozoic.

II. Three characteristic olivine microstructures develop in response to evolving PT conditions:

- Olivine porphyroclasts (M1) grew under static mantle conditions at high temperature (>>870 °C)
- Olivine "foam" structures (M2) formed pervasively in a Km-shear zone at 750-830°C - 2±1 Gpa
- Olivine "mortar" structures (M3) formed heterogeneously within localized shear zones at 550-600°C- 0,45-0,6 Gpa

III. A retrograde PT evolution dictates transition from SCLM (M1) to crustal conditions (M3) during the early Caledonian orogeny (~450 Ma). Olivine foam microstructures (M2) represent a transitional stage

IV. Exhumation of the KSP occurred by plate tectonic processes related to continental eduction (exhumation) during the the subduction-eduction cycle of the SNC

V. Between 750-830°C and P > 1.0 GPa deformation of the peridotite occured by ductile dislocation creep processes (M2) producing dominant E-type CPO's and subordinate C-type CPO's by the operation of the [100](001) and [001](100) slip systems.

VI. All dynamically recrystallized M2 olivine grains have an annealed microstructure defined by strain-free grains and straight grain boundaries meeting into triple point junctions. Annealing did not erase the previous strong olivine CPO.

VII. The "relatively LT" olivine "foam" microstructure and related CPO's might be used to discriminate orogenic peridotite massifs (mantle wedge peridotites) from other peridotite types (i.e. ophiolite), at least in the Scandinavian Caledonides

9 FUTURE WORKS

I. Re-Os on sulphide grains within olivine M1 porphyroclasts is the ultimate proof to support or deny an Archean origin for the KSP

II. REE analyses and Sm-Nd isotope chemistry of harzburgite and dunite layers should give a more solid base for the refertilization events.

III. A CPO study of olivine M1 porphyroclasts and olivine M2 Type I grains (foam microstructure) might give important constraints to an early deformation event(s) in the mantle

IV. A detailed study of trace elements in order to define whether the KSP is affected by subduction fluid signature. Positive or negative feedback might help to discriminate the mantle provenance (i.e. hanginwall vs footwall configuration)

V. The olivine method – M2 microstructure as indicator of sub-continental provenance- should be tested in order to verify the validity. I suggest a pilot test on some of the widespread ultramafic bodies in the SNC.

VI. A petrological and microstructural comparison with orogenic peridotites from other mountain belts (Himalaya, Alps, Andes etc..) in order to verify whether the olivine microstructure as geodynamic indicator is a method extendable worldwide

10 ACKNOWLEDGEMENTS

First and foremost, I would like to thank my supervisor of this MSc project, Dr. H.L.M. v. Roermund for the great guidance and advice. His experience and willingness to motivate me contributed enormously to improve the MSc thesis and my passion for metamorphic geology. As a matter of fact, I am more motivated than ever to pursue a career involving my beloved high pressure metamorphic rocks!

I also want to thank Mattia, Janneke and Alex for the support and good time in the office and during the lab-research.

Special thanks to my family for their love financial support all along my stydyng career.

11 REFERENCES

Anonymous, (1972). Penrose field conference on ophiolites. Geotimes **17** (12): 22–24

Andréasson, P.G., (1980). Metamorphism in extensive nappe terrains: A study of the Central Scandinavian Caledonides. Geologiska Föreningens i Stockholm Förhandlingar, **102**, 335-357

Andréasson, P.G., (1994). The Baltoscandian Margin in Neoproterozoic–early Palaeozoic times. Some constraints on terrane derivation and accretion in the Arctic Scandinavian Caledonides. Tectonophysics **231**, 1–32.

Arai, S., (1994). Characterization of spinel peridotites by olivine–spinel compositional relationships: review and interpretation. Chemical Geology **113**, 191–204

Ballhaus, C., Berry R.F., Green D.H., (1991). High pressure experimental calibration of the olivine–orthopyroxene–spinel oxygen geobarometer: implications for the oxidation state of the upper mantle. Contributions to Mineral and Petrology **107**:27–40

Bernstein S., Kelemen P.B., Brooks C.K., (1998). Depleted spinel harzburgite xenoliths in Tertiary dykes from East Green- land: restites from high degree melting. Earth and Planetary Science Letters **154**:221–235

Bernstein, S., and Brooks, C. K., (1999). Mantle xenoliths from Tertiary lavas and dykes at Ubekendt Ejland, West Greenland. Geological Survey of Greenland Bulletin **180**, 152–154

Bernstein, S.H., Kelemen, K., Peter B. Brooks, P.B., Kent, C., (2006). Ultra-depleted, shallow cratonic mantle beneath West Greenland: dunitic xenoliths from Ubekendt Ejland. Contributions to Mineralogy and Petrology **152**, 335-347

Bernstein, S.H., Kelemen, K., Hanghøj, K., (2007). Consistent olivine Mg# in cratonic mantle reflects Archean mantle melting to the exhaustion of orthopyroxene. Geology 35, 459–462.

Beyer, E.E., Griffin, W.L., O'Reilly, S.Y., (2006). Transformation of Archean lithospheric mantle by refertilization: evidence from exposed peridotites in the Western Gneiss Region, Norway. Journal of Petrology **47**, 1611–1636

Biermann, C., (1979). Investigations into the development of microstructures in amphibole bearing rocks from the Seve-Köli Nappe Complex.

Bodinier, J.-L., and Godard, M., Orogenic, Ophiolitic, and Abyssal Peridotites in: Carlson, R.W., The mantle and core. Elsevier B.V. Amsterdam, pp 103-171 (2005)

Brueckner, H. K., and Medaris, L.G., (1998). A tale of two orogens: The contrasting P-T-t history and geochemical evolution of mantle in high- and ultrahigh-pressure metamorphic terranes of the Norwegian Caledonides and the Czech Variscides, Schweiz. Mineral. Petrogr. Mitt, **78**, 293–307.

Brueckner, H. K.,. and Medaris, L.G., (2000). A general model for the intrusion and evolution of 'mantle' garnet peridotites in high-pressure and ultra-high- pressure metamorphic terranes. Journal Metamorphic Geology, **18**, 123– 133.

Brueckner, H. K., and Van Roermund, H.L.M., (2004). Dunk tectonics: A multiple subduction/eduction model for the evolution of the Scandinavian Caledonides. Tectonics, **23**, 1–20.

Brueckner, H.K., and van Roermund, H.L.M., Pearson, N.J., (2004). An Archean (?) to Paleozoic Evolution for a Garnet Peridotite Lens with Sub-Baltic Shield Affinity within the Seve Nappe Complex of Jämtland, Sweden, Central Scandinavian Caledonides. Journal of Petrology **45**, 415-437

Brueckner, H.K., van Roermund, H.L.M., (2007) Concurrent HP meta- morphism on both margins of Iapetus: Ordovician ages for eclogites and garnet pyroxenites from the Seve Nappe Complex, Swedish Caledonides. Journal Geological Society of London **164**, 117–128

Brueckner, H.K., Carswell, D.A., Griffin, W.L., Medaris, L.G., Van Roermund, H.L.M., Cuthbert, S.J., (2010). The mantle and crustal evolution of two garnet peridotite suites from the Western Gneiss Region, Norwegian Caledonides: an isotopic investigation. Lithos **117**, 1–19.

Bogdanova, S.V., Gorbatschev, R., and Stephenson, R., (2001). EUROBRIDGE: Palaeoproterozoic accretion of Fennoscandia and Sarmatia. Tectonophysics, **339** (1-2)

Bucher-Nurminen, K., (1988). Metamorphism of ultramafic rocks in the Central Scandinavian Caledonides. Norges Geologiske Undersùkelse Special Publication **3**, 86-95.

Bucher-Nurminen, K., (1991). Mantle fragments in the Scandinavian Caledonides. Tectonophysics **190**, 173-192.

Bucher, K., Metamorphism of Ultramafic Rocks in: Petrogenesis of Metamorphic Rocks. Springer-Verlag Berlin Heidelberg edition; Berlin, Heidelberg, pp 191-223 (2011)

Calon, T.K., (1979). A study of the Alpine-type peridotites in the Seve-Köli Nappe Complex, central swedish Caledonides, with special reference to the Kitttelfjäll peridotite.

Carswell, D.A., Tucker, R.D., O'Brien, P.J., Krogh, T.E., (2003a). Coesite micro-inclusions and the U/ Pb age of zircons from the Hareidland Eclogite in the Western Gneiss Region of Norway. Lithos **67**, 181–190.

Carswell, D.A., Brueckner, H.K., Cuthbert, S.J., Mehta, K., O'Brien P. J., (2003b), The timing of stabilization and the exhumation rate for ultra- high pressure rocks in the Western Gneiss Region of Norway. Journal Metamorphic Geology, **21**, 601–612.

Cocks, L.R.M., and Torsvik, T.H., (2007). Siberia, the wandering northern terrane, and its changing geography through the Palaeozoic. Earth-Science Reviews, **82** (1-2), 29–74.

Coleman, R.G., (1971). Plate tectonic emplacement of upper mantle peridotites along continental edges. Journal of Geophysical Research, **76,** 1212-1222.

Condie, K.C., Plate Tectonics and Crustal Evolution. Butterworth-Heinemann Ltd. (4th Edition); Oxford, UK, 282 p. (1997)

deCapitani, C.,, Petrakakis, K., (2010). The computation of equilibrium assemblage diagrams with Theriak/Domino software. American Mineralogist **95**, 1006-1016, 2010

Den Tex, E., (1969). Origin of ultramafic rocks, their tectonic setting and history: A contribution to the discussion of the paper ''The origin of ultramafic and ultrabasic rocks'' by P. J. Wyllie. Tectonophysics **7**, 457–488.

Dewey, J., (1976). Ophiolite obduction. Tectonophysics **31**, 93–120.

Dick, H.J.B., Bullen T., (1984). Chromium spinel as a petrogenetic indicator in abyssal and alpine-type peridotites and spatially associated lavas. Contribution to Mineral Petrology **86,** 54–76

Du Rietz, T., (1935). Peridotites, serpentinites and soapstones ofnorthern Sweden.

Geologiska Foreningens i Stockholm Forhandlingar **57/2**, 133-260.

Fleet, M.E., and Angeli, N., (1993). Oriented chlorite lamellae in chromite from Pedra Branca Mafic-Ultramafic complex, Ceara, Brazil. American mineralogist **78**, 68-75

Friend, C.R.L., Bennett, V.C., Nutman, A.P., (2002). Abyssal peridotites >3,800 Ma from southern West Greenland: field relationships, petrography, geochronology, whole-rock and mineral chemistry of dunite and harzburgite inclusions in the Itsaq Gneiss Complex. Contributions to Mineralogy and Petrology **143**, 71-93

Gaál, G., Gorbatscheb, R., (1987). An Outline of the Precambrian Evolution of the Baltic Shield. Precambrian Research **35**, 15-52

Gademan, M., MSC thesis, (2011). Finnmarkian Monazite EMP ages in the Central belt of the Seve Nappe, north Jämtland/south Västerbotten, Sweden.

Gademan, M., Hogerwerf, M.A., Verbaas, J., van Roermund, H., (2011)., Evidence for a Finnmarkian (~500 Ma) continental collision/subduction zone in the central belt of the Seve Nappe Complex, northern Jämtland-southern Västerbotten, Sweden; Constraints from chemical EMP monazite ages and orogenic mantle wedge garnet peridotite. EGU meeting Vienna 2011, Subduction zone dynamics

Gee, D.G., Fossen, H., Henriksen, N., Higgins, A.K., (2008). From the Early Paleozoic Platforms of Baltica and Laurentia to the Caledonide Orogen of Scandinavia and Greenland. Episodes **31**

Gee, D.G., Juhlin, C., Pascal, C., Robinson, P., (2010). Collisional Orogeny in the Scandinavian Caledonides (COSC). GFF **132**, 29–44

Gilio, M., MSc thesis (2013).Olivine fabrics and microstructures of the Friningen garnet peridotite, Seve Nappe Complex, central Swedish Caledonides.

Hartog, S. A. M. Den., MSC thesis, (2008). Microphysics of Subgrain Development and Dynamic Recrystallization with Implications for Strength Evolution in Translithospheric Shear Zones.

Herzberg, C., (2004). Geodynamic information in peridotite petrology. Journal of Petrology **45**, 2507–2530.

Hogerwerf M.A., MSC thesis, (2011). Age dating project in the Central Belt of the SeveNappe Complex of Southern Västerbotten, Sweden,leading to a construction of a new geodynamic model of the formation of the Caledonian Orogeny

Iyer, K., Austrheim, H., John, T., Jamtveit, B., (2007). Serpentinization of the oceanic lithosphere and some geochemical consequences: Constraints from the Leka Ophiolite Complex, Norway. Chemical Geology **249**, 66-90

Janák M., Van Roermund, H.L.M., Majka J.C., Gee, D.G., (2013). UHP metamorphism recorded by kyanite-bearing eclogite in the Seve Nappe Complex of northern Jämtland, Swedish Caledonides. Gondwana Research **23** (3), 865-879

Jung, H., Karato, S., (2001). Water-induced fabric transitions in olivine. Science **293**, 1460–1463.

Jung, H., Katayama, I., Jiang, Z., Hiraga, T., Karato, S., (2006). Effect of water and stress on

the lattice preferred orientation (LPO) in olivine. Tectonophysics **421**, 1–22.

Jung, H., Mo, W., Green, H.W., (2009). Upper mantle seismic anisotropy resulting from pressure-induced slip transition in olivine. Nature Geoscience **2**, 73–77

Karson, J.A., (1998). Internal structure of oceanic lithosphere:a perspective from tectonic windows. Buck, W.R., Delayny, P.T., Karson, J.A. andLagabrielle,Y. (eds.). Faulting and magmatism at Mid-ocean Ridges. American Geophysical Union **106**, 177–218

Katayama, I., Jung, H., and Karato, S., (2004). New type of olivine fabric from deformation experiments at modest water content and low stress. Geology **32**, 1045–1048.

Katayama, I., and Karato, S., (2008). Low-temperature, high-stress deformation of olivine under water-saturated conditions. Physics of the Earth and Planetary Interiors, **168** (3-4), 125–133

Klemme, S., (2004).The influence of Cronthe garnet–spinel transition in the Earth's mantle: experiments in the system MgO–Cr2O3–SiO2 and thermodynamic modeling. Lithos **77**, 639–646.

Kohlstedt, D.L., Goetze, C., Durham, W.B., Vander Sande, J., (1976). New technique for decorating dislocations in olivine. Science **191**, 1045-1046

Krogh, T.E., Kamo, S.L., Robinson, P., Terry, M.P., Kwok, K., (2011). U–Pb zircon geochronology of eclogites from the Scandian Orogen, northern Western Gneiss Region, Norway: 14–20 million years between eclogite crystallization and return to amphibolite-facies conditions. Canadian Journal of Earth Sciences **48**, 441–472

Lee, C.T., Rudnick, R.L., (1999). Compositionally stratified cratonic lithosphere: petrology and geochemistry of peridotite xenoliths from the Labait volcano, Tanzania. Proc 7th Int Kimberlite Conf, The JB Dawson Vol, 503–521

Lloyd, G.E., Farmer, A.B., Mainprice, D., (1997). Misorientation analysis and orientation of subgrain and grain boundaries. Tectonophysics **279**, 55-78.

Majka, J., Be'eri-Shlevin, Y., Gee, D. G., Ladenberger, a., Claesson, S., Konečný, P., and Klonowska, I., (2012). Multiple monazite growth in the Åreskutan migmatite: evidence for a polymetamorphic Late Ordovician to Late Silurian evolution in the Seve Nappe Complex of west-central Jämtland, Sweden. Journal of Geosciences **57**, 3–23.

Mørk, M.B.E., Kullerud, K. and Stabel, A., (1988). Sm–Nd dating of Seve eclogites, Norrbotten, Sweden—evidence for early Caledonian (505Ma) subduction. Contributions to Mineralogy and Petrology **99**, 344–351.

Müntener, O., and Manatschal, G., (2006). High degrees of melt extraction recorded by spinel harzburgite of the Newfoundland margin: the role of inheritance and consequences for the evolution of the southern North Atlantic. Earth and Planetary Science Letters, **252**, 437–452.

Palasse, L.N., (2008). Microstructural evolution and seismic anisotropy of upper mantle rocks in rift zones. GEOLOGICA ULTRAIECTINA **300**

Passchier, C.W., and Trouw, R.A.J., Deformation Mechanisms, in: Microtectonics. Springer-Verlag Berlin Heidelberg edition; Berlin, Heidelberg, pp 25-63 (2005)

Qvale, H., and Stigh, J., (1985). Ultramafic rocks in the Scandinavian Caledonides. In Gee, D.G., and Sturt, B.A. (eds) The Caledonide Orogen and Scandinavia and Related Areas.Wiley, Chichester, pp. 693-715.

Reverdatto, V.V., Selyatitskiy, A.Yu., Carswell, D.A., (2008). Geochemical distinctions between "crustal" and mantle-derived peridotites/pyroxenites in high/ultrahigh pressure metamorphic complexes. Russian Geology and Geophysics **49,** 73–90

Roberts, D., and Gee, D.G., (1985). An introduction to the structure of the Scandinavian Caledonides: In: D.G. Gee and B.A. Sturt (Editors), The Caledonide Orogen: Scandinavia and Related Areas. Wiley, Chichester, pp. 55- 68.

Roberts, D., Heldal, T., Melezhik, V.M., (2001). Tectonic structural features of the Fauske conglomerates in the Løvgavlen quarry, Nordland, Norwegian Caledonides, and regional implications. Nor. Geol. Tidsskr **81**, 245– 256.

Roberts, D., (2003). The Scandinavian Caledonides: event chronology, paleogeographic settings and likely modern analogues. Tectonophysics **365**(1-4), 283–299.

Root, D.B., and Corfu, F., (2011). U–Pb geochronology of two discrete Ordovician high-pressure metamorphic events in the Seve Nappe complex, Scandinavian Caledonides. Contributions to Mineralogy and Petrology **163**, 769–788

Sachtleben, T., Seck, H.A., (1981). Chemical control of Al-solubility in orthopyroxene and its implications on pyroxene geothermometry. Contributions to Mineral Petrology **78**,157-165

Shimizu, I., (1998). Stress and temperature dependence of recrystallized grain size: a subgrain misorientation model. Geophysical Research Letters **25**(22), 4237-4240

Spengler, D., van Roermund, H.L.M., Drury, M., Ottolini, L., Mason, P. .D., and Davies, G., (2006). Deep origin and hot melting of an Archaean orogenic peridotite massif in Norway Nature, **440**(7086), 913–7

Stephens, M., Gee D.G., (1985). A tectonic model for the evolution of the eugeoclinal terranes in the central Scandinavian Caledonides. In: Gee, D.G., Sturt, B.A., (eds) The Caledonide Orogen – Scandinavia and Related Areas. J. Wiley and Sons, Chichester, pp 953–978

Stigh, J., (1979) Ultramafites and detrital serpentinites in the central and southern parts of the Caledonian Allochthon in Scandinavia. Department of Geology, Chalmers University of Technology, Goteborg, Publications **A27**, pp 222

Terry, M. P., Robinson, P., Hamilton, M.A., Jercinovic, M.J., (2000a). Monazite geochronology of UHP and HP metamorphism, deformation and exhumation, Nordøyene, Western Gneiss Region, Norway. Am. Mineral. **85**, 1651–1664

Terry, M. P., and Robinson P., (2003). Evolution of amphibolite-facies structural features and boundary conditions for deformation during exhumation of high- and ultrahigh-pressure rocks, Nordøyane, Western Gneiss Region, Norway. Tectonics **22**(4)

Torsvik, T. H., and Cocks, L.R.M., (2009). The Lower Palaeozoic palaeogeographical evolution of the northeastern and eastern peri-Gondwanan margin from Turkey to New Zealand. Geological Society London, Special Publications, **325**(1), 3–21

Trouw, R.A.J., (1973). Structural Geology of the Marsfjällen area Caledonides of Västerbotten Sweden, Sveriges Geologiska Undersökning, årsbok **67** (7)

Tucker, R.D., Robinson, P., Solli, A., Gee, D.G., Thorsnes, T., Krogh, T.E., Nordgulen, Ø., Bickford, M.E., (2004). Thrusting and extension in the Scandian hinterland, Norway: new U–Pb ages and tectono-stratigraphic evidence. American Journal Scientist **304**, 477–532

Yoshinobu, A.S., Barnes, C.G., Nordgulen, O., Prestvik,T., Fanning, M., R. B. Pedersen (2002).

Ordovician magmatism, deformation and exhumation in the Caledonides of central Norway: An orphan of the Taconic orogeny? Geology **30**, 883–886.

Van der Wal, D., Chopra, P., Drury, M., Fitz Gerald, J., (1993). Relationships between dynamically recrystallized grain size and deformation conditions in experimentally deformed olivine rocks. Geophysical Research Letter **20**, 1479–1482.

Van Roermund, H.L.M, Bakker, E., (1984). Structure and metamorphism of the Tangen-Inviken area, Seve Nappes, Central Scandinavian Caledonides, GFF **105**, 301-309

Van Roermund, H.L.M., (1989). High-pressure ultramafic rocks from the allochthonous nappes of the Swedish Caledonides. In: Grayer R. A. (Ed.), The Caledonide Geology of Scandinavia, Graham and Trotman, Norwell, Massachusets, 205 – 219

Van Roermund, H.L.M., (2009). High-pressure ultramafic rocks from the allochthons nappes of the Swedish Caledonides. European Journal of Mineralogy **21**, 1085-1096

Veerbas, J., MSC thesis, (2011). The tectonometamorphic evolution of a garnet peridotite lens, N. Jämtland, Sweden: From Sub-Continental Lithospheric Mantle to Orogenic Garnet Peridotite exposed at the surface

Walter, M.J., (1998). Melting of garnet peridotite and the origin of komatiite and depleted lithosphere. J. Petrology **39**, 29–60

Webb, S.A.C, Wood, B.J., (1986). Spinel-pyroxene-garnet relationships and their dependence on Cr/Al ratio. Contributions to Mineralogy and Petrology **92**, 471-480

Whattam, S. A., (2009). Arc-continent collisional orogenesis in the SW Pacific and the nature, source and correlation of emplaced ophiolitic nappe components. Lithos **113**(1-2), 88–114.

Williams, P. F., Zwart, J., (1977). A model for the development of the Seve-Köli Caledonian Nappe Complex. In S.K. Saxena S. Bhattacharji (eds.):Energetics of geological processes, 169-187. Springer Verlag, New York.

Witt-Eickschen, G., Seck, H.A., (1991). Solubility of Ca and Al in Orthopyroxene from spinel peridotite — an improved version of an empirical geothermometer. Contributions to Mineralogy and Petrology **106**, 431–439.

Wortel, M.J.R., and Spakman, W., (2000). Subduction and slab detachment in the Mediterranean- Carpathian Region. Science **290**, 1910–1917.

Zwart, H.J., (1974). Structure and metamorphism in the Seve–Köli Nappe Complex (Scandinavian Caledonides) and its implications concerning the formation of metamorphic nappes. In: Bellière, J., and Duchesne, J.C., (eds) Géologie des Domains Cristallins. Centenaire de la Société Géologique de Belgique, Liège, 129–144.

11 APPENDIX

Appendix 1 Kitttelfjäll spinel peridotite geological map

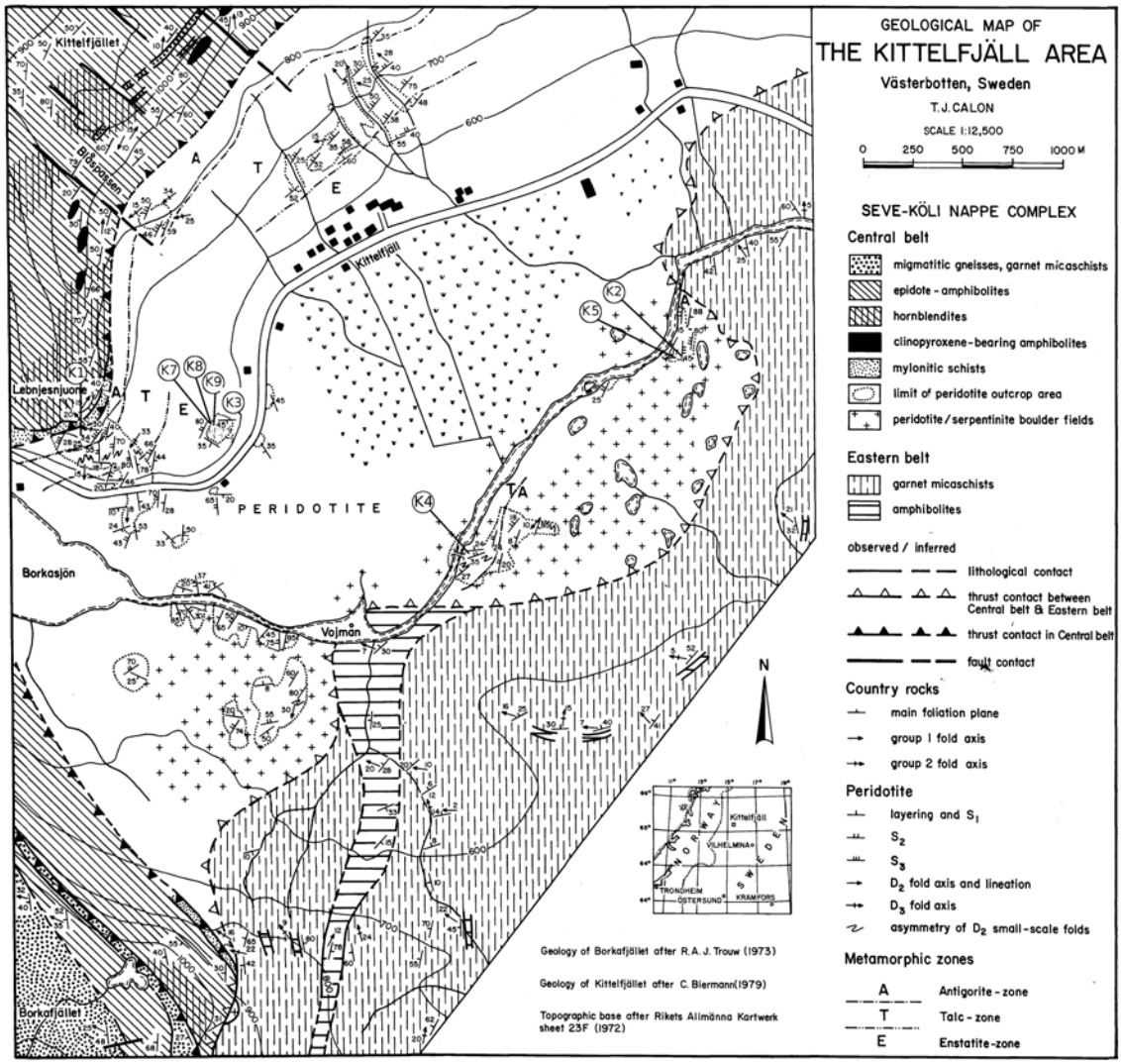

Geological map of the Kittelfjäll area (after Calon, 1979) with location of representative samples collected with the following **GPS coordinate:**

K1 : **33W 0521495** (Serpentinite)
7234650

K4: **33W 0523291** (Dunite sample with olivine "mortar" microstructure)
7234141

K2-K5: **33W 0521495** (Dunite sample with deformed "foam" microstructure)
7234650

K3-K7-K8-K9: **no GPS data available,** samples located in the quarry near Lebnjesnuone (Dunite K3-K7-K8; Harzburgite K9)

Appendix 2 Olivine M1 porphyroclast linescan

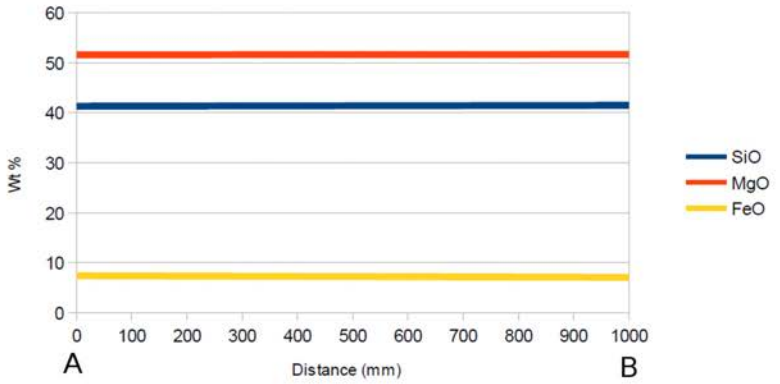

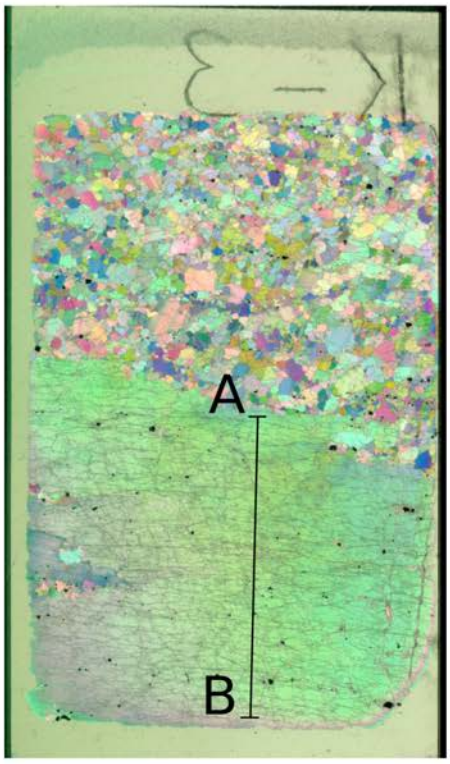

Distance (A-B)(um)	SiO	MgO	CaO	FeO	MnO	Cr2O3	NiO	TOTAL
26	41,310	51,593	2.59359e-09	7,427	0,096	0,005	0,373	100,802
51	41,341	51,758	0,002	7,061	0,100	1.75062e-08	0,408	100,671
77	41,256	51,689	2.5946e-09	7,223	0,090	1.7494e-08	0,391	100,649
103	41,111	51,804	0,004	7,436	0,072	1.74796e-08	0,357	100,784
128	41,108	51,353	2.59449e-09	7,232	0,096	0,009	0,346	100,143
154	41,055	51,308	2.59331e-09	7,419	0,106	1.74758e-08	0,382	100,271
179	41,072	51,499	2.59415e-09	7,262	0,102	1.74883e-08	0,392	100,327
205	41,101	51,648	2.59245e-09	7,591	0,110	0,004	0,388	100,841
231	40,843	51,216	0,025	7,282	0,094	0,004	0,391	99,855
256	41,066	52,012	2.5934e-09	7,421	0,106	1.74788e-08	0,391	100,995
282	40,964	51,834	2.59298e-09	7,460	0,099	1.74726e-08	0,427	100,784
308	41,128	51,747	0,001	7,253	0,066	1.74931e-08	0,363	100,558
333	41,035	51,540	2.59361e-09	7,373	0,084	1.74798e-08	0,405	100,436
359	41,236	51,634	2.59236e-09	7,672	0,097	1.74614e-08	0,356	100,995
385	41,128	51,747	0,001	7,253	0,066	1.74931e-08	0,363	100,558
410	41,035	51,540	2.59361e-09	7,373	0,084	1.74798e-08	0,405	100,436
436	41,236	51,634	2.59236e-09	7,672	0,097	1.74614e-08	0,356	100,995
462	41,235	51,726	0,001	7,466	0,104	1.74763e-08	0,374	100,907
487	41,075	51,445	2.59418e-09	7,234	0,104	0,013	0,399	100,269
513	41,297	51,761	2.59386e-09	7,370	0,082	0,013	0,392	100,914
538	41,410	51,596	2.59346e-09	7,462	0,092	1.74768e-08	0,391	100,951
564	41,314	51,638	2.59377e-09	7,359	0,089	1.74821e-08	0,433	100,833
590	41,333	51,647	2.59472e-09	7,172	0,095	0,012	0,416	100,675
615	41,251	51,599	0,007	7,156	0,091	0,008	0,371	100,483
641	41,321	51,610	2.59453e-09	7,279	0,078	1.74916e-08	0,364	100,652
667	41,368	51,295	2.59351e-09	7,436	0,070	0,002	0,418	100,590
692	41,162	51,656	2.59387e-09	7,345	0,080	1.74833e-08	0,411	100,655
718	41,019	51,702	2.59441e-09	7,187	0,105	0,015	0,397	100,426
744	41,217	51,695	2.59329e-09	7,472	0,090	1.74751e-08	0,391	100,865
769	41,270	51,510	2.59444e-09	7,260	0,097	1.74914e-08	0,369	100,506
795	41,409	51,961	2.59458e-09	7,278	0,089	1.74935e-08	0,368	101,105
821	41,508	51,656	2.59448e-09	7,288	0,091	0,000	0,382	100,925
846	41,365	51,838	2.59321e-09	7,499	0,072	1.74734e-08	0,434	101,207
872	41,479	51,711	2.59357e-09	7,400	0,095	1.74795e-08	0,454	101,139
897	41,387	51,664	2.59334e-09	7,478	0,088	1.74753e-08	0,405	101,021
923	41,512	51,654	2.59371e-09	7,437	0,079	1.74797e-08	0,400	101,082
949	41,588	51,493	0,002	7,366	0,078	0,015	0,339	100,882
974	41,438	51,882	2.59385e-09	7,395	0,095	1.74832e-08	0,393	101,202
1000	41,500	51,671	2.59566e-09	7,091	0,079	1.75076e-08	0,361	100,701

Compositional profile (A-B), optical micrograph (XPL) and EMPA of Olivine M1 porphyroclast in sample K3 (dunite).

Appendix 3 Orthopyroxene M1 porphyroclast linescan

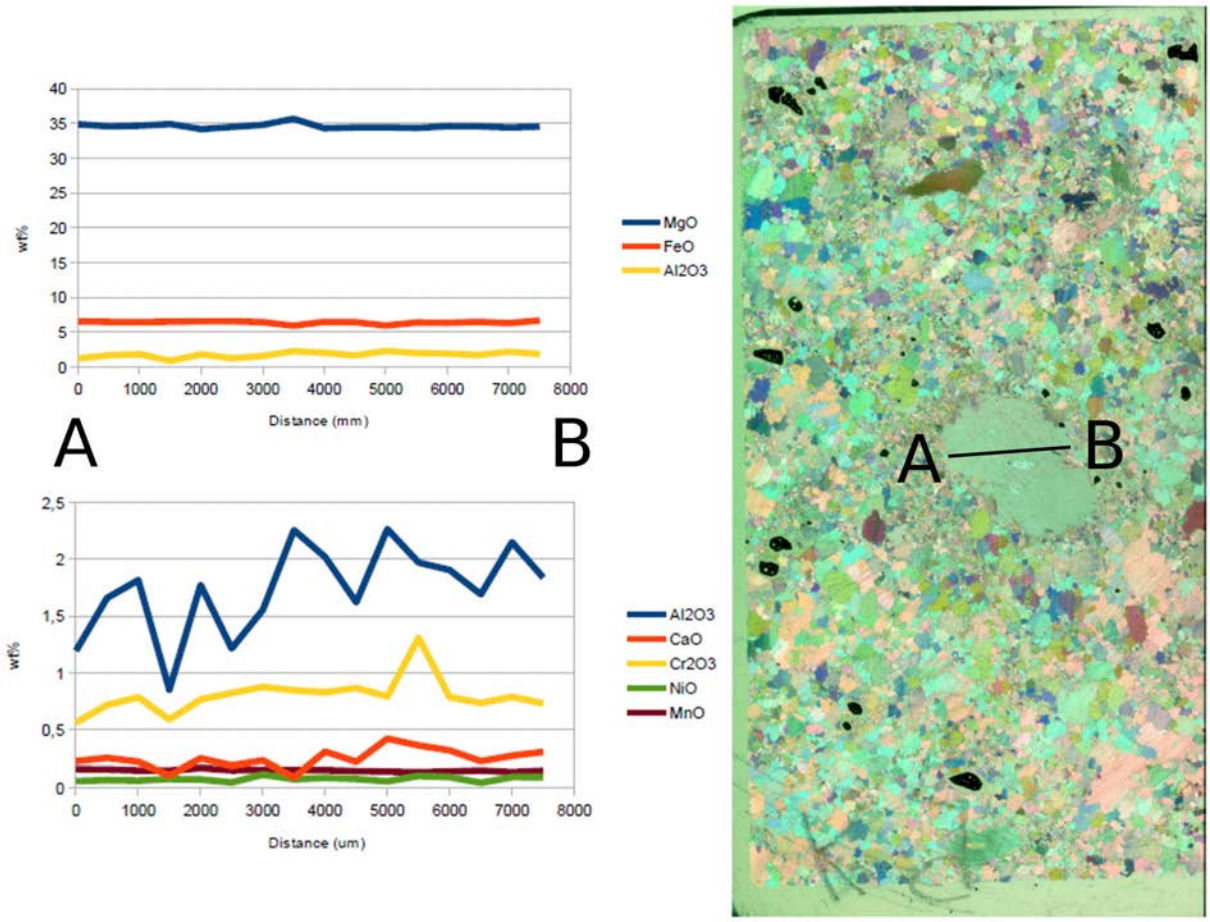

Distance (um)	SiO	Al2O3	FeO	MnO	MgO	CaO	NaO	TiO	Cr2O3	NiO	TOTAL
0	57,25	1,19	6,53	0,16	34,86	0,23	-	0,02	0,57	0,06	100,87
500	56,86	1,66	6,45	0,16	34,56	0,26	0,06	0,01	0,72	0,07	100,80
1000	56,73	1,81	6,43	0,15	34,65	0,22	0,01	0,00	0,79	0,06	100,87
1500	57,19	0,85	6,49	0,15	34,89	0,11	-	-	0,59	0,08	100,35
2000	56,19	1,77	6,55	0,17	34,17	0,25	0,02	0,01	0,77	0,07	99,97
2500	56,74	1,22	6,55	0,15	34,48	0,19	0,00	0,01	0,83	0,05	100,21
3000	56,68	1,56	6,40	0,15	34,77	0,23	0,00	-	0,88	0,11	100,79
3500	56,47	2,25	5,89	0,15	35,64	0,09	0,08	-	0,85	0,07	101,51
4000	56,36	2,02	6,45	0,15	34,28	0,31	0,02	0,00	0,83	0,09	100,51
4500	56,58	1,62	6,40	0,14	34,41	0,22	0,00	0,01	0,87	0,08	100,33
5000	56,42	2,26	5,92	0,14	34,41	0,43	0,00	-	0,79	0,06	100,44
5500	56,10	1,97	6,37	0,14	34,34	0,36	0,04	0,03	1,31	0,10	100,76
6000	56,63	1,90	6,32	0,14	34,60	0,32	0,04	0,01	0,79	0,09	100,85
6500	56,89	1,69	6,46	0,15	34,56	0,23	0,05	0,00	0,74	0,04	100,81
7000	56,51	2,15	6,26	0,14	34,41	0,28	0,14	0,02	0,79	0,09	100,79
7500	56,59	1,84	6,65	0,15	34,52	0,31	0,00	-	0,73	0,09	100,89

Compositional profile (A-B), optical micrograph (XPL) and EMPA of orthopyroxene M1 porphyroclast in sample K9 (Harzburgite)

Appendix 4 Electron Microprobe Analysis

Sample	Lithology	SiO	MgO	FeO	MnO	Cr2O3	CaO	NiO	Total	Mg#
k3	Dunite (Foam M2)	41,32	52,00	7,23	0,09	0,23	2.59329e-09	0,41	101,29	92,70
K3	Dunite (Foam M2)	41,25	51,75	7,50	0,07	0,01	2.59339e-09	0,35	100,93	93,41
K3	Dunite (Foam M2)	41,29	51,64	7,33	0,09	1.74872e-08	2.59416e-09	0,37	100,72	93,60
K3	Dunite (Foam M2)	41,18	51,53	7,40	0,08	1.74802e-08	2.59372e-09	0,38	100,57	93,10
K3	Dunite (Foam M2)	41,12	51,46	7,58	0,07	0,02	2.5927e-09	0,36	100,61	92,90
K3	Dunite (Foam M2)	41,17	51,65	7,41	0,08	0,01	2.59332e-09	0,45	100,77	93,10
K3	Dunite (Foam M2)	41,30	51,69	7,17	0,09	0,00	2.59466e-09	0,45	100,70	93,30
K3	Dunite (Foam M2)	41,04	51,40	7,44	0,10	0,00	0,02	0,40	100,41	93,10
K9	Harz. (Foam M2)	41,00	49,95	9,27	0,14	1.73261e-08	2.58333e-09	0,37	100,72	91,20
K9	Harz. (Foam M2)	40,84	50,08	9,07	0,10	1.73408e-08	2.58445e-09	0,37	100,45	91,30
K9	Harz. (Foam M2)	40,66	49,61	8,81	0,10	0,01	2.58546e-09	0,37	99,56	91,40
K9	Harz. (Foam M2)	40,70	49,74	8,97	0,11	0,01	2.58463e-09	0,37	99,90	91,40
K9	Harz. (Foam M2)	40,17	49,87	8,77	0,10	0,01	2.58527e-09	0,38	99,30	92,24
K9	Harz. (Foam M2)	40,06	50,08	9,09	0,10	1.73312e-08	2.5836e-09	0,39	99,72	92,60
K9	Harz. (Foam M2)	40,61	50,02	8,80	0,13	1.73615e-08	2.58543e-09	0,37	99,93	91,80
K9	Harz. (Foam M2)	40,39	50,01	8,91	0,12	0,01	2.58455e-09	0,40	99,84	92,20
K9	Harz. (Foam M2)	40,51	50,30	9,26	0,12	1.73225e-08	2.58295e-09	0,41	100,60	92,16
K9	Harz. (Foam M2)	40,82	49,96	8,82	0,12	1.73602e-08	2.58542e-09	0,41	100,13	91,45
K9	Harz. (Foam M2)	40,41	49,73	8,75	0,12	0,01	2.58551e-09	0,36	99,37	91,60
K9	Harz. (Foam M2)	40,56	49,81	8,91	0,12	0,01	2.58485e-09	0,36	99,77	91,48
K9	Harz. (Foam M2)	40,69	50,09	9,11	0,11	0,01	2.5839e-09	0,40	100,41	91,70
K9	Harz. (Foam M2)	40,76	50,19	9,14	0,12	1.73364e-08	0,00	0,33	100,55	91,60
K4	Harz. (Mortar M3)	41,03	50,47	8,81	0,10	0,01	2.58593e-09	0,38	100,79	91,70
K4	Harz. (Mortar M3)	40,97	50,30	8,92	0,11	1.73528e-08	2.58522e-09	0,40	100,69	91,60

EMP analysis of representative major element oxides for olivine M2 foam microstructure and olivine M3 mortar microstructure in dunite and harzburgite (Harz.).

Sample	Lithology	SiO	MgO	FeO	MnO	Al2O3	CaO	NaO	TiO	Cr2O3	NiO	TOTAL	Mg#
K9	Porph. M1	57,25	34,86	6,53	0,16	1,19	0,23	-	0,02	0,57	0,06	100,87	91,15
K9	Porph. M1	56,86	34,56	6,45	0,16	1,66	0,26	0,06	0,01	0,72	0,07	100,80	91,5
K9	Porph. M1	56,73	34,65	6,43	0,15	1,81	0,22	0,01	0,00	0,79	0,06	100,87	91,6
K9	Porph. M1	57,19	34,89	6,49	0,15	0,85	0,11	-	-	0,59	0,08	100,35	91,6
K9	Porph. M1	56,19	34,17	6,55	0,17	1,77	0,25	0,02	0,01	0,77	0,07	99,97	91,5
K9	Porph. M1	56,74	34,48	6,55	0,15	1,22	0,19	0,00	0,01	0,83	0,05	100,21	91,5
K9	Porph. M1	56,68	34,77	6,40	0,15	1,56	0,23	0,00	-	0,88	0,11	100,79	91,9
K9	Porph. M1	56,47	35,64	5,89	0,15	2,25	0,09	0,08	-	0,85	0,07	101,51	94,79
K9	Porph. M1	56,36	34,28	6,45	0,15	2,02	0,31	0,02	0,00	0,83	0,09	100,51	91,8
K9	Porph. M1	56,58	34,41	6,40	0,14	1,62	0,22	0,00	0,01	0,87	0,08	100,33	91,6
K9	Porph. M1	56,42	34,41	5,92	0,14	2,26	0,43	0,00	-	0,79	0,06	100,44	92
K9	Porph. M1	56,10	34,34	6,37	0,14	1,97	0,36	0,04	0,03	1,31	0,10	100,76	92,2
K9	Porph. M1	56,63	34,60	6,32	0,14	1,90	0,32	0,04	0,01	0,79	0,09	100,85	92
K9	Porph. M1	56,89	34,56	6,46	0,15	1,69	0,23	0,05	0,00	0,74	0,04	100,81	91,5
K9	Porph. M1	56,51	34,41	6,26	0,14	2,15	0,28	0,14	0,02	0,79	0,09	100,79	92,2
K9	Porph. M1	56,59	34,52	6,65	0,15	1,84	0,31	0,00	-	0,73	0,09	100,89	91,5
K9	Eq. Foam M2	56,45	34,62	6,35	0,13	1,33	0,24	0,00	0,02	0,21	0,05	99,39	91,6
K9	Eq. Foam M2	56,55	34,69	6,40	0,13	0,89	0,21	0,01	-	0,25	0,05	99,19	92
K9	Eq. Foam M2	56,56	34,60	6,36	0,15	1,22	0,14	0,03	0,01	0,64	0,07	99,77	91,2
K9	Eq. Foam M2	56,69	34,87	6,43	0,16	0,98	0,12	0,01	0,01	0,56	0,07	99,89	92
K9	Eq. Foam M2	55,78	34,34	6,35	0,18	1,37	0,16	0,06	0,01	0,70	0,09	99,04	91,5
K9	Eq. Foam M2	55,96	34,45	5,87	0,13	1,82	0,33	0,05	-	0,75	0,09	99,46	91,1
K9	Eq. Foam M2	55,86	34,16	6,10	0,15	1,88	0,35	0,02	-	0,72	0,08	99,31	92,2
K9	Eq. Foam M2	56,14	34,18	6,31	0,11	1,30	0,28	0,03	0,01	0,71	-	99,08	92,5

EMP analysis of representative major element oxides for orthopyroxene M1 porphyroclast and orthopyroxene M2 in harzburgite.

Sample	Mineral/Texture	SiO	TiO	Al2O3	Cr2O3	FeO	MnO	MgO	CaO	NaO	KO	TOTAL
k3	Chlorite	31,55	0,04	13,59	4,01	2,82	0,06	33,42	0,02	0,01	-	85,52
K3	Chlorite	33,01	0,01	12,49	4,44	2,48	0,01	34,01	0,00	0,02	-	86,47
K3	Chlorite	32,87	0,01	13,08	4,77	3,01	0,03	32,94	0,14	0,02	-	86,89
K3	Chlorite	34,55	-	10,51	4,27	2,34	0,04	34,59	0,01	-	-	86,32
K3	Chlorite	31,80	0,01	12,50	3,66	2,61	0,03	33,53	0,00	0,01	-	84,16
K9	Chlorite	32,23	0,01	14,80	2,78	2,71	0,03	33,52	-	0,00	-	86,08
K9	Chlorite	32,00	-	12,36	4,33	2,20	-	33,59	0,01	0,01	-	84,51
K9	Chlorite	33,17	0,02	12,08	4,19	2,29	0,06	33,52	0,04	0,01	-	85,37
K9	Tremolite in Eq. With olivine M2 foam structure	57,49	0,03	0,50	1,22	2,13	0,12	23,93	11,88	0,68	0,03	98,01
K9	Tremolite in Eq. With olivine M2 foam structure	57,64	0,02	0,44	0,14	1,81	0,07	23,94	12,11	0,62	0,04	96,82
K9	Tremolite in Eq. With olivine M2 foam structure	57,36	0,02	0,79	0,33	1,84	0,07	23,82	12,02	0,86	0,04	97,15
K3	Tremolite incl. Olivine M1 Porphyroclast	57,41	0,01	0,25	0,05	1,44	0,07	21,22	12,53	0,39	0,01	93,37
K3	Tremolite incl. Olivine M1 Porphyroclast	58,72	0,00	0,11	0,03	1,25	0,07	21,52	12,56	0,41	0,02	94,69

EMP analysis of representative major element oxides for amphiboles and chlorite in dunite and harzburgite.

Appendix 6 XRF bulk rock analysis

	TGA	Wt%															
Sample	LOI (105-1000)	SiO2	Al03	TiO2	FeO	MnO	CaO	MgO	Na2O	K2O	P2O5	TOTAL	TOTAL+LOI	Cr	Ni	Sr	Ba	Zr
K7	0,27	40,48	0,09	0,01	8,97	0,12	0,11	51,35	<0,01	0,01	<0,01	101,13	101,40	2582,70	3058,02	<5	<30	<5
K9a	0,38	42,37	0,43	0,01	10,10	0,14	0,46	46,89	<0,01	0,01	<0,01	100,39	100,77	3021,57	2569,04	<5	<30	<5
K9B	0,39	42,56	0,57	0,01	9,81	0,14	0,70	45,97	0,03	0,01	0,00	100,88	101,27	3533,41	2558,71	-	-	12,58

XRF major element oxides analysis for dunite (K7) and harzburgites (K9a-K9b) samples. All Fe is considered FeO.

		Wt%										
Sample	Lithology	SiO2	Al03	TiO2	FeO	MnO	CaO	MgO	Na2O	K2O	P2O5	TOTAL	Mg#
K7	Dunite	40,03	0,09	0,01	8,87	0,12	0,11	50,77	0,00	0,01	0,00	100,0	92,4
K9a	Harzburgite	42,20	0,43	0,01	10,06	0,14	0,46	46,71	0,00	0,01	0,00	100,0	91,1
K9B	Harzburgite	42,19	0,57	0,01	9,73	0,14	0,69	45,57	0,03	0,01	0,00	100,00	91

XRF major element oxides analysis for dunite (K7) and harzburgites (K9a-K9b) samples recalculated to 100%

Appendix 6

Olivine fabric analysis

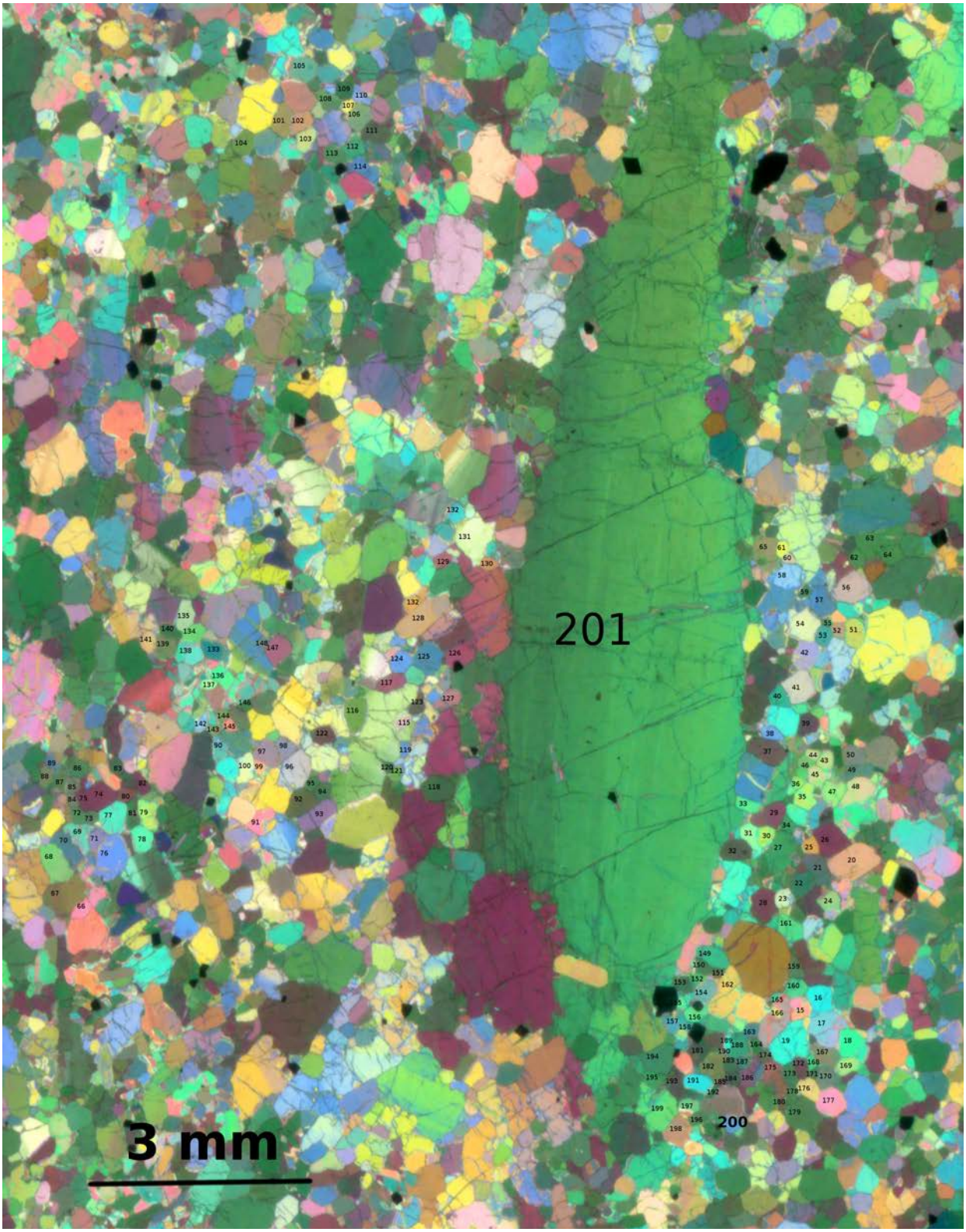

Optical micrograph of sample K8c (dunite). CPO measurements on olivine M2 type II grains are defined by number from 1 to 200, and the parental olivine M1 porphyroclast has the number 201. Every number is related to relative crystallographic major axis of olivine crystals plotted in Fig. 37.